

**POLITECNICO DI TORINO**

Collegio di Ingegneria Elettrica

**Corso di Laurea Magistrale in Ingegneria Elettrica**

Tesi di Laurea Magistrale

**Modelling and lab-setting  
for hydrogen-electricity integration  
in the energy transition context**



**Relatori**

Dott. Andrea Mazza

Dott. Abouzar Estebsari

Prof. Ettore Francesco Bompard

**Correlatore**

Prof. Harm Lok

**Candidato**

Giulia Morandi

ID n. 232881

Luglio 2019



# Executive Summary

The aims of this thesis have been:

- The configuration of the lab setup, for local measurements on on-site resources (PV panels and electrolyser);
- The arrangement of the remote connection between labs and creation of a multi-site co-simulation lab layout, for reproducing the measurements in remote;
- The experimental-based modelling of a PV-field, for studies aiming to integrate PtG plants in the electrical grid;
- The experimental-based modelling (static and dynamic) of a PEM electrolyser, again for studies aiming to integrate PtG plants in the electrical grid;
- The application of the lab setup and the models previously built in order to test and validate the correct functioning of the remote connection.

The models of energy transition sources created in this thesis will be later merged into large-scale power grid simulations for investigating the interactions between hydrogen production and renewable sources, as well as their influences on the grid. The multi-site laboratory layout will be applied to remotely test the local resources by realizing a “geographically distributed real-time co-simulation” based on Remote Power Hardware-In-the-Loop concepts.

# Contents

Executive Summary .....	3
Contents .....	4
List of Figures.....	7
List of Tables.....	10
List of Acronyms and Nomenclature.....	11
Chapter 1: Theoretical background.....	13
1.1 H <sub>2</sub> production .....	13
1.2 Focus on electrolysis .....	14
1.2.1 Water-splitting reaction .....	14
1.2.2 Electrolysis technologies.....	15
1.2.2.1 Alkaline electrolysis .....	15
1.2.2.2 PEM electrolysis .....	17
1.2.2.3 Solid Oxide electrolysis .....	18
1.3 PtG-based multi-energy system .....	19
1.3.1 PtG concept.....	19
1.3.1.1 Conversion Power-to-Gas .....	20
1.3.1.2 Conversion Gas-to-Power .....	21
1.4 Electrical aspects of PtG .....	21
1.4.1 Requirements of electrolyzers for PtG applications .....	21
1.4.1.1 Alkaline electrolyser .....	22
1.4.1.2 PEM electrolyser .....	22
1.4.2 PtG applications in the electrical system.....	23
1.4.2.1 Generation side.....	24
1.4.2.2 Transmission side .....	24
1.4.2.3 Distribution side .....	25
1.4.2.4 Utilization side .....	26
1.4.3 Configurations for hydrogen-electricity integration .....	27
1.4.3.1 Off-grid applications .....	27
1.4.3.2 Grid-connected applications .....	29
Chapter 2: Groningen laboratory setup .....	31
2.1 Aim of the laboratory .....	31
2.2 Overview of the facilities at Entrance's demonstration site.....	32
2.2.1 Physical components.....	33
2.2.2 Virtual connections .....	34
2.3 Focus on the devices used for the experiments.....	36
2.3.1 Power analyzer: electrical measurements.....	36
2.3.1.1 Power analyzer characteristics .....	36
2.3.1.2 Power analyzer software.....	37
2.3.2 Electrolyser: hydrogen production characterization .....	38
2.3.2.1 Electrolyser specifications .....	38
2.3.2.2 Electrolyser structure and functioning .....	38
2.3.2.3 Electrolyser efficiency .....	42
2.3.2.4 Hydrogen process measurements and control: PLC, HOGEN40 software and flow controller .....	44
2.3.3 PV-field: renewable source characterization .....	47



2.3.3.1 PV-field specifications .....	47
2.3.3.2 PV-field efficiency .....	48
2.3.3.3 Weather conditions measurements: pyranometer and temperature sensors .....	49
Chapter 3: Model of the PV panels .....	51
3.1 Aim of the modelling .....	51
3.2 Concept of the PV panels model .....	51
3.3 Collecting the measurements .....	52
3.4 Processing the data .....	55
3.4.1 Active power, reactive power and solar irradiance .....	55
3.4.2 Air temperature .....	59
3.5 Creation of the model .....	60
3.6 Validation of the model .....	65
Chapter 4: Model of the electrolyser .....	67
4.1 Concept of the electrolyser model .....	67
4.2 First approach: static .....	67
4.2.1 Collecting the measurements .....	67
4.2.2 Processing the data .....	73
4.2.3 Creation of the model .....	80
4.3 Second approach: dynamic .....	82
4.3.1 Collecting the measurements .....	82
4.3.2 Validation of the model .....	87
Chapter 5: Multi-site laboratory setup and remote simulation .....	90
5.1 Aim of the multi-site lab .....	90
5.2 Explanation of the Remote Power Hardware-In-the-Loop .....	90
5.2.1 What is it? .....	90
5.2.2 Why is it important? .....	91
5.2.3 How do we use it? .....	92
5.3 Network connection .....	93
5.4 Test cases .....	94
5.4.1 First test set .....	95
5.4.2 Second test set .....	98
Conclusion and future work .....	103
Appendix A .....	105
A.1 How to get started with DataLogger software .....	105
A.1.1 Connection .....	105
A.1.2 Software main screen .....	106
A.1.3 Measure Mode .....	108
A.2 Importing CSV files into Excel .....	110
Appendix B .....	111
B.1 Electrolyser operating manual .....	111
B.1.1 Hydrogen risks and safety measures .....	111
B.1.2 How to start up the electrolyser system .....	111
B.1.3 How to shut down the electrolyser system .....	115
Appendix C .....	117
C.1 Electrolyser software manual .....	117
C.1.1 How to interface with the PLC .....	117

C.1.2 How to connect to the PLC in remote .....	117
C.1.3 How to retrieve the measured data from the electrolyser PLC .....	118
C.1.3.1 Retrieving data by connecting a PC to the PLC via miniUSB-USB cable .....	119
C.1.3.2 Retrieving data by pulling out the SD card and plugging it into a PC .....	120
C.1.4 How to retrieve the measured data from the electrolyser unit .....	122
C.1.4.1 Connection via RS232 serial cable.....	122
C.1.4.2 Connection via Ethernet .....	122
C.1.4.3 Data logging .....	123
Appendix D .....	125
D.1 How to arrange the PV panels connections within the lab setup .....	125
D.2 How to arrange the electrolyser connections within the lab setup .....	125
Appendix E.....	127
References.....	128

# List of Figures

Fig. 1 – Hydrogen production methods .....	13
Fig. 2 – Schematic diagrams of (a) a gap cell; (b) a zero-gap cell and.....	16
Fig. 3 – Schematic working principle of alkaline water electrolysis.....	16
Fig. 4 – Schematic working principle of PEM electrolysis .....	17
Fig. 5 – Schematic working principle of high-temperature water electrolysis .....	18
Fig. 6 – Power-to-Gas system.....	19
Fig. 7 – Illustration of the electrical network structure .....	23
Fig. 8 – Grid-independent hydrogen production system .....	28
Fig. 9 – Grid-independent integrated energy system with hydrogen as renewable energy storage.....	28
Fig. 10 – Grid-assisted hydrogen production system.....	29
Fig. 11 – Grid-connected system with hydrogen as renewable energy storage.....	30
Fig. 12 – Grid-connected integrated energy system (or hydrogen energy chain) .....	30
Fig. 13 – Components for the integration hydrogen production-renewable energy sources.	31
Fig. 14 – Picture of the Entrance Micro-Grid Lab.....	32
Fig. 15 – Schematic of the Entrance’s Micro-Grid Lab setup .....	32
Fig. 16 – Picture of the N4L’s PPA1500 power analyzer .....	36
Fig. 17 – Analog input diagram of the PPA1500 power analyzer.....	36
Fig. 18 – Proton’s Hogen40 PEM electrolyser .....	38
Fig. 19 – Picture of the electrolyser container at the Entrance test site .....	39
Fig. 20 – Picture of one side of the electrolyser cabin .....	39
Fig. 21 – Picture of the other side of the electrolyser cabin .....	40
Fig. 22 – Inside of the Proton’s Hogen40 PEM electrolyser.....	40
Fig. 23 – PFD and measuring equipment of the hydrogen production process .....	46
Fig. 24 – Picture of the PV panels and inverter at the Entrance test site .....	47
Fig. 25 – Picture of the pyranometer at the PV installation under study .....	49
Fig. 26 – Picture of the air temperature sensor at a neighbor PV installation .....	50
Fig. 27 – Scheme of the concept for the implementation of the PV panels model.....	52
Fig. 28 – PPA measurements: active power.....	53
Fig. 29 – PPA measurements: reactive power .....	54
Fig. 30 – Pyranometer measurements: solar irradiance .....	54
Fig. 31 – Temperature sensor measurements: air temperature .....	55
Fig. 32 – Function $Q(P)$ .....	63
Fig. 33 – PV panels model .....	63
Fig. 34 – PV panels model: PV Panels subsystem .....	64
Fig. 35 – PV panels model: PV_model subsystem.....	64
Fig. 36 – PV panels model: Counter subsystem .....	64
Fig. 37 – PV panels model: comparison between estimated and measured active power.....	65
Fig. 38 – PV panels model: comparison between estimated and measured active power.....	65
Fig. 39 – Scheme of the concept for the implementation of the electrolyser model .....	67
Fig. 40 – Three-phase active power at full-load.....	70
Fig. 41 – Three-phase reactive power at full-load .....	70
Fig. 42 – Active power of phase 1 by varying the load .....	70
Fig. 43 – Reactive power of phase 1 by varying the load.....	71
Fig. 44 – DC power by varying the load.....	71

Fig. 45 – H <sub>2</sub> output flow by varying the load .....	71
Fig. 46 – Three-phase active power at 25% of full-load and time step of 20 ms.....	72
Fig. 47 – Three-phase active power at 25% of full-load and time step of 1 s.....	72
Fig. 48 – Three-phase reactive power at 25% of full-load and time step of 20 ms .....	73
Fig. 49 – Three-phase reactive power at 25% of full-load and time step of 1 s .....	73
Fig. 50 – Active power of phase 1 at 25% of full-load after the overlaying process (with zoom) .....	77
Fig. 51 – Reactive power of phase 1 at 25% of full-load after the overlaying process (with zoom).....	78
Fig. 52 – Result of the data processing: active power of phase 1 by varying the load.....	79
Fig. 53 – Result of the data processing: reactive power of phase 1 by varying the load .....	80
Fig. 54 – Electrolyser model .....	80
Fig. 55 – Electrolyser model: Electrolyser subsystem .....	81
Fig. 56 – Electrolyser model: electrical data_25 subsystem .....	81
Fig. 57 – Active power of phase 1, 2 and 3 – start-up and step to 25% of full-load.....	84
Fig. 58 – Active power of phase 1, 2 and 3 – step from 25 to 50% of full-load .....	84
Fig. 59 – Active power of phase 1, 2 and 3 – step from 50 to 75% of full-load .....	85
Fig. 60 – Active power of phase 1, 2 and 3 – step from 75 to 100% of full-load .....	85
Fig. 61 – H <sub>2</sub> output flow - start-up and step to 25% of full-load (with zoom) .....	86
Fig. 62 – H <sub>2</sub> output flow - step from 25 to 50% of full-load (with zoom).....	86
Fig. 63 – Electrolyser model: Electrolyser subsystem with flow_setpoint control signal.....	87
Fig. 64 – Electrolyser model: comparison between real and simulated power profiles (case 0- 25%).....	88
Fig. 65 – Electrolyser model: comparison between real and simulated power profiles (case 25-50%) .....	88
Fig. 66 – Electrolyser model: comparison between real and simulated power profiles (case 50-75%) .....	89
Fig. 67 – Electrolyser model: comparison between real and simulated power profiles (case 75-100%) .....	89
Fig. 68 – Power Hardware-In-the-Loop schematic.....	91
Fig. 69 – General scheme of the plan for PHIL collaboration between Hanze and PoliTo .....	92
Fig. 70 – Schematic of the VPN communication between Hanze and PoliTo.....	93
Fig. 71 – Multi-site lab network topology .....	94
Fig. 72 – Active power withdrawn by the electrolyser - Local measurements.....	96
Fig. 73 – Active power withdrawn by the electrolyser - RHIL measurements.....	96
Fig. 74 – Production of H <sub>2</sub> - Local measurements .....	97
Fig. 75 – Production of H <sub>2</sub> - RHIL measurements .....	97
Fig. 76 – Simulink model subsystem: Flow controller Modbus writing .....	99
Fig. 77 – Simulink model subsystem: Flow controller Modbus reading .....	99
Fig. 78 – Simulink model subsystem: Power analyzer TCP reading .....	99
Fig. 79 – Active power withdrawn by the electrolyser - Local measurements (from Simulink) .....	100
Fig. 80 – Active power withdrawn by the electrolyser - RHIL measurements (from Simulink) .....	100
Fig. 81 – Production of H <sub>2</sub> - Local measurements (from Simulink) .....	101
Fig. 82 – Production of H <sub>2</sub> - RHIL measurements (from Simulink) .....	102
Fig. 83 – PPA REMOTE menu.....	105

Fig. 84 – PPA REMOTE menu - detail.....	105
Fig. 85 – Configure PPA connection .....	106
Fig. 86 – Communications window .....	106
Fig. 87 – DataLogger Software main screen.....	107
Fig. 88 – Results panel in Measure mode .....	108
Fig. 89 – Multilog window .....	109
Fig. 90 – First room detail: main valve of the feedwater tube .....	112
Fig. 91 – First room details: (a) two ion exchange units; (b) RO unit and pump control panel .....	112
Fig. 92 – Second room details: valves. BV-09 in green, BV-04 in blue, BV-013 in orange, PCV-01 in yellow .....	113
Fig. 93 – Second room details: (a) electrolyser main switch; (b) PLC display .....	114
Fig. 94 – Electrolyser display .....	114
Fig. 95 – Second room details: manometers .....	115
Fig. 96 – PLC display: (a) main screen; (b) general setting screen .....	117
Fig. 97 – Remote Operator main screen .....	118
Fig. 98 – SD Card Explorer selection.....	119
Fig. 99 – SD Card Explorer main screen.....	120
Fig. 100 – SD Card Manager selection.....	120
Fig. 101 – SD Card Manager main screen .....	121
Fig. 102 – HOGEN40 Communications window .....	122
Fig. 103 – HOGEN40 Diagnostics.....	123
Fig. 104 – HOGEN40 System Monitoring .....	124
Fig. 105 – Detail switches and sockets (inverter side) .....	125
Fig. 106 – Detail switches and sockets (PPA side).....	125

# List of Tables

Tab. 1 – Technical parameters of the major electrolyser technologies [3,4] .....	18
Tab. 2 – Comparison of characteristics of alkaline and PEM electrolyzers in the context of PtG [3,4] .....	23
Tab. 3 – Proton’s Hogen40 PEM electrolyser specifications.....	38
Tab. 4 – PLC monitored variables.....	45
Tab. 5 – HOGEN40 monitored variables .....	45
Tab. 6 – Trina Solar’s PV panels specifications.....	47
Tab. 7 – SolarEdge’s three-phase inverter specifications .....	48
Tab. 8 – <b>PQ_real</b> [17279x7].....	55
Tab. 9 – <b>Irrad_real</b> [1441x2].....	55
Tab. 10 – <b>PQ_lin</b> [17281x7].....	56
Tab. 11 – <b>Irrad_lin</b> [17281x2].....	57
Tab. 12 – <b>PQ_Econs</b> [17281x7].....	59
Tab. 13 – <b>Irrad_Econs</b> [17281x2] .....	59
Tab. 14 – <b>Ta_31_10</b> [205x2] .....	59
Tab. 15 – <b>Ta_01_11</b> [205x2] .....	59
Tab. 16 – <b>Ta</b> [17281x2] .....	60
Tab. 17 – <b>P_lookup</b> [17269x2] .....	62
Tab. 18 – <b>Q_lookup</b> [17269x2].....	62
Tab. 19 – <b>PQ_25_2h_real</b> [6910x7] .....	74
Tab. 20 – <b>PQ_25_30s_real</b> [1501x7] .....	74
Tab. 21 – <b>PQ_25_2h_lin</b> [360001x7].....	75
Tab. 22 – <b>PQ_25_30s_lin</b> [1501x7] .....	75
Tab. 23 – <b>PQ_25_2h_Econs</b> [360001x7] .....	76
Tab. 24 – <b>PQ_25_30s_Econs</b> [1501x7].....	76
Tab. 25 – <b>PQ_25_Econs_final</b> [360001x7] .....	79
Tab. 26 – Electrolyser display details .....	114

# List of Acronyms and Nomenclature

A/D	Analog/Digital
AC	Alternating Current
CC	Carbon Capture
CHP	Combined Heat and Power
CO	Carbon Monoxide (chemical compound)
CO <sub>2</sub>	Carbon Dioxide (chemical compound)
CSV	Comma-Separated Values (file format)
DC	Direct Current
DER	Distributed Energy Resource
$\Delta G$	Gibbs free energy
$\Delta H$	Enthalpy
$\Delta S$	Entropy
DPS	Distributed Power System
DSP	Digital Signal Processor
FPGA	Field Programmable Gate Array
G-RTSLab	Global Real-Time Simulation Lab (at PoliTo)
GtP	Gas-to-Power
H <sub>2</sub>	Hydrogen (chemical element)
H <sub>2</sub> O	Water (chemical compound)
HER	Hydrogen Evolution Reaction
HIL	Hardware-In-the-Loop
HuT	Hardware under Test
LAN	Local Area Network
MEA	Membrane Electrode Assembly
NG	Natural Gas
NOCT	Nominal Operating Cell Temperature
O <sub>2</sub>	Oxygen (chemical element)
OER	Oxygen Evolution Reaction
PEM	Proton Exchange Membrane (or Polymer Electrolyte Membrane)
PFD	Process Flow Diagram
PHIL	Power Hardware-In-the-Loop
PLC	Programmable Logic Controller
PM	Power Module
PPA	Power Analyzer
PtG	Power-to-Gas
PV	Photo-Voltaic
RES	Renewable Energy Source
RHIL	Remote Power Hardware-In-the-Loop
RO	Reverse Osmosis
RoS	Rest of the System
RPH	Renewable Power Hydrogen

RPM	Renewable Power Methane
RTS	Real-Time Simulation
RTT	Real-Time Target
SNG	Synthetic Natural Gas (or Syngas)
SOE	Solide Oxide Electrolysis
SOEC	Solide Oxide Electrolysis Cell
STC	Standard Test Conditions
TCP	Transmission Control Protocol (network protocol)
TCP/IP	Transmission Control Protocol/Internet Protocol
TSV	Tab-Separated Values (file format)
UDP	User Datagram Protocol (network protocol)
VPN	Virtual Private Network



# Chapter 1

## Theoretical background

### 1.1 H<sub>2</sub> production

Hydrogen production is the primary step towards the transition to a hydrogen economy and the replacing of conventional fuels. It can be realized by processing a wide variety of raw materials employing primary energies from different resources. Accordingly, the processes available for H<sub>2</sub> production can be divided into two main categories, namely *conventional* and *renewable* technologies. The former category is based on fossil fuels (exhaustible and limited, such as natural gas, coal, etc.) used both as raw material and source of energy; the latter comprises methods based on the use of renewable energy sources (non-exhaustible, such as solar, wind or tidal energy and geothermal heat) for the processing of renewable materials (either biomass or water).

The classification of the major current technologies is presented in Figure 1, and, in what follows, a short overview is given [1,2].

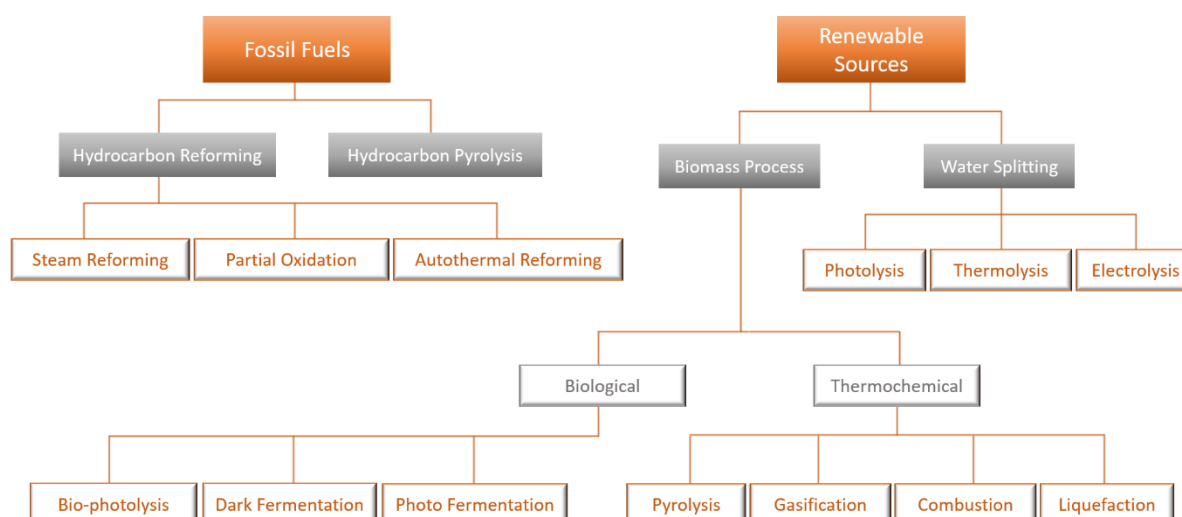


Fig. 1 – Hydrogen production methods

*Fossil fuels* are up to now the most commonly used feedstock for producing hydrogen. These methods are the most cost-effective because of the maturity level of the technology, which is based on well-developed techniques with highly efficient energy conversion and making use of already existing infrastructures. In this context, the main technologies are *hydrocarbon reforming* and *pyrolysis*, which are by far the most developed ones, alone covering almost the entire hydrogen demand. However, the dependence on fossil fuels appears disadvantageous as a significant amount of CO<sub>2</sub> byproduct is generated and released in the atmosphere. These key limitations, along with the related environmental issues and concerns for fossil fuels depletion, lead to the necessity of developing alternative methods for H<sub>2</sub> production in a clean and sustainable way.

*Renewable sources*-based methods for H<sub>2</sub> production are numerous but not commonly implemented as usual production methods and some of them even at the developing stage.

Specifically, this wide variety can be divided into *biomass* processes and *water-splitting* technologies.

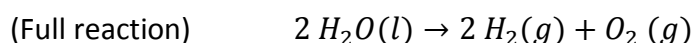
- *Biomass* is a renewable energy source consisting of organic matter derived from plants and animal materials such as, energy crops including herbaceous, woody, forest and agricultural residues or industrial and municipal wastes. Biomass can be used to generate hydrogen in a sustainable way by reducing CO<sub>2</sub> emissions to the atmosphere with respect to the use of fossil fuels. In fact, the amount of CO<sub>2</sub> released when the biomass is gasified is equal to the amount that was previously absorbed from the atmosphere during the organism lifetime. Technologies for hydrogen production from biomass can be classified into *thermochemical* and *biological*. They both constitute an effective means for sustainable development and waste minimization, representing a step forward the achievement of a climate with zero emission of greenhouse gases.
- *Water-splitting* represents another sustainable alternative. This technology in fact produces H<sub>2</sub> by using water, which is one of the most available raw materials on Earth. Moreover, this process is liable for CO<sub>2</sub> emissions only when fossil fuels are used to generate the required electricity, while, if the electrical energy comes from RES, the resulting H<sub>2</sub> is the cleanest energy carrier. The main technologies in this field are *thermolysis*, *photolysis* and, mostly, *electrolysis*.

## 1.2 Focus on electrolysis

*Electrolysis* is the most established and valuable method for water splitting. Since this reaction is non-spontaneous, the required energy must be provided to the system externally by means of electricity and the device used for this process is the so-called *electrolyser*. This hydrogen production unit contains multiple electrolysis cells, series-connected to form the electrolysis stack. The elementary electrolysis cell consists of two metallic electrodes, an anode and a cathode, facing each other and immersed in a liquid electrolyte. A thin electrolytic layer, consisting in a diaphragm impregnated with the electrolyte, is placed between the electrodes and acts as an electric isolator. Electrical work is applied to the cell in order to dissociate water molecules into its constituents and generate gaseous hydrogen. Since individual cells are of limited production capacity, they are stacked together to obtain the production capacity most appropriate for process requirements.

### 1.2.1 Water-splitting reaction

Specifically, the principle of water electrolysis is the following. Direct current passes between the two electrodes – where the charge carriers are the electrons as in the external circuit, and then flows through the electrolyte – with the charges being carried by the mobile ions. This current flow provides the necessary energy to split the water molecules into its constituent elements. The diaphragm serves as electric isolator and maintains the evolving gas streams separated, to prevent their spontaneous chemical recombination by diffusion in the interpolar area. As a result of the process, oxygen is formed at the anodic (positive) terminal and hydrogen at the cathodic (negative) terminal, the production being directly proportional to the current flowing through the electrodes. The following reaction is satisfied:



Assuming standard conditions of temperature and pressure ( $T^\circ = 298 \text{ K}$ ,  $P^\circ = 1 \text{ bar}$ ),  $\text{H}_2\text{O}$  is liquid while  $\text{H}_2$  and  $\text{O}_2$  are gaseous. Enthalpy, entropy and Gibbs free energy standard changes for this reaction are, respectively<sup>1</sup>:

$$\Delta H_d^\circ(\text{H}_2\text{O}(l)) = +285.84 \text{ kJ mol}^{-1}$$

$$\Delta S_d^\circ(\text{H}_2\text{O}(l)) = +163.15 \text{ kJ mol}^{-1} \text{ K}^{-1}$$

$$\Delta G_d^\circ(\text{H}_2\text{O}(l)) = \Delta H_d^\circ(\text{H}_2\text{O}(l)) - T \cdot \Delta S_d^\circ(\text{H}_2\text{O}(l)) = +237.22 \text{ kJ mol}^{-1}$$

As consequence of the highly endothermic enthalpy contribution, the Gibbs free energy change is positive and, therefore, the reaction is non-spontaneous.

As a comment, it is worth to say that state functions change with temperature<sup>2</sup>. While the total amount of energy required for water splitting  $\Delta H$  is roughly constant over the temperature range of practical interest, the entropic contribution  $T \cdot \Delta S$  (heat demand) increases and the Gibbs free energy  $\Delta G$  (electricity demand) decreases by increasing the operating temperature. In particular,  $\Delta G$  becomes negative at very high temperatures ( $> 2500 \text{ K}$ ) and this makes the reaction to happen spontaneously. Although direct water thermo-dissociation cannot be applied in practice because of material-related constraints, high-temperature water electrolysis appears as a promising solution. By providing heat to the system, a higher operating temperature is obtained so that the dissociation of water is facilitated and in turn less electricity is required<sup>3</sup>[2].

## 1.2.2 Electrolysis technologies

Different technologies of electrolyzers are available nowadays. Low temperature electrolyzers are already commercially available and among these the most developed and commonly used are alkaline electrolyzers and Proton Exchange Membrane<sup>4</sup> (PEM) electrolyzers. In addition, a third type called Solid Oxide Electrolyte (SOE) electrolyser, based on high temperature electrolysis, is still at the development stage. The mentioned technologies, as their names suggest, can be distinguished according to the nature of the electrolyte as well as the structure and functioning of the electrolysis cell. In this regard, the following section provides an overview on the related characteristics and operating principles.

### 1.2.2.1 Alkaline electrolysis

Alkaline water electrolysis uses a liquid alkaline electrolyte and a cell structure so-called *zero-gap cell* (Figure 2(b)). This is aimed at improving the *gap cell* concept (Figure 2(a)), i.e. the most conventional and simple cell configuration.

<sup>1</sup> State functions depend on temperature and pressure. At operating temperature  $T$  and pressure  $P$ ,  $\Delta H(T, P)$  represents the total amount of energy that is needed to split 1 mole of water, where  $\Delta G(T, P)$  is the amount of electrical work required and  $T \cdot \Delta S(T, P)$  is the demanded heat. The relationship among these quantities at atmospheric pressure is:  $\Delta H(T, 1) = \Delta G(T, 1) + T \cdot \Delta S(T, 1)$

<sup>2</sup> The change with pressure is less significant.

<sup>3</sup> The total energy required for the electrolysis process comes for the 85% from electricity and 15% from heat at standard temperature. The percentages turn into 66.6% and 33.3% respectively at  $1000^\circ\text{C}$ . This is important since electricity is more costly than heat, with a cost ratio kWh of electricity/kWh of heat usually around 3-5 [2].

<sup>4</sup> Or proton conducting Polymer Electrolyte Membrane.

It is composed by two planar electrodes placed face to face in the liquid electrolyte and separated by a porous diaphragm impregnated with the electrolyte itself. A certain distance between electrodes and diaphragm is needed in order to let formed gas streams evolve freely. This gap, however, leads to increased ohmic losses, thus to a limit on the maximum operating current density. The improved cell concept, instead, implies to suppress the gap between anode and cathode by using porous electrodes directly pressed onto the separator. This allows the produced gaseous streams to be released through the pores on the backside, and, at the same time, allows the ohmic losses to be reduced, so that considerably higher current densities can be reached without significant efficiency drops.

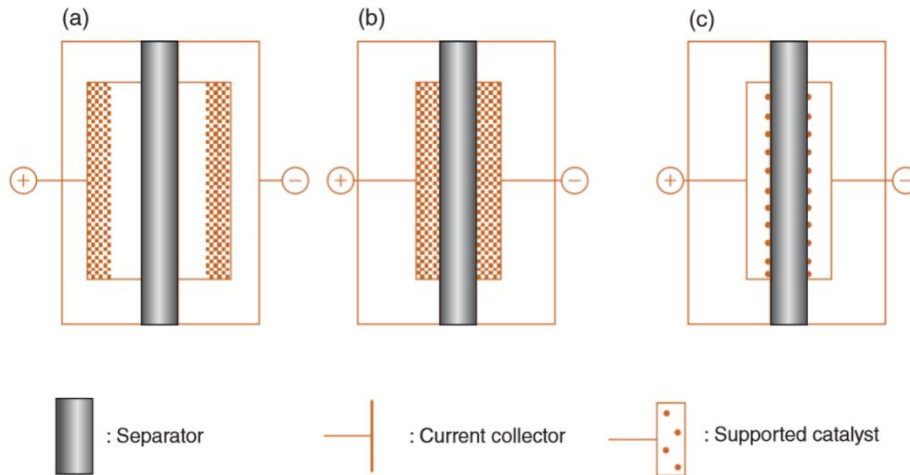


Fig. 2 – Schematic diagrams of (a) a *gap cell*; (b) a *zero-gap cell* and (c) a *PEM* (polymer electrolyte membrane) *cell*

In alkaline water electrolysis cells, water is introduced at the cathode and here is dissociated into hydrogen and hydroxide ions.  $H_2$  is separated from water in an external separator, while  $OH^-$  ions move through the liquid electrolyte to the anode where are recombined into  $O_2$ . The processes taking place at anode and cathode are respectively known as the oxygen evolution reaction (OER) and the hydrogen evolution reaction (HER). The corresponding equations are written as follows (alkaline media):

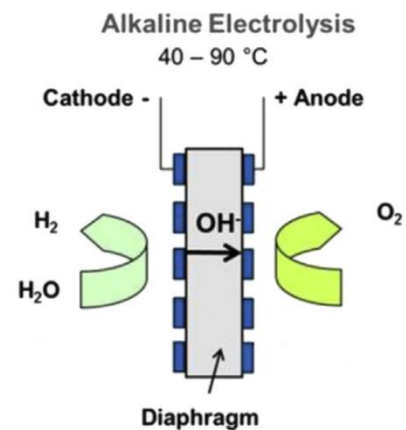
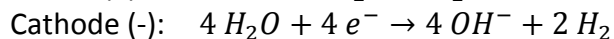
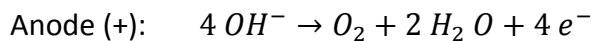


Fig. 3 – Schematic working principle of alkaline water electrolysis

Alkaline water electrolysis is a well-established technology and electrolyzers of this kind have been commercialized for decades, with units of nominal power from tens of kW up to 3.5 MW. Current densities are rather low, being in the range  $0.2\text{--}0.4 \text{ A/cm}^2$ . Maximum operating pressures are up to 30 bar, with average operating temperatures around  $80^\circ\text{C}$ . Most efficient units can reach maximum stack efficiencies of about 70% [2-4]. The major technical parameters are reported in Table 1.

### 1.2.2.2 PEM electrolysis

PEM electrolysis is realized in an acidic electrolyte and through the application of the so-called *PEM cell* structure (Figure 2(c)). This configuration constitutes an improvement of the cell type used in alkaline technology which, because of the necessity of a liquid electrolyte, is unsuitable to operate in acidic media (for problems related to metals corrosion). In the PEM cell, instead, the electrolyte is not liquid but confined inside a thin polymeric membrane with proton-conducting ability. This layer has the double purpose of acting both as cell separator, to separate gas products and avoid recombination, and as electrolytic media, to move ionic charges between the electrodes. The membrane surface is coated on both sides by two porous catalytic layers, on which current collectors are pressed to create electric contacts for the electrodes. The obtained layout is known as Membrane Electrode Assembly (MEA). As a final result, no liquid electrolyte is present in the cell and the only aqueous element circulating is de-ionized water feeding the electrochemical reaction. This makes it possible to use acidic media (protons being more mobile than hydroxide ions) while avoiding the dissolution of metallic catalysts due to the highly acidic environment.

In PEM cells, water is introduced at the anode and here is dissociated into oxygen and hydrogen ions.  $O_2$  remains within the aqueous admixture, which is ejected from the anode, while  $H^+$  protons move through the polymer electrolyte membrane to the cathode where are recombined with electrons to form  $H_2$ . The conversions at both sides (OER and HER) are realized according to the following formulas (acidic media):

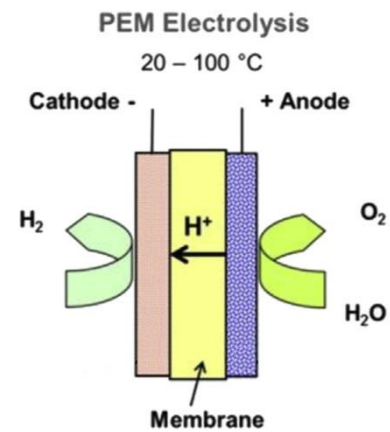
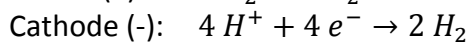
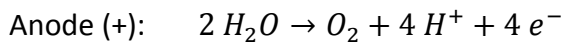


Fig. 4 – Schematic working principle of PEM electrolysis

PEM electrolyzers have been developed for approximately 20 years and, nowadays, units are available only for small and medium scale applications. However, PEM offers several notable advantages compared to alkaline technology: thinner electrolysis cells are obtained resulting in a more compact setup, with excellent properties of chemical and mechanical stability and durability, improved efficiency at high current density and possibility to operate more safely under pressure. In fact, the compact MEA design, along with the absence of liquid electrolyte, allows the operation at elevated current densities in the range  $0.5\text{--}2\text{ A/cm}^2$  as well as pressure differences between electrodes potentially up to 100 bar. In this way, highly compressed hydrogen can be produced on one side, while simultaneously the feedwater and the produced oxygen can be kept at atmospheric pressure on the opposite side, thus reducing the risks associated with the handling of pressurized oxygen. Maximum operating temperatures are around  $100\text{ °C}$  due to thermic limitations of the polymeric material. At last, the drawbacks concern the overall efficiency and the cost. In fact, although the cell efficiency is comparable to that of alkaline electrolyzers, the stack efficiency is lower due to the relatively smaller size of PEM modules (up to 67%) [2-5]. The main technical parameters are summarized in Table 1.

Tab. 1 – Technical parameters of the major electrolyser technologies [3,4]

Type	Rated power [MW]	Rated production [Nm <sup>3</sup> /h]	Energy consumption [kWh/Nm <sup>3</sup> ]	Efficiency [%]	Operating pressure [bar]	Operating temperature [°C]	Current density [A/cm <sup>2</sup> ]
Alkaline	0.055÷3.5	0.4÷760	4.3÷7.5	47÷70	1÷30	65÷100	0.2÷0.4
PEM	0.008÷2	0.53÷400	5.8÷6.7	48÷67	10÷30	20÷100	0.5÷2

### 1.2.2.3 Solid Oxide electrolysis

Solide Oxide Electrolysis (SOE) is a high-temperature steam electrolysis technology which makes use of the so-called Solid Oxide Electrolysis Cell (SOEC).

The solide oxide electrolyte is alkaline and O<sup>2-</sup> ion conductor, so that the half-cell reactions, dependent on the electrolyte pH, are similar to that of the alkaline water electrolysis cell. The SOEC system differs in the fact that the water-splitting reaction is carried out at high temperatures with water steam instead of liquid. In this way, only a portion of the required total energy amount has to be supplied in electricity form, while the remaining portion can be provided by means of heat. In this case, the conversions at both sides (OER and HER) are realized according to the following formulas (acidic media):

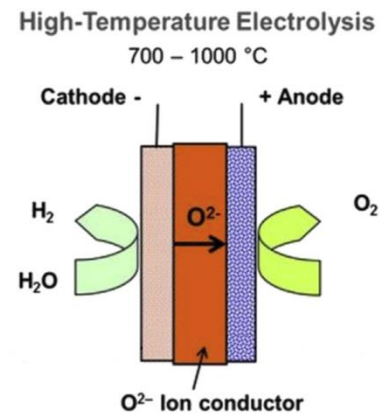
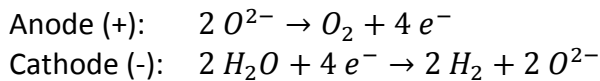


Fig. 5 – Schematic working principle of high-temperature water electrolysis

High-temperature steam electrolysis was developed for the first time in Germany between the 1970s and 1980s and is still at the development stage. It can be currently operated at temperatures of approximately 700-1000 °C (in contrast to maximum 100-130 °C for low-temperature electrolysis). Therefore, since part of electrical energy used for conventional electrolysis is replaced by thermal energy, this constitutes a very promising technology in many aspects. Operational expenses are in fact lower than for low-temperature electrolysis (with electricity consumptions of 4–7 kWh/Nm<sup>3</sup>H<sub>2</sub> for alkaline and PEM technologies, 3.4 kWh/Nm<sup>3</sup>H<sub>2</sub> for SOE technology) and further savings can be achieved through the recovery of industrial heat wastes. In spite of the numerous potential advantages, the technology is relatively immature and its further development is limited by material constraints [2,3].

## 1.3 PtG-based multi-energy system

### 1.3.1 PtG concept

The Power-to-Gas concept is based on the conversion of electricity into gas, this identified with different final products (hydrogen or SNG), through a series of processes. The main step is represented by the so-called Power-to-Hydrogen process, in which the electricity coming from renewable energy sources is used to generate hydrogen by water electrolysis. In this sense, hydrogen constitutes a chemical fuel able to store electrical energy. As such, it can be applied as energy carrier in the context of a multi-vector energy system. In the form of gas vector, hydrogen can be delivered to the customer either directly or further processed into SNG for end uses such as heating, mobility, mechanical energy production and so on. Both gases can then be converted back into the electricity vector by means of the reverse concept of Gas-to-Power, for the final uses pertaining to electricity. Briefly, the coupling of these two concepts makes it possible to create a close link between gas and electricity sectors, allowing them to operate in synergy [3,6].

A graphical representation of the Power-to-Gas and reverse Gas-to-Power concepts is provided in Figure 6 [7,8]. This is followed by a schematic explanation of the functioning of the overall system.

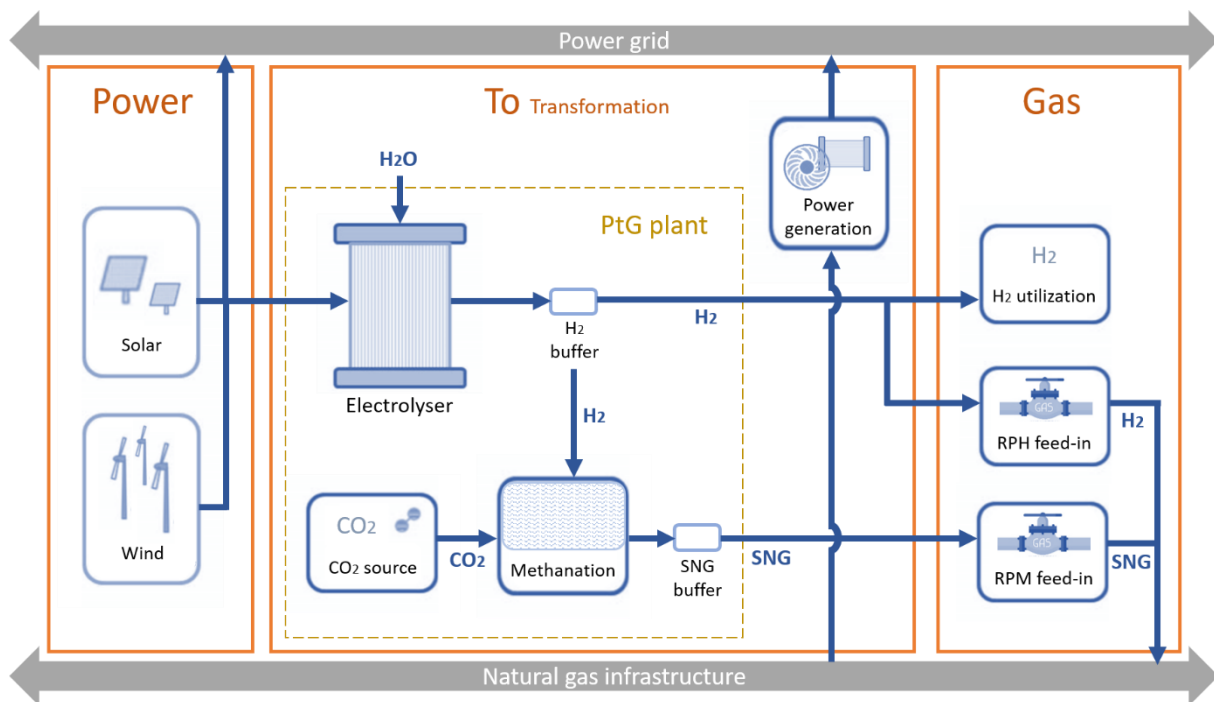


Fig. 6 – Power-to-Gas system

### 1.3.1.1 Conversion Power-to-Gas

#### POWER

The power comes from renewable energy sources, mainly solar and wind, and is injected into the electrical grid when the system is capable to absorb the production. In times of negative residual load, when the renewables produce more electric power than required by electrical loads, the excess is converted into gas (either hydrogen or SNG) by PtG plants [7].

#### TO: Transformation

A typical PtG plant includes four main components [3]:

- An *electrolyser*: this device takes feedwater and electricity from renewables as input and, through the process of electrolysis, produces  $H_2$  and  $O_2$ . In fact, water electrolysis appears to be the best option to deal with the transient electrical power profiles of renewables. The resulting hydrogen is indicated as renewable power hydrogen (RPH) and it can be used directly in applications pertaining to  $H_2$  or upgraded through further processing.
- A *methanation process device*: the methanation process consists in the production of methane or SNG by using  $H_2$  and  $CO_2$  (or  $CO$ )<sup>5</sup> as input and the releasing of a consistent amount of heat. The final product resulting from the methanation of the produced RPH is called renewable power methane (RPM). This is regarded as the direct substitute of conventional natural gas and, as such, it can be used in the same applications without the limitations associated to  $H_2$  usage. Other positive aspects of RPM production are the possibility of processing  $CO_2$  to avoid its release into the atmosphere and the recovering of heat to be used for industrial purposes.

A *source of  $CO_2$* :  $CO_2$  is necessary for the methanation step and must be provided through efficient and cost-effective means, ideally with high purity and a controllable flow rate to follow the fluctuating demand. Possible  $CO_2$  sources are [3,4,9]:

- $CO_2$  from fossil power plants, obtained by means of Carbon Capture (CC) technologies;
  - $CO_2$  from biomass, derived through the processes of fermentation, gasification and combustion;
  - $CO_2$  from industrial processes, obtained as a byproduct;
  - $CO_2$  from air.
- *Storage facilities*. These are proper containers added to the plant in order to store the gases involved in the process ( $H_2$ ,  $CO_2$  and SNG).

---

<sup>5</sup> Also  $CO$  can be used as a reactant together with  $H_2$  to obtain methane, if a source of  $CO$  exists (the methanation process requires a step less).



## GAS

Three alternative pathways for the final gas, either RPH or RPM, are currently being considered:

- Direct feed-in of RPH into the existing NG grid;
- Feed-in of RPM into the existing NG grid;
- Utilization of RPH in a dedicated infrastructure for each hydrogen application (such as fuelling stations for hydrogen-based vehicles, storing facilities for industrial processes).

Regarding the option of direct RPH feed-in, the maximum allowable  $H_2$  concentration is limited in order to assure the safe operation of distribution infrastructures originally designed for natural gas. On the other hand, by considering the solution of further processing the produced RPH, the feed-in of obtained RPM into the natural gas grid would be possible in unlimited quantities. In this regard, current research is aimed at investigating and comparing the various alternatives on the basis of efficiency and economics criteria [4].

### 1.3.1.2 Conversion Gas-to-Power

The reverse concept of Gas-to-Power allows to transform gas back to electricity and to close the energy loop, which can then be regarded as a fully reversible energy storage device. In times of positive residual loads, when power production from renewables is lower than the load demand, GtP facilities use gas (either hydrogen or SNG) to generate electricity and compensate for the difference. Specifically, fuel cells are employed to generate electricity from pure hydrogen. GtP facilities can also include natural-gas-based power plants, such as Combined-Cycle Gas Turbine (CCGT), Open-Cycle Gas Turbine (OCGT) or Internal Combustion Engine (ICE) power plants. These facilities use the gaseous fuel from the public gas network to produce mechanical power that in turn drives an alternator and produce electricity [2,3,6].

## 1.4 Electrical aspects of PtG

### 1.4.1 Requirements of electrolyzers for PtG applications

The listed parts of the PtG system need a certain amount of power for working and this is taken from the electrical grid to which they are connected. To this extent, the different devices composing the PtG plant have a direct impact on the operation of the electrical network. Specifically, electrolyser,  $CO_2$  production, and  $H_2$  compression/storage can be considered the most power consuming. Among these, the most important role is played by the electrolysis system since, thanks to its controllability, it can adapt the power consumption in order to participate actively in the operation of the system.

Therefore, electrolyzers for PtG applications have the following specific requirements [3,4]:

- High efficiency, to minimize the energy losses
- Highly dynamic behavior, to follow the fluctuations of power input from renewables
- Extremely low minimum load, to enable stand-by mode with nearly zero energy consumption
- Low capital costs and long lifetime, to allow for cost-effective hydrogen production

- Additional possibility to produce compressed hydrogen, to reduce energy demand and investment costs for compressors

#### 1.4.1.1 Alkaline electrolyser

Some issues associated with the application of alkaline electrolyzers in a PtG system concern:

- Dynamic behavior:
  - Transient operation is possible with this technology, but the dynamics is slower than that of PEM electrolyzers due to the higher inertia of the cell. Nevertheless, the maximum ramping rate equal to about 10%  $P_N$ /s results in a typical response time of seconds or minutes, which is considered to be sufficient for grid applications.
  - The cold and hot start-up are relatively long. The starting time ranges from 10 min to few h mainly depending on the purity of the final gas, while the restarting time after shutdown lie in the range 30–60 min due to the necessary purging operations.
- The minimum load: the minimal load capability is usually limited within the range 10÷40%  $P_N$ , due to gas conductivity issues of the diaphragm for low gas flows. It follows that, if the input power falls below the critical value, the electrolyser has to be switched off.

The investment costs of large-scale units are estimated to be about 1000 €/kW and projected to drop to about 500-600 €/kW in the near future [3,4].

#### 1.4.1.2 PEM electrolyser

In the context of PtG concepts, PEM electrolyzers presents several advantages, in regard to:

- Dynamic behavior:
  - The complete ramping up and down is possible in only few seconds, so that, in contrast to alkaline electrolyzers, these devices are well-suited to highly dynamic applications in the electrical network and operation with transient power loads.
  - Multiple power on/off cycles can be sustained and a cold start-up can be completed in just few minutes, leading to a higher flexibility in comparison to alkaline technology.
- Minimum load: a very low partial load of 0-5%  $P_N$  is allowed due to the impermeability of the membrane to the gaseous components. This means that the unit is able to work in the 0÷100% control range, much wider than that of alkaline devices.

For all these reasons, PEM electrolyzers are well-adapted and the well-suited to be coupled with intermittent renewable energy sources, such as solar and wind. Moreover, PEM electrolyzers offer the additional advantage to perform pressurized water electrolysis for directly supplying compressed hydrogen at the requested pressure value (potentially up to 100 bar). In fact, the PEM cell is designed to enable the operation under elevated pressure differences between the electrodes and to produce high-pressure hydrogen without significant extra energy costs compared to atmospheric water electrolysis. This feature allows for saving on the capital and operational cost for compression.

Nevertheless, the major issue and key barrier of this technology is related to the cost of the unit itself. In spite of an acceptable durability, PEM cells are still rather expensive due to the required noble materials used as catalysts.

The current investment costs are valued around 2000 €/kW, but a potential cost reduction to 500 €/kW is expected in case alternative materials would be used and efficiency would be improved by upscaling effects [3,4].

For the sake of completeness, a comparison between the main characteristics of alkaline and PEM electrolyzers in the context of PtG applications is shown in Table 2.

Tab. 2 – Comparison of characteristics of alkaline and PEM electrolyzers in the context of PtG [3,4]

Type	Cold start-up time	Hot start-up time (from stand-by)	Load change [%P <sub>N</sub> /s]	Minimum load [%P <sub>N</sub> ]	Cost [€/kW]
Alkaline	min to h	s to min	<10	10÷40	≈1000
PEM	min	s	10÷100	0÷5	≈2000

### 1.4.2 PtG applications in the electrical system

In order to further explore the aspects related to the connection and potential impact of PtG facilities on the electrical system, a schematic overview on the function carried out in the different sectors constituting the electrical power industry is provided. This vision includes current solutions and perspective applications to the generation, transmission, distribution and utilization of electricity (Figure 7) and is important to envisage how PtG technology can be effectively deployed in the present and future electricity system [3,6].

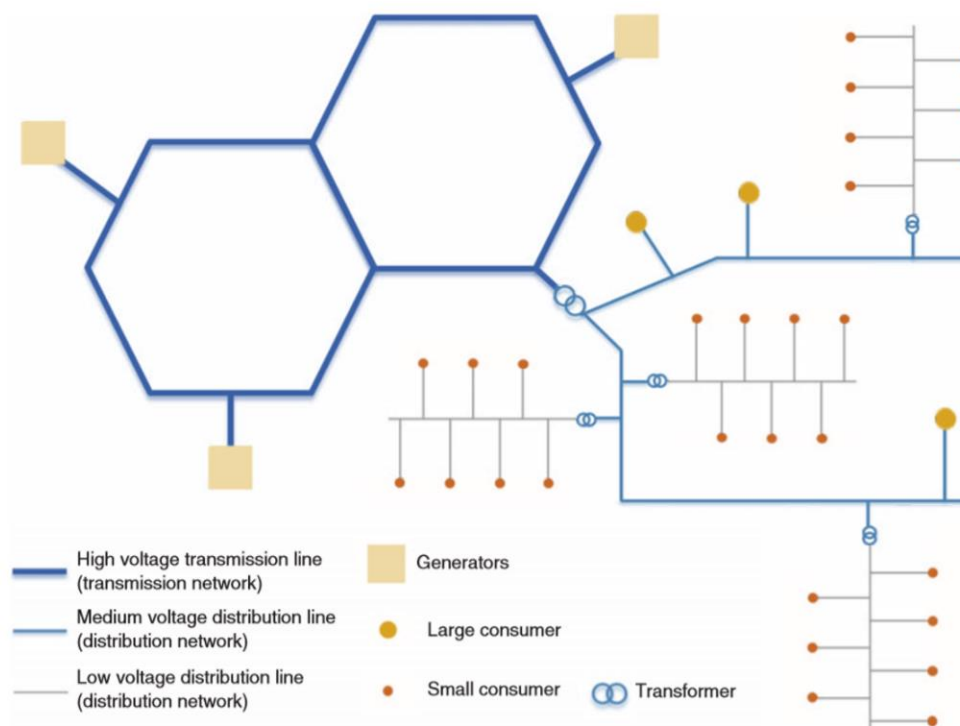


Fig. 7 – Illustration of the electrical network structure

#### 1.4.2.1 Generation side

On the generation side, a differentiation is made between dispatchable and non-dispatchable power plants. The former includes plants with controllable generators (such as based on fossil, hydro and nuclear primary energy sources) while the latter involves non-controllable generators (mainly RES-based). The benefits that come with the application of PtG in both cases regard a more efficient and cost-effective utilization of the plant.

##### *DISPATCHABLE UNITS*

The application of PtG to dispatchable plants concern:

- *Additional flexibility*, which the link between gas and electricity can provide to the plant, in terms of production control purposes or provision of reserve services. For instance, the integration of PtG facilities can contribute to keep the production profile of nuclear and fossil fuel power plants as flat as possible or to reduce the mismatch between real and scheduled production of RES-based and CHP plants. A further advantage is that the heat recovery from methanation can be used for pre-heating in steam or gas-fired plants.
- *Arbitrage opportunity*, owing to the introduction of energy-shifting possibilities between electricity and gas in a system that may be supplied either by power or fuel. This must involve a careful economic assessment of the provision of services and the costs of selling and purchasing both energy vectors.
- *CO<sub>2</sub> emission reduction*, because of the possibility to employ the carbon dioxide resulting as a byproduct of the plant for the process of methanation. This leads to a more viable production from both environmental and economical point of view, by offering the opportunity to participate to greenhouse gas emission allowance trading in energy-related markets.

##### *NON-DISPATCHABLE UNITS*

On the other hand, the application of PtG to non-dispatchable plants can lead to:

- *Reduction of renewable energy curtailment*, due to the electricity storage function provided by the conversion of electricity into gas during peak power production periods. This allows to increase the plant load factor, leading to improvements in economy and efficiency.
- *Introduction of an integrated energy system* based on renewable energy, thanks to the improvement of the dispatchability of renewable sources. The gas-electricity integration facilities can help in shaping the intermittency and enhancing the inertia of renewable energy sources. In this sense, they may be able to increase the penetration level of renewables, simultaneously ensuring the reliability of the electrical system.

#### 1.4.2.2 Transmission side

On the transmission side, the applications of PtG can be distinguished in ancillary services, energy storage and RES integration, system management.

##### *ANCILLARY SERVICES*

Ancillary services consist in a variety of operations beyond generation and transmission, necessary to support the operation and assure the reliability of the transmission network in

terms of stability and security. These services can be categorized according to their duration in very short (from few ms to 5 min), short (from 5 min to 1 h), intermediate (from 1 h to 3 days) and long (seasonal). The possibility for the PtG plant to provide ancillary services of any duration is directly connected to the performance of the electrolyser in terms of electrical response. In particular, the applications for which PtG has proven to be most suitable are:

- *Spinning reserve* (short), consisting in a generator that is already online and can rapidly be dispatched to respond to a fast change in demand and ensure the balance between energy generated and load required. PtG shows characteristics suitable for the substitution of conventional power plants in spinning reserve operations and black starting of offline generators.

- *Frequency and voltage regulation* (very short), referring to the task of maintaining grid frequency and voltage within specific ranges. This task is becoming more difficult because the increasing power injection from renewables into the electrical network impacts on the voltage profiles and, leading to mismatch between production and consumption at grid level, causes variations of the system frequency. PtG has the potential to solve these technical issues acting as a RES production filter.

In addition, the characteristics of PtG are adapted for:

- *Load following and load levelling* (intermediate) – services provided to shape load and generation profiles in order to, respectively, make them match or make the load as uniform as possible.

- *Unit commitment* (intermediate) – service aimed at covering the mismatch between the forecasted and actual renewable production that may result from unforeseen weather conditions.

#### *BULK ENERGY STORAGE AND RES INTEGRATION*

PtG appears to be a suitable solution for energy storage, in particular on long-term basis (seasonal). As such, this technology can be used to shift power profiles in time in order to balance the power grid and reduce the network congestion time. This results in a general improvement of the network flexibility, which represents a key factor for the integration of RES in the electrical system and the prospective achievement of a 100% renewable energy-based system.

#### *SYSTEM MANAGEMENT*

PtG technology is a conversion asset able to create a link between the sectors of electricity and heating. The integration between the two systems would allow to simultaneously manage the two main infrastructures of transmission system and gas network on the basis of joint technical and economic assessments. The major results would be the alleviation of both gas and electricity networks congestion caused by transfer limits, as well as the modification of gas and electricity prices in accordance to market trends.

#### **1.4.2.3 Distribution side**

On the distribution side, many problems are arising due to the gradual increase of renewable energy-based plants that, because of their small-medium size, are being connected to the distribution network. Therefore, the distribution system is changing from the traditional

passive network (where active power was received from a single supply point and transported downstream to the customers) into an active network (where the distributed energy resources introduce multiple additional power inputs). This is altering the way distribution systems are operating, requiring the application of PtG as a possible solution, specifically, for voltage control and network upgrade deferral. In addition, PtG can be used for the management of the system in synergy with other sectors.

#### *VOLTAGE CONTROL*

Up to now, the control of the electrical system has been focused more on the transmission system than on the distribution system, due to their different structure and purposes. However, the strategy for the operation of the distribution network is changing, moving towards an active control approach. In this regard, PtG can help to actively control the voltage and maintain it within its operational range.

#### *NETWORK UPGRADE DEFERRAL*

The introduction of distributed energy sources and following increase in power injection at the final nodes of the feeders are causing problems related to the inversion of power flow (as active and reactive power start flowing backwards along the feeder when production is higher than load consumption). This all leads to the necessity of expensive interventions for upgrading the protective schemes, substituting transformers and improving the measuring system. Moreover, the increasing power injection of DER causes distribution network congestions and the consequent need of interventions for extending the network. In this regard, PtG can help in delaying the necessity for structural measures and avoiding related investments.

#### *SYSTEM MANAGEMENT*

In the same way as for the transmission system, PtG can play the role of coupling facility between the electrical and gas network also at distribution level, where the conversion can be guaranteed by using PtG facilities and gas turbines of smaller size. The optimal management of the integrated system would likewise lead to improvements in the operation of both networks.

#### **1.4.2.4 Utilization side**

On the utilization side, PtG applications can be divided according to the size in small, medium, and large scale applications.

- *Small size* applications include private or semi-detached houses, installing small PtG plants to produce gas for heating and hot water usage or for sale.
- *Medium size* applications indicate the integration of PtG facilities with small CHP plants, supplying blocks of apartment buildings.
- *Large size* applications refer to the installation of PtG facilities in large industrial or commercial sites, either for integration with large-scale CHP plants or for production of car fuel.

Generally, the integration of PtG in a local energy system contributes to the extension of the idea of electricity prosumer to the more general concept of global energy prosumer. While an electricity prosumer is both a producer and a consumer of electrical energy, the global

prosumer identifies an entity capable to operate multi-energy facilities in a coordinated way. It represents a key figure in the context of a rational energy management.

### 1.4.3 Configurations for hydrogen-electricity integration

For the purpose of PtG application at the utilization side, different configurations integrating hydrogen production with renewable energy sources in a local energy system are possible. Besides the two main parts represented by electrolyser and renewable source, some additional components are needed depending on the considered application and the function it is aimed at. In general, these components are the following ones:

- A *local or remote H<sub>2</sub> user*, to feed with the produced hydrogen;
- A *hydrogen storage system*, to act as a buffer for the local user or to store and transport hydrogen to remote locations;
- A *fuel cell system*, to generate electricity back from stored hydrogen;
- A *connection to the electric grid*, to allow the integrated system to withdraw and inject energy as needed;
- A *short-term electricity storage system* (such as batteries), to assist the system during transient operations and facilitate the absorption of fast power changes;
- A *power conditioning, management and control system* (power converter with DC/DC stage for PV panels and AC/DC or DC/DC for wind turbines), to support power transient and control the energy flow between all the system components;
- An *electrical load* to be satisfied.

The various configurations for H<sub>2</sub>-RES integration can be basically divided into off-grid (or autonomous) and grid-connected applications.

#### 1.4.3.1 Off-grid applications

This option is mainly applied in case the grid is not accessible and implies the electrolyser and renewable energy source to work autonomously without connection to the electrical network. The main off-grid configurations are below introduced.

If the purpose is hydrogen production for local or remote use, the scheme to be realized is presented in Figure 8. The electrolyser is directly supplied by the renewable source, leading to the production of completely renewable hydrogen, which can either be used locally in a variety of applications or transported to remote utilization sites. However, the direct connection would expose the electrolyser to power variations due to the transient renewable energy supply. As most of the commercial electrolysis units are not designed for highly dynamic operations, a power converter and a battery bank must be added to the system to deal with fast power transience.

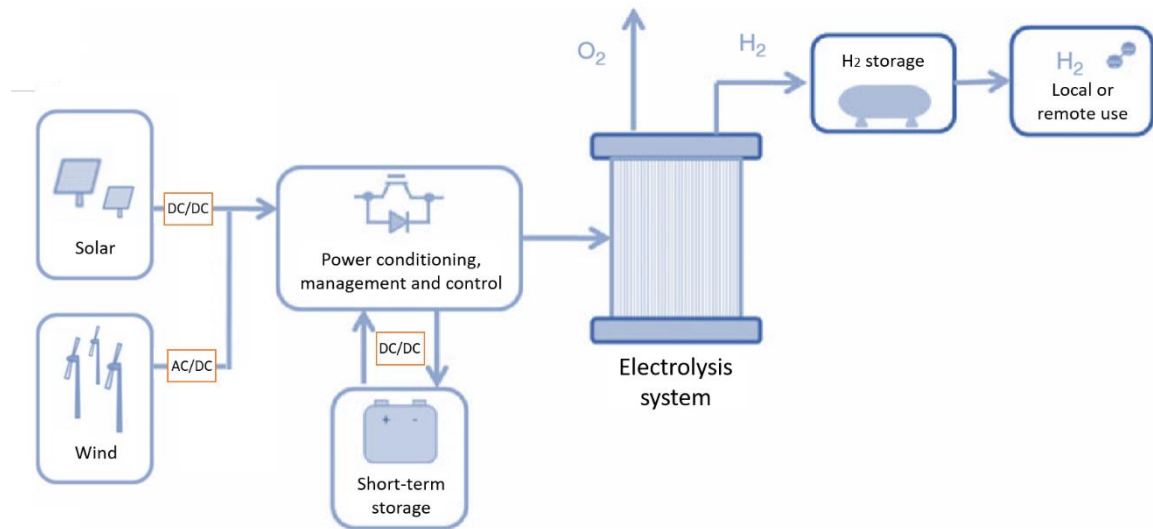


Fig. 8 – Grid-independent hydrogen production system

If the purpose is the electricity production to supply a local load, hydrogen can be used as a storage for the excess of electrical energy and, in accordance, the previous scheme is modified as depicted in Figure 9. In this case, when renewable source overproduction occurs, the electrolyser can turn the excess of energy into hydrogen in order to be stored. Conversely, when underproduction occurs (due to weather conditions or at night), the stored hydrogen can be used in a fuel cell to generate electricity back and fill up the gap. In this way, this stand-alone power supply system ensures the availability of electricity for satisfying the load and, in addition, allows to use the produced hydrogen for other end uses.

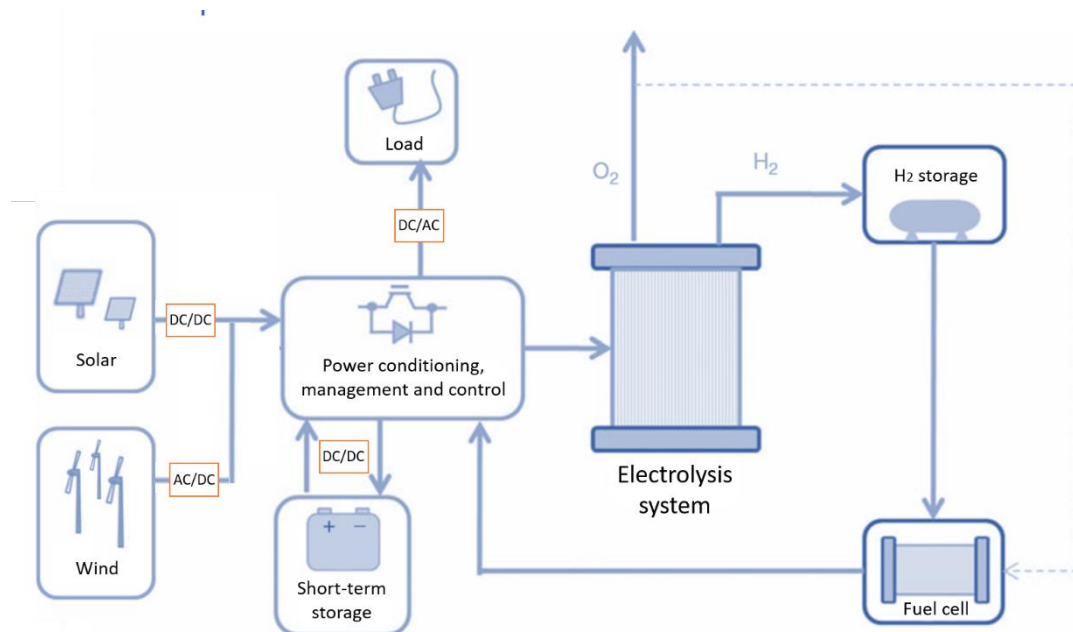


Fig. 9 – Grid-independent integrated energy system with hydrogen as renewable energy storage



### 1.4.3.2 Grid-connected applications

In this case, the access to the grid is available so that electrolyser and renewable source are connected, respectively, for power consumption and power injection. The major grid-connected configurations are summarized as follows.

When the final objective is the production of hydrogen, the grid-assisted scheme in Figure 10 represents an alternative to the previous grid-independent. In this case, intermittent operation is avoided by combining the renewable energy with the electricity supplied from the grid so that the electrolyser can be operated at the desired load. Specifically, when renewable power is higher than the needed electrolysis power, the electrolyser is only supplied by the renewable source. In contrast, when renewable power is lower, the missing amount is withdrawn from the electrical grid.

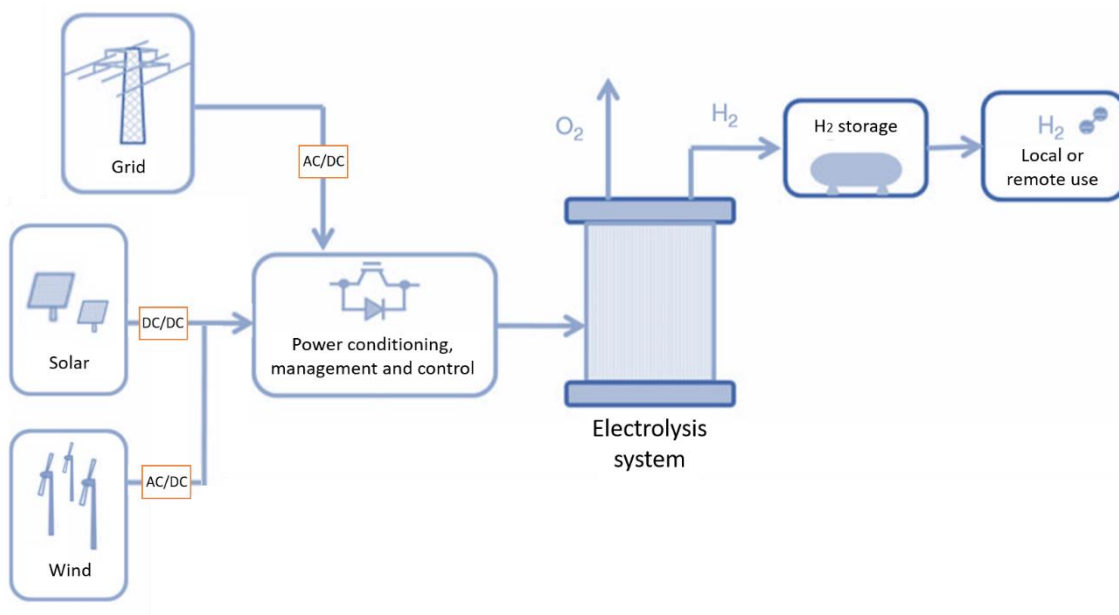


Fig. 10 – Grid-assisted hydrogen production system

In order to reduce renewable energy curtailment and to enhance the integration of renewable energy sources in the electrical system, a possible solution is to apply the configuration schematized in Figure 11. When the power produced by the renewable source cannot be absorbed by the grid due to grid congestion problems or to a low electrical energy demand, the strategy is to turn the excess into hydrogen by means of the electrolyser (renewable energy peak shaving). On the contrary, supposing that the grid is always able to absorb the entire renewable power production, an alternative approach consists in operating the electrolyser at constant power and injecting the surplus into the grid (base-load consumption).

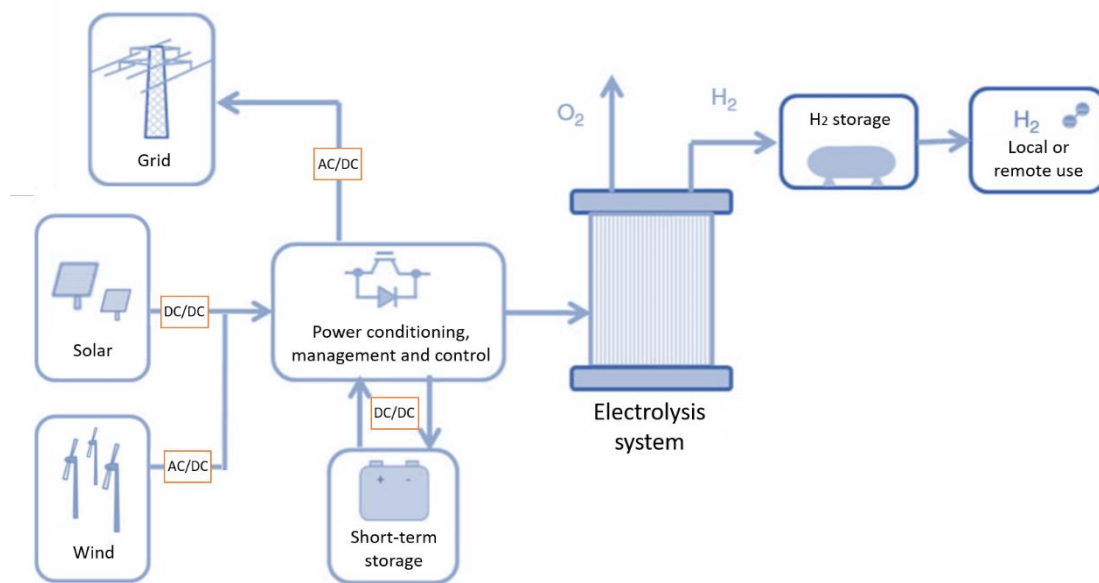


Fig. 11 – Grid-connected system with hydrogen as renewable energy storage

At last, the so-called hydrogen energy chain represented in Figure 12 is the most complete configuration, realized by combining all the above listed component. This integrated energy system can be used to improve the grid operation by helping to reach the instantaneous balance between power generation and consumption as well as to supply the local electrical load with a pre-determined energy pattern. In fact, by applying a proper control strategy to the direct and inverse hydrogen-electricity conversion, it is possible to inject the desired power profile into the grid or into any electrical load. The main drawback of employing a hydrogen chain as an energy storage means is the relatively low overall efficiency (25–35%, hydrogen compression excluded).

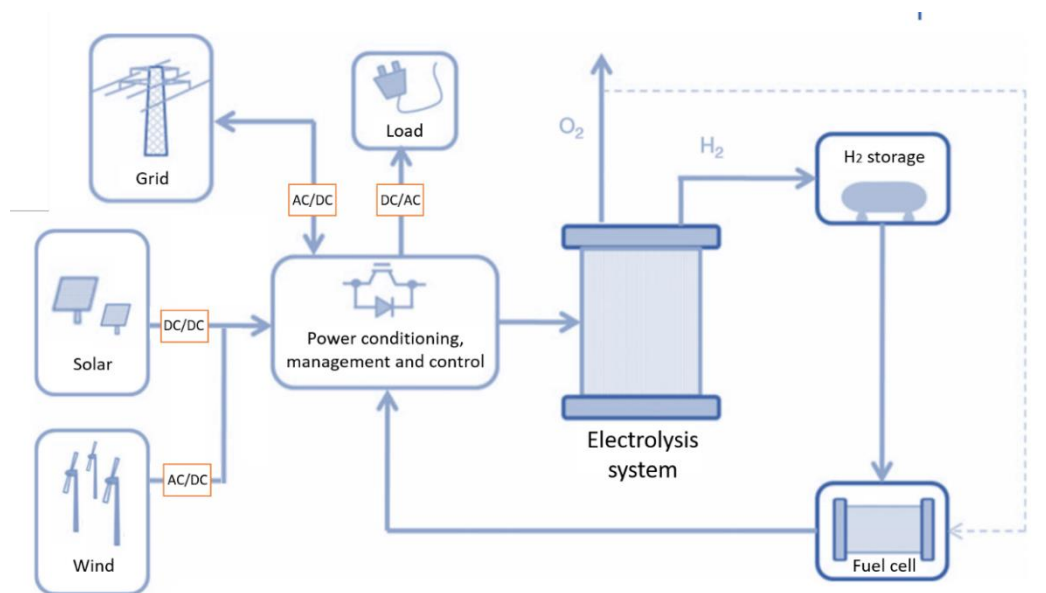


Fig. 12 – Grid-connected integrated energy system (or hydrogen energy chain)

For a complete description of the various configurations and examples of actual demonstration plants see [2].

# Chapter 2

## Groningen laboratory setup

### 2.1 Aim of the laboratory

The Real-Time Micro-Grid Lab, situated at the Energy Transition Center (Entrance) building of the Hanze University of Applied Sciences (Groningen, the Netherlands), is a test site that has been designed and built for the purpose of PtG grid integration experiments in the context of the STORE&GO project [34]. The laboratory setup comprises new energy transition sources and all the additional components necessary to investigate the integration of hydrogen production by water electrolysis with renewable energy sources (Figure 13). The research method is based on the characterization of these sources, comprising electrolyser, PV panels, wind turbines, fuel cells, and others, through the acquisition of appropriate data in order to produce mathematical models based on the real-time and dynamic measurements.

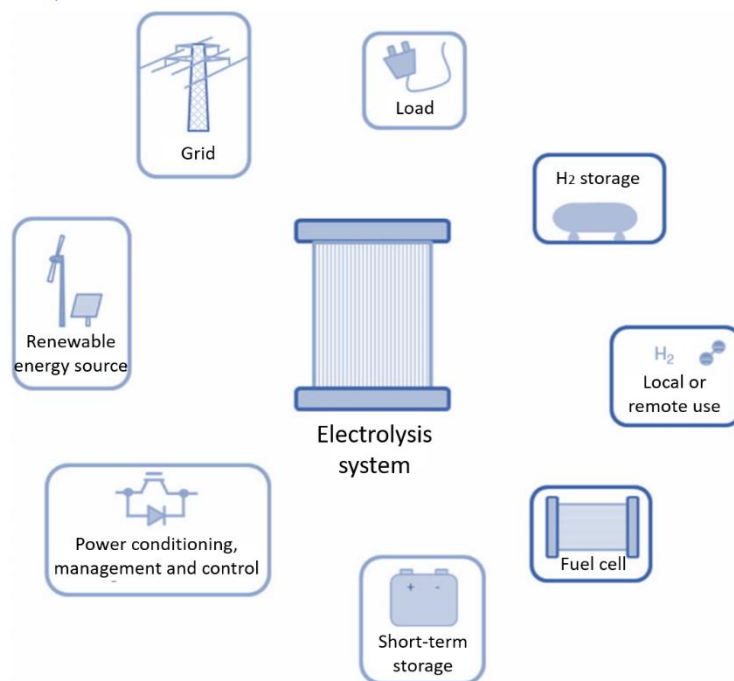


Fig. 13 – Components for the integration hydrogen production-renewable energy sources

Another important aspect is that the complete setup has now been configured to be accessible through a low latency data connection by remote use. This allows to establish a communication between the Micro-Grid Lab and the Global Real-Time Simulation Lab (G-RTSLab) located at the Politecnico di Torino. In this way, the laboratory equipment in Groningen can be accessed from Turin for the purpose to remotely collect real-time data to merge into large-scale grid models and with the final aim to realize a distributed real-time co-simulation.

## 2.2 Overview of the facilities at Entrance's demonstration site

The Real-Time Micro-Grid Lab is located into the cabin C6 of the Entrance demonstration site. A picture of the inside of the cabin is shown in Figure 14.



Fig. 14 – Picture of the Entrance Micro-Grid Lab

The laboratory setup is modular in design and realization. It follows that the various subsystems and both the physical and virtual connections between them can be represented schematically as in Figure 15. The different components appearing in the scheme are briefly presented below.

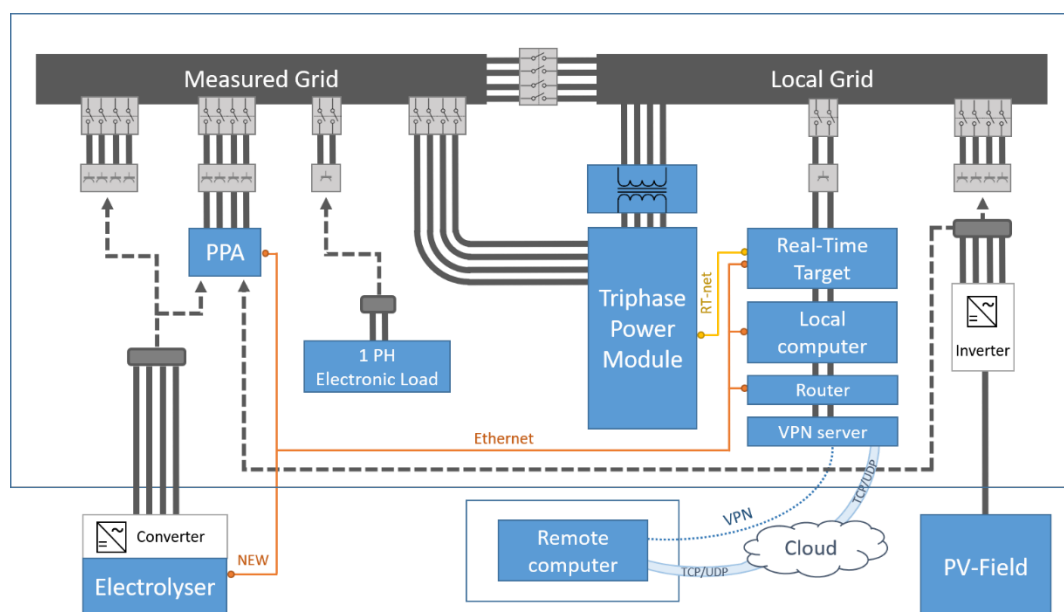


Fig. 15 – Schematic of the Entrance's Micro-Grid Lab setup

## 2.2.1 Physical components

### *GRID*

In the lab environment, two portions of grid can be distinguished: the one called *local grid* is the part that supply the Micro-Grid Lab directly from the main external grid; the one called *measured grid* is a main-grid independent and galvanic separated grid, which thus constitutes the primary component of the micro-grid itself.

The measured grid is configured as a three-phase with neutral conductor (3PH+N) and is functionally equivalent to the most common European three-phase AC networks. The setup is fitted with a locked switch to bypass the local grid to the micro-grid environment. After closing this switch, it is possible to connect energy sources or loads > 15 kW so that they can send energy to or use and store energy from the local grid. Connections of the single subsystems to both local and measured grid are safely realized through interconnected junction boxes.

### *ENERGY TRANSITION SOURCES: ELECTROLYSER AND PV PANELS*

The energy transition sources already installed at the Micro-Grid simulation site are a small industrial electrolyser and a PV installation. Both can be connected to the micro-grid environment through outside wiring.

The electrolyser is supplied by DC power, so that the unit must include an AC/DC converter. The entire electrolysis subsystem can be connected to the internal grid either directly or through the power analyzer, which allows power consumption and other electrical variables on the AC side to be measured.

The PV installation is equipped with a three-phase inverter to transform the generated DC power into AC. Similarly to the electrolyser, the inverter can be connected to the measured grid through the power analyzer, so that the power production and all the related electrical variables can be monitored and logged. Otherwise, by connecting the inverter to the local grid, the power production is sent directly into the electrical network.

It is important to notice that the current setup allows only one between electrolyser and PV-field to be monitored by the power analyzer at a time. It follows that, if both energy transition sources are intended to be operated at the same time, the connection options are:

- electrolyser connected to the internal grid through the power analyzer and its power input measured; PV-field off-line or connected to the external grid and its power output sent into the electrical network;
- PV-field connected to the internal grid through the power analyzer and its power output measured; electrolyser shut down or connected to the internal grid directly.

The specifications of the electrolyser system and PV-field are fully presented in the following section 2.3, which is focused on the devices characterization. Details on the electrical behavior of, respectively, PV panels and electrolyser unit will be provided in the following Chapters 3 and 4, which are entirely dedicated to their modelling.

## *ELECTRONIC LOAD*

The setup also includes the possibility to connect a single phase electronic load. This can be switched to either of the three-phase conductors and create a programmed load pattern in order to test individual phase reactions or achieve a predefined unbalance in the three phases.

## *TRIPHASE*

To achieve a controlled grid voltage and frequency, a Triphase Distributed Power System (DPS) is used. This has the ability to realize a scalable, flexible and open platform for rapid prototyping of power conversion and power system applications or for Power-Hardware-In-the-Loop testing. With this system a complete controlled micro-grid can be obtained.

The DPS product includes a 15 kW bidirectional isolated Power Module (PM), suited for bidirectional energy flow between the grid and DC or single/three-phase AC loads and sources. The module incorporates power amplifiers, power converters, sensors, connection contactors, safety features and signal processing units. This setup can be interfaced through software libraries that come with the DPS product for a high-end real-time control. In this way, the system can be configured either as voltage source/generator or as current source/load, and controlled with a specific pattern, harmonic signature, independent phase shift angle, etc. This is possible by switching over the numerous internal switches with many inductive and capacitive configurable components under the law of Virtual Circuit Control. Theoretical basis on the Triphase PM structure, functioning and control law can be found in [10-13].

As an example, by configuring the Triphase PM as programmable voltage source, it is possible to simulate the main grid generator. Its voltage can be controlled in terms of amplitude, phase, frequency and harmonic content, with the purpose to analyze the consequent behavior of the devices connected to the internal grid. On the other hand, when the Triphase PM is configured as current source, it is possible to simulate a preprogrammed load with the aim of analyzing what is needed to suppress a certain grid disturbance. For instance, when a device connected to the internal grid creates a capacitive phase shift, the virtual model can be controlled to simulate an inductive load able to fully compensate the disturbance.

## 2.2.2 Virtual connections

### *ETHERNET AND REAL-TIME NETWORKS*

The LAN of the laboratory is made up by a router directly connected to the internet backbone of the Hanze's datacenter. This provides a high-speed and reliable Ethernet connection, with a speed of 1 GB/sec and a latency lower than 50 ms. Within the laboratory environment, the LAN encompasses the following devices: local engineering PC, Real-Time Target and power analyzer. Ethernet connection is by definition based on a TCP/IP protocol [14], thus each interconnected device has to be provided with its own IP address, assigned within a certain range identifying the LAN.

Furthermore, for virtual operation the Triphase PM is connected over a real-time communication bus, indicated as XC Real-Time Network, to its powerful PC-based real-time control unit. This Real-Time Target (RTT) has the task to run the models for all kind of customized sources or loads in real-time. The models are first implemented on the engineering workstation and then sent to the RTT over Ethernet connection.

In general, with the described network setup: the Triphase models can be sent from the local computer to the RTT and then to the Triphase PM; the devices connected to the internal grid can be real-time monitored by the power analyzer while the data can be accessed and logged by the local computer.

In addition, a new Ethernet line connecting the electrolyser subsystem with the internal lab environment has been constructed within the time frame of this work. Now the local computer can access the measurements related to the hydrogen production process and performed by sensors inside the electrolyser cabin, up to now accessible only on site via serial connection. Also some start-up and shut down automated operations can now be carried out from the engineering workstation, of course after the unit has been manually prepared to be operated. Previously, in contrast, all the steps to start-up and shut down the system had to be carried out manually on site.

### *VPN COMMUNICATION*

To the described network topology, a server has been added to make up a connection over the Internet with the remote computer in Turin and allow the communication of the two laboratories with each other. Specifically, the server task is to forward data between the remote instances, drop invalid packets, collect statistics of the communication link and run other arbitrary operations on the sent and received data if required. The protocol used by this device for exchanging data is the User Datagram Protocol (UDP).

For the sake of security, the communication is realized via a Virtual Private Network (VPN) tunnel. The solution is based on the open source VPN software called OpenVPN, which is able to establish a completely decentralized virtual network on top of the Internet and enable point-to-point data exchange. This method is fundamental to protect all data and equipment against undesired use.

More details on the VPN communication between the two laboratories for the creation of the multi-lab setup and implementation of the related experiments can be found in the dedicated Chapter 5.

### *5G NETWORK*

Concerning the virtual connections, it is also worth to mention a current test aimed at using a 5G low latency network to remotely monitor renewable sources like the PV resources present on site and wind turbines located in a neighbor test site. The PV-field connected to the lab setup is already monitored through an energy meter and a pyranometer, while the related data of instantaneous produced power and solar irradiance are saved on a cloud storage. This can be accessed through a private Hanze account via website or by means of a smartphone app. Moreover, in the near future, a real-time connection to a new high-power wind generator close by will be established in collaboration with Entrance 5G Research Lab. The generated energy will be measured on site and the collected data will be delivered to the lab via the low latency 5G network.

## 2.3 Focus on the devices used for the experiments

### 2.3.1 Power analyzer: electrical measurements

#### 2.3.1.1 Power analyzer characteristics

In order to measure the power consumption or generation of the connected resource, the laboratory setup is equipped with a power analyzer – model PPA1500, fabricated by Newtons4th Ltd. This is shown in Figure 16.

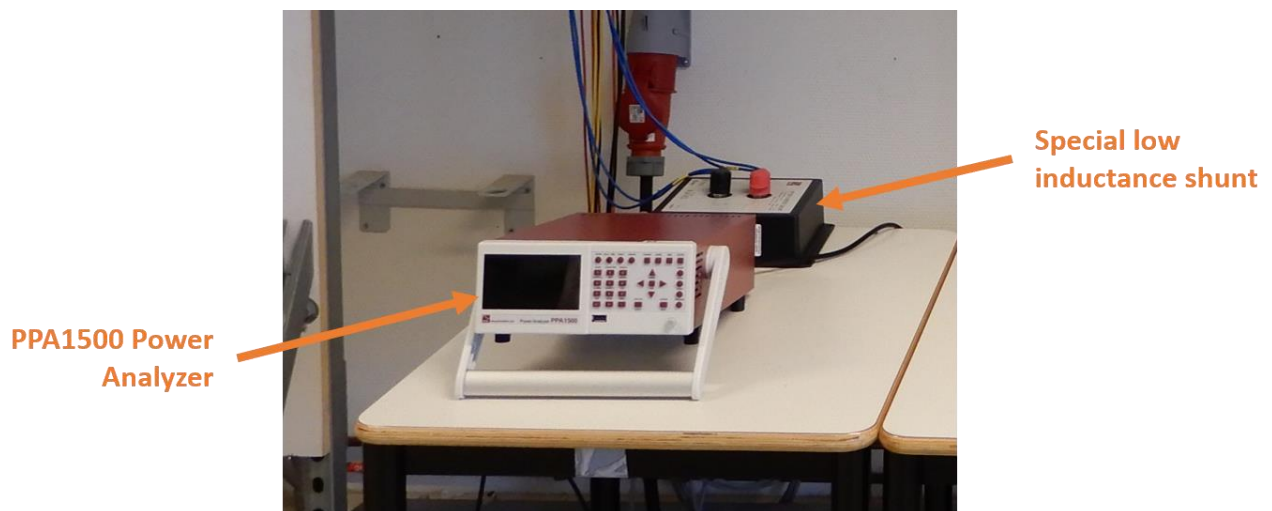


Fig. 16 – Picture of the N4L's PPA1500 power analyzer

This high-speed model has been selected because of its excellent properties in real-time analysis. It is capable to dynamically measure electrical parameters over all three phases, perform the harmonic analysis, compute the power factor and real RMS values, for a total of 60 data parameters logged in one time frame (the lowest being 1 ms according to the instrument specifications). The fundamental dynamic feature is that the data processing is carried out “on the fly”, thus continuously and in parallel over the three-phase conductors. The power analyzer internal structure, necessary for gaining such an accurate real-time measurement, is depicted in Figure 17.

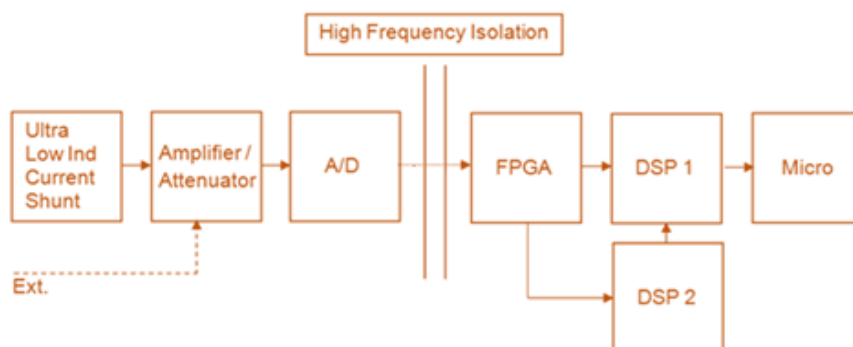


Fig. 17 – Analog input diagram of the PPA1500 power analyzer

This scheme includes six independent and galvanically separated measure channels for the three-phase voltage and current. Each channel contains an amplifier/attenuator and a high-speed high-resolution A/D converter. After passing through a high-frequency isolation buffer, the channels lead to a FPGA, followed by two independent digital signal processors (DSPs).



The instrument functioning is as follows. At first, the analyzer samples the voltage and current waveforms entering or exiting the channels, within a typical sampling time of  $0.5\mu\text{s}$ . Once sampled, the data is processed by the FPGA and the various required parameters are calculated by the DSPs within the same time frame. Specifically, DSP 1 is aimed at processing true RMS signals and other complex derivative signals, while DSP 2 is entirely dedicated to Fourier analysis of frequency and harmonics. The memory buffer is continually emptied as the samples are processed.

For the N4th PPA1500 instrument specifications and usage, see [15,16].

In addition, it is important to point out that a phase power imbalance was observed when analysing the electrolyser power data. This is due to the fact that the DC voltage required by the electrolytic process is rectified via a single phase only. Therefore, since the current consumption on this phase exceeds the  $30\text{ A}_{\text{RMS}}$  current limit reported by the instrument specifications, a  $100\text{ A}_{\text{RMS}}$  current shunt has been installed. This is a special shunt designed and optimised to have a flat response throughout the frequency range. The component is visible in Figure 16 behind the power analyzer.

### 2.3.1.2 Power analyzer software

The Newtons4th Ltd's power analyzer is provided by the company with two different software programs for setting configurations, reading measurements and logging data directly on the user's laptop, namely, PPA CommView and PPA DataLogger. In order to interface with the device, the former makes use of commands in the form of lines of code, which means that the user has to type functions in a specially designed programming language in order to execute the various operations. The latter, instead, is much more user friendly. It is fitted with a graphical interface designed to be very simple and intuitive. For these reasons, DataLogger has been adopted as the main reference software for the performed measurements. Specifically, it allows to connect the PC to the power analyzer via RS232, USB and LAN and comprises all measurement modes which reflect the instrument operating options. It also enables to export text files in CSV format or directly to Microsoft Excel.

Appendix A provides information on the individual features and options of this software which have been useful during the performed experiments. For further specifications on both the programs, refer to [17] for CommView and [18] for DataLogger.

## 2.3.2 Electrolyser: hydrogen production characterization

### 2.3.2.1 Electrolyser specifications

The electrolyser under study is a Proton Exchange Membrane (PEM) water electrolysis system of 8 kW. When supplied with power and deionized water it is capable of producing up to 1.05 Nm<sup>3</sup> of H<sub>2</sub> per hour with a continuous output stream. The electrolysis unit is depicted in Figure 18 while its specifications are summarized in Table 3.



Fig. 18 – Proton's Hogen40 PEM electrolyser

Tab. 3 – Proton's Hogen40 PEM electrolyser specifications

Proton Energy Systems, S-Series Hogen40 Hydrogen generator	
Supply Voltage	200-240 V <sub>AC</sub>
Number of Phases	1~
Full Load Current	44 A
Frequency	50/60 Hz
Hydrogen Product Rate	1.05 Nm <sup>3</sup> /h
Hydrogen Output Pressure	13.8 barg
Altitude	1520 m
Ambient Temperature	5 °C to 40 °C
DI Water Conductivity	>1 MΩ·cm
Installation	Indoor

### 2.3.2.2 Electrolyser structure and functioning

The unit is designed for indoor operation only, thus located in a container outside right next to the laboratory. A picture of the electrolyser cabin is visible in Figure 19.



Fig. 19 – Picture of the electrolyser container at the Entrance test site

The container consists of two separate rooms. One side houses the PLC and the water preparation system, where tap water is treated by means of a Reverse Osmosis (RO) unit and ion exchange filters to create suitable water for electrolysis (Figure 20). The deionized water then flows to the room on the other side where the electrolyser itself is situated (Figure 21). This room also houses a system of valves and two 5L storage cylinders for storing the produced hydrogen. The tanks can be emptied afterwards by venting the contained hydrogen outside. Produced hydrogen can also be directly vented during operation, without filling the tanks. The former production method will be further referred to as tanks filling mode, the latter as venting mode. A flow controller has been added at last to the setup to control the flow of hydrogen while vented to the outside air. For the sake of completeness, Figure 23 shows the PFD of the hydrogen production process as well as the position of the various elements along the pathway.

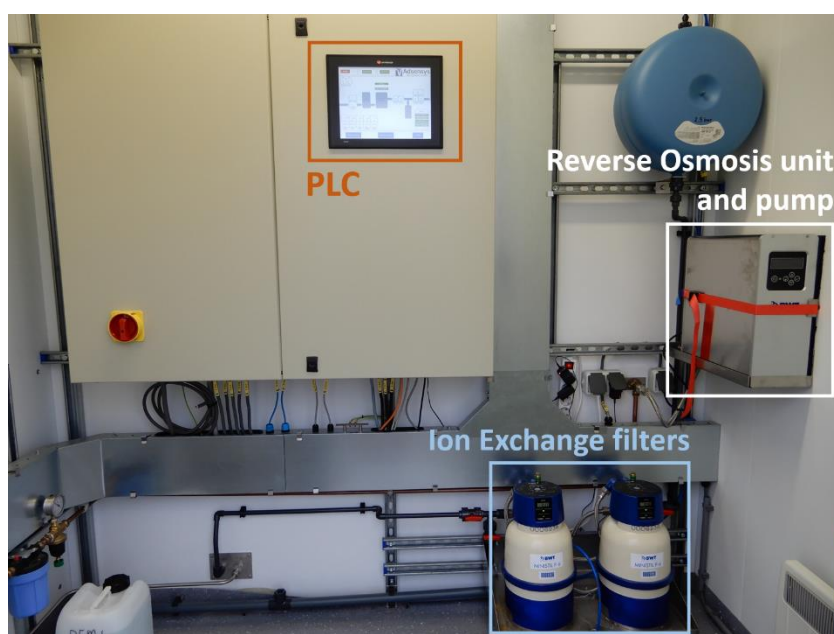


Fig. 20 – Picture of one side of the electrolyser cabin

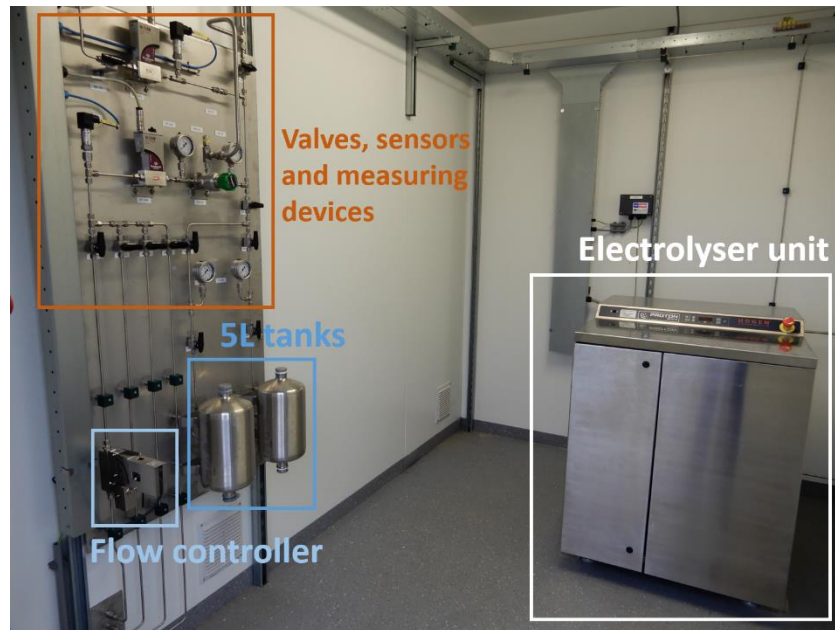


Fig. 21 – Picture of the other side of the electrolyser cabin

The electrolyser unit contains an electrolysis cell stack and auxiliary equipment, required for regulating electrolysis operations (circulating water, drying hydrogen, pressurizing hydrogen, performing safety operations and shutting down the system). The internal part of the unit and the functional elements included therein are illustrated in Figure 22.

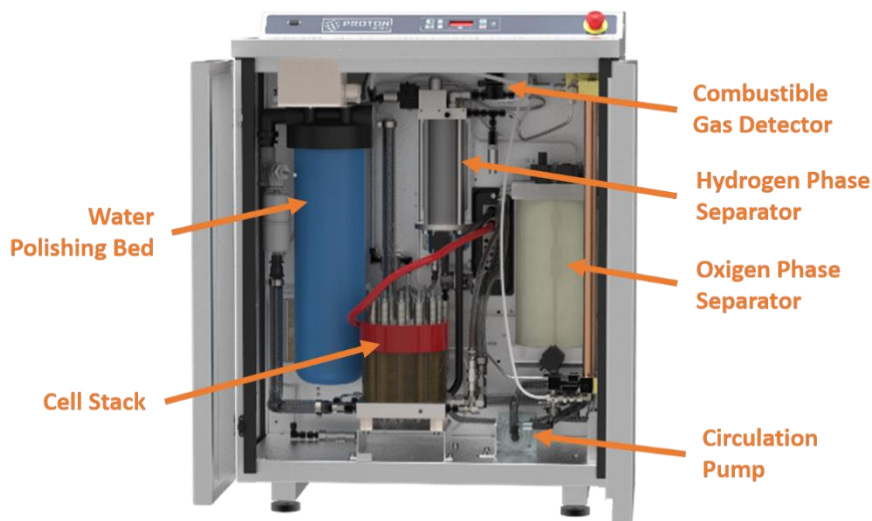


Fig. 22 – Inside of the Proton's Hogen40 PEM electrolyser

A control board and on-board sensors are also inside the unit for the sake of monitoring performance and automating operations<sup>6</sup>. Specifically, this control system deals with the automation of normal and security operations, by turning on and off auxiliary equipment (such as ventilation fans, circulation pumps etc.) when needed or shutting off the entire system if something goes wrong during the process.

<sup>6</sup> The sensors monitor system and process conditions whereas the regulator, along with proper transducers, controls the system operations accordingly.

The control also allows to regulate the H<sub>2</sub> production in accordance to the pressure set-points. The two set-points that can be set are:

- System pressure, which represents the H<sub>2</sub> pressure in the H<sub>2</sub> separator inside the unit;
- Product pressure, which represents the pressure of the H<sub>2</sub> flowing out of the system from the H<sub>2</sub> port.

For the sake of security, both of them are fixed and properly preset by a specialized technician to approximately 15 bar.

Briefly, the electrolysis unit is internally controlled and fully automated in every state and process. The operator only has to start the system up at the beginning and shut it down at the end of operation. Instructions on how to carry out these tasks are provided in the brief user's manual in Appendix B. Throughout the electrolyser start-up and functioning described therein, various operating states can be distinguished. The states definitions are given in the Proton's electrolyser manual [19] and, since an explanation is useful for the purpose of the electrolyser characterization, these are shortly introduced below:

- **PRE-START:** The state is initiated as soon as the main power switch is turned on. The system flushes itself out of water if water quality is below the required conductivity. Water levels in the two separators (oxygen/water and hydrogen/water) are adjusted if they are low. When the PRE-START operation is completed, it is possible to let the generator maintain this idle state or it can be started up bringing the system into next state.
- **GENERATE-VENT:** In this mode, the circulation pump is started up and the system verifies the process values of water flow rate and water quality. Full current is applied to the stack after 120 seconds and hydrogen generation is started. Now the system checks both separator levels, voltage conditions in the stack and rectifier operation, venting hydrogen and oxygen outside during this process. If the process values pass all checkpoints, the electrolyser will stop venting and start to build up pressure, leading to next state.
- **PRESSURIZE STORAGE:** In this state, the system pressure is increased up to the system pressure set-point while the hydrogen lines are pressurized up to the product pressure set-point. Once the set-point levels are reached, the process goes into steady-state.
- **STEADY-STATE:** The generator produces hydrogen that flows out of the system through the H<sub>2</sub> product port. Full flow of gas is produced when the system pressure is below its set-point and, similarly, full flow of gas is delivered when the product pressure is below the respective set-point. When the set-points are reached, the power used for hydrogen generation is switched off and the electrolyser remains in idle state. When the pressure drops below the set-points, the generator will deliver full gas production until it reaches the pressure set-points again.

A comment on the last operating state seems necessary. During steady-state, in fact, it has been observed that the described control influences the electrolyser behavior both in tanks filling mode and venting mode.

When producing in tanks filling mode, it has been noted that the tanks are not capable of storing H<sub>2</sub> for a long time but, due to leaks, the H<sub>2</sub> is continuously lost and dispersed into the air. It follows that, when the tanks are filled up completely, the product pressure reaches its set-point and the electrolyser stops the production. When the H<sub>2</sub> is lost, the product pressure drops and the electrolyser starts back to generate again.

During the performed measurements for the purpose of the electrolyser modelling, the H<sub>2</sub> was instead blown out to the outside air in order to simulate the H<sub>2</sub> load supply. In order to get the reduced load operation, the desired H<sub>2</sub> flow was obtained by manually acting on the valves on the tubes leading to the outside air. By closing the valves, the output pressure increases so that the product pressure is constantly kept around its set-point. It follows that during this state the electrolyser supply is switched on and off intermittently.

For more information about the electrolyser construction, specifications, installation, operation and maintenance refer to the manuals [19-21].

### 2.3.2.3 Electrolyser efficiency

The efficiency is an important parameter for characterizing the electrolyser performances. It reflects the difference in energy required for the actual process of hydrogen production with respect to the theoretical one.

The first cause of limitation of the electrolyser efficiency are the irreversibilities related to the real electrolysis reaction, mainly overvoltages and parasitic currents [2,22]. In fact, the actual voltage applied to the cell (i.e.  $V_{cell}$ ) must be considerably higher than the thermodynamic voltage (i.e. reversible cell voltage  $V_{rev}$  – the lowest voltage required for the electrolysis to take place) to overcome the losses and let a relevant current density flow across the cell. In particular, the electrolysis cell voltage  $V_{cell}$  can be expressed as the sum of the reversible voltage and the additional overvoltages appearing in the cell:

$$V_{cell} = V_{rev} + V_{ohm} + V_{act} + V_{con} \quad (1)$$

The various overvoltage terms in the formula have the following meaning:

- $V_{ohm}$  is the overvoltage caused by ohmic losses: it is due to the resistance of electrodes and other several cell elements to the electrons flow, as well as to the electric resistivity of the electrolyte.
- $V_{act}$  is the activation overvoltage: it is generated across the electrodes as a result of the energy barrier that the charges have to overcome to move across the electrodes and the reactants.
- $V_{con}$  is the concentration overvoltage: it is caused by the mass transport phenomena of convection and diffusion happening inside the cell.

Besides the losses occurring in the electrolysis process, other causes of non-ideality are the energy losses in the electric power supply and power electronic conversion. Furthermore, an additional energy consumption comes from the peripherals and auxiliary equipment included in a complete hydrogen production system (magnetic valves, microprocessors, sensors, electrolyte cooling systems, units for oxygen purification and moisture removing from the

generated hydrogen). At last, losses of hydrogen product have to be considered (such as the amount of hydrogen needed by purity sensors, leaking from valves or lost in the electrolyser water feeding system). All these causes of additional losses must be taken into account when calculating the global efficiency of the hydrogen production system.

Given these considerations, the electrolyser efficiency  $\eta_E$  can be expressed as the ratio between the energy content of the hydrogen generated and the amount of electrical energy required, considering either only the electrolysis process or the global hydrogen production system. Consequently,  $\eta_E$  can be easily calculated through the formula [22]:

$$\eta_E = \frac{HHV_{H_2}}{C_E} \cdot 100 \text{ [%]} \quad (2)$$

where,  $HHV_{H_2}$  is the hydrogen higher heating value, equal to 3.54 kWh/Nm<sup>3</sup> [23]  
 $C_E$  is the specific energy consumption, expressed in kWh/Nm<sup>3</sup>

The specific energy consumption relates the energy consumed to the hydrogen produced through the following formula:

$$C_E = \frac{P}{\dot{V}} \quad (3)$$

The terms appearing therein have different meaning depending on whether the electrolysis efficiency or the global one is considered:

In the former case,  $P = P_{DC}$  is the DC power applied to the stack [kW]

$\dot{V} = \dot{V}_{stack}$  is the ideal hydrogen production rate of the stack [Nm<sup>3</sup>/h]

In the latter case,  $P = P_{AC}$  is the total AC power applied to the entire system [kW]

$\dot{V} = \dot{V}_{syst}$  is the actual hydrogen flow rate, net of losses [Nm<sup>3</sup>/h]

The efficiency of the electrolyser under study is now calculated by making use of the formulas reported above. At first, the DC power applied to the stack is considered, so that the obtained result represents the efficiency of the stack only. Afterwards, the calculation is performed by considering the total AC power applied to the entire unit, thus the outcome is the overall system efficiency which also takes the AC/DC conversion losses and the power for the auxiliaries into account. The needed parameters are taken from measurements performed on the unit at full rate production:

- the estimated hydrogen production rate in the stack equals 19 L/min<sup>7</sup>;
- the actual hydrogen flow rate measured at the output of the whole system equals 1.05 Nm<sup>3</sup>/h<sup>8</sup>;
- the DC power applied to the stack is 6 kW;
- the total AC power input to the system is 8 kW.

<sup>7</sup> By using the conversion factor 1000 L/m<sup>3</sup>: (19 L/min · 60 min/h) / 1000 L/m<sup>3</sup> = 1.14 m<sup>3</sup>/h

<sup>8</sup> Also equal to the hydrogen product rate declared by the manufacturer in the datasheet.

### *ELECTROLYSIS OR STACK EFFICIENCY*

The specific energy consumption for the electrolysis process can be calculated as:

$$C_E = \frac{P_{DC}}{\dot{V}_{stack}} = \frac{6}{1.14} = 5.263 \text{ kWh/Nm}^3$$

Then, the stack efficiency is calculated through the ratio:

$$\eta_E = \frac{HHV_{H_2}}{C_E} \cdot 100 = \frac{3.54}{5.263} \cdot 100 = 67.3\%$$

### *OVERALL HYDROGEN PRODUCTION SYSTEM EFFICIENCY*

In this case, the specific energy consumption is calculated by considering the total power input as follows:

$$C_E = \frac{P_{AC}}{\dot{V}_{syst}} = \frac{8}{1.05} = 7.619 \text{ kWh/Nm}^3$$

At last, the overall efficiency of the electrolyser is obtained:

$$\eta_E = \frac{HHV_{H_2}}{C_E} \cdot 100 = \frac{3.54}{7.619} \cdot 100 = 46.5\%$$

#### 2.3.2.4 Hydrogen process measurements and control: PLC, HOGEN40 software and flow controller

The hydrogen production process parameters and the system input/output variables can be monitored and logged in two separate ways:

- The PLC installed on one side of the container stores the process input/output data (related to water inlet and hydrogen outlet) on a SD card plugged into the PLC itself. It is possible to read out the data on it either by connecting a laptop via USB-cable and opening the SD card with the program called SD Card Suite or by taking out the SD card when the system has no power and plugging it into the laptop. A short user's manual reporting instruction on how to retrieve the measurements from the PLC is reported in Appendix C.
- The data from the electrolyser itself, related to the electrolysis process, can be acquired by using a program called HOGEN40 and a USB-to-RS232 serial converter cable to make a laptop communicate with the system. With this program, it is possible to both log real-time data and monitor the process values in order to see which state the system is in. A short user's manual showing how to retrieve the measurements via HOGEN40 software can be found in Appendix C.

Since during the making of this project both electrolyser and PLC have been arranged to be accessed via Ethernet connection, it is now possible to perform all the above measurements directly through a computer connected to the laboratory LAN – without the necessity of being on site and using a serial cable.

By comparing both Tables 4 and 5 with the numerical symbols in Figure 23, one can understand the type of measurement devices present in the system, their location in the process flow diagram and whether their data can be accessed from the PLC side or the electrolyser side.



Tab. 4 – PLC monitored variables

N	PLC monitored variables	
1	H <sub>2</sub> O inlet volume flow	[ml/min]
2	Produced H <sub>2</sub> volume flow (upstream of the tanks)	[m <sup>3</sup> /h]
3	Produced H <sub>2</sub> pressure (upstream of the tanks)	[bar]
4	Produced H <sub>2</sub> volume flow (downstream of the tanks)	[m <sup>3</sup> /h]
5	Produced H <sub>2</sub> pressure (downstream of the tanks)	[bar]

Tab. 5 – HOGEN40 monitored variables

N	HOGEN40 monitored variables	
1	Gas detect	[%LeL]
2	Product pressure	[psi]
3	System pressure	[psi]
4	Water quality	[MΩ]
5	Stack voltage	[V]
6	Stack current	[A]
7	System temperature	[°C]
8	Water flow rate	[lpm]

Other variables related to the converter monitoring are:  
 3.3 V<sub>DC</sub> sense, 24.0 V<sub>DC</sub> sense, +5.0 V<sub>DC</sub> sense, 2.5 V reference, -5.0 V<sub>DC</sub> sense, board temperature

Among the mentioned measuring equipment, a flow controller has been recently added on the output product pipe leading to the outside air and its communication channel connected to the laboratory LAN via Ethernet (as done for the other instruments already installed). In this way, the device allows both to control and measure the amount of produced gas flowing through it while all its data and settings can be accessed by an engineering computer connected to the same LAN. The instrument is based on Modbus TCP/IP communication protocol [24], thus it is possible to interact with it either through a software interface specially designed for Modbus registers reading/writing or by implementing a code for carrying out the same task in Matlab. A brief overview on the chosen Modbus interface – Modbus Tester developed by Schneider Electric, and an explanation of the Matlab code used during the performed experiments is reported in Appendix E. The characteristics of the instrument as well as instruction for installation can be found in [25].

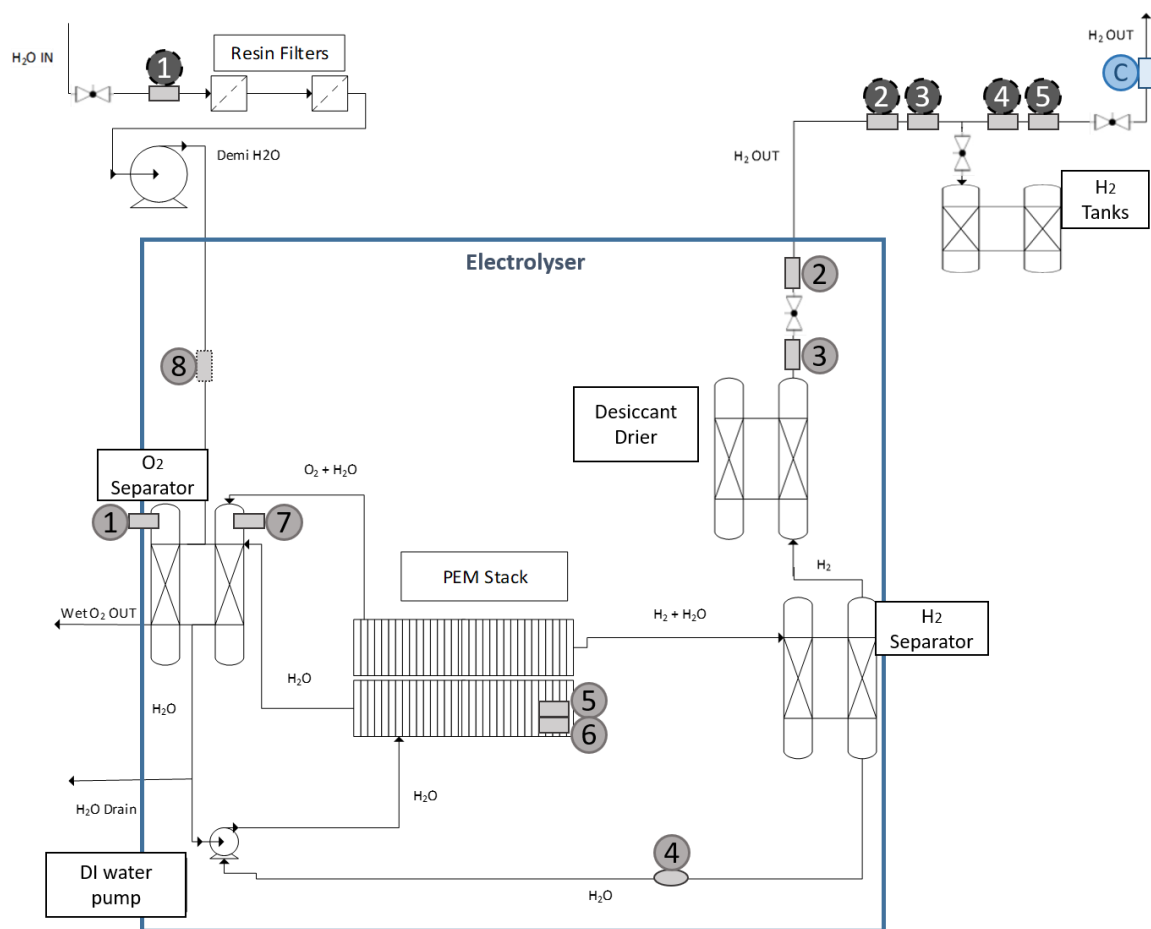


Fig. 23 – PFD and measuring equipment of the hydrogen production process

Note: the newly installed flow controller is marked with C in the upper right side of Figure 23.

## 2.3.3 PV-field: renewable source characterization

### 2.3.3.1 PV-field specifications

The PV-field under study consists of 16 PV panels with a maximum power output of 260 W<sub>p</sub> each, thus the total nominal power equals 4.16 kW<sub>p</sub>. The most important technical specifications of panels and inverter are reported in Tables 6 and 7, respectively. A picture of the PV modules and associated inverter is visible in Figure 24.



Fig. 24 – Picture of the PV panels and inverter at the Entrance test site

Tab. 6 – Trina Solar's PV panels specifications

Trina Solar, PV panel model TSM-260PC05A	
ELECTRICAL DATA @ STC	
Peak Power - P <sub>MAX</sub> [W <sub>p</sub> ]	260
Maximum Power Voltage – V <sub>MPP</sub> [V]	30.6
Maximum Power Current - I <sub>MPP</sub> [A]	8.50
Open Circuit Voltage – V <sub>OC</sub> [V]	38.2
Short Circuit Current – I <sub>SC</sub> [A]	9.00
Module efficiency - $\eta_m$ [%]	15.9
MECHANICAL DATA	
Solar cells	Multicrystalline 156 x 156 mm
Module dimensions	1650 x 992 x 35 mm
Weight	18.6 kg
TEMPERATURE RATINGS	
Nominal Operating Cell Temperature (NOCT)	44 °C (±2 °C)
Temperature Coefficient of P <sub>MAX</sub>	-0.41 %/°C
Temperature Coefficient of V <sub>OC</sub>	-0.32 %/°C
Temperature Coefficient of I <sub>SC</sub>	0.053 %/°C
Operational Temperature	-40~+85 °C

Note: Values important for calculations presented in the following sections.

Standard Test Conditions (STC): Air Mass AM1.5. Irradiance 1000 W/m<sup>2</sup>. Cell Temperature 25 °C; Power measurement tolerance: ±3%.

Nominal Operating Cell Temperature (NOCT): Irradiance 800 W/m<sup>2</sup>. Ambient Temperature 20 °C. Wind Speed 1 m/s; Power measurement tolerance: ±3%.

Tab. 7 – SolarEdge’s three-phase inverter specifications

SolarEdge, Three-phase inverter model SE4K	
<b>OUTPUT</b>	
Rated AC Output Power	4000 W
Maximum AC Output Power	4000 W
Nominal Operating Voltage	220/230 V <sub>AC</sub> (L-N) 380/400 V <sub>AC</sub> (L-L)
Maximum Output Current	6.5 A <sub>AC</sub>
Nominal Operating Frequency	50/60 Hz
<b>INPUT</b>	
Maximum DC Power (Module STC)	5400 W
Input Voltage range	680 – 950 V <sub>DC</sub>
Maximum Input Current	7 A <sub>DC</sub>
Maximum Inverter Efficiency	98%
<b>INSTALLATION SPECIFICATIONS</b>	
Protection Rating	IP65
Installation	Indoor

For the complete datasheets refer to [26] and [27].

### 2.3.3.2 PV-field efficiency

In order to characterize the PV installation, the efficiency can be calculated from the ratings reported above. The efficiency of a photovoltaic system is the amount of solar energy per square meter of surface that the plant can convert into electricity. Since the photovoltaic performance also varies according to the operating temperature, the standard operating conditions, so-called STC, are generally taken as reference. The formula used for the calculation is as follows:

$$\eta = \frac{\frac{P_{tot,PV}}{A_{tot,PV}}}{1000} \cdot 100 [\%] \quad (4)$$

where,  $P_{tot,PV}$  is the PV system total nominal power [W]

$A_{tot,PV}$  is the PV system total surface [m<sup>2</sup>]

$G_{STC} = 1000 \text{ W/m}^2$  is the irradiance reference value at STC

In this case:

$$P_{tot,PV} = 4160 \text{ W}_p, A_{tot,PV} = 26.18 \text{ m}^2$$

so that the formula returns:

$$\eta = \frac{\frac{4160}{26.18}}{1000} \cdot 100 = 15.89\%$$

This is roughly equivalent to the module efficiency specified by the PV module datasheet [26] and reported in Table 6. It represents the percentage amount of solar energy that is actually converted into usable electrical energy by the plant, under standard operating conditions.

### 2.3.3.3 Weather conditions measurements: pyranometer and temperature sensors

The PV installation comes equipped with a pyranometer, instrument used for measuring the solar irradiance on a planar surface, also referred to as solar radiation flux density ( $[W/m^2]$ ). The datasheet of the instrument is available at [28] and a picture of the device is shown in Figure 25. The measurements are performed at 1 min interval and for the whole 24 hours in a day. The measured values are then automatically uploaded and saved every day onto a cloud storage, accessible through a private Hanze's account. The database contains 24 hours solar irradiance data for each day, from 1<sup>st</sup> June 2017 till the current date.

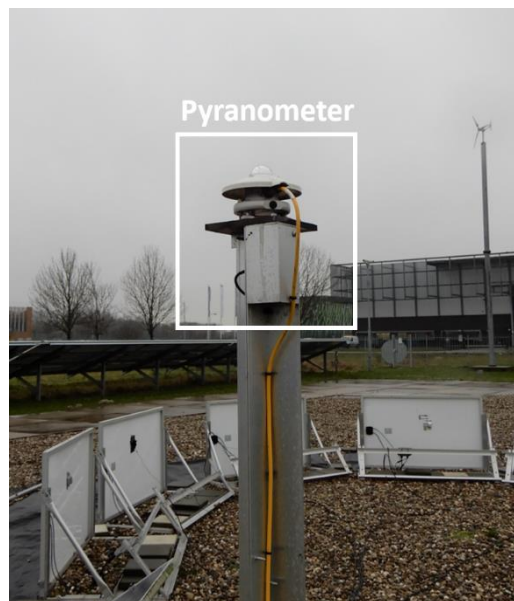


Fig. 25 – Picture of the pyranometer at the PV installation under study

The PV panels model, whose implementation will be described step by step in the following Chapter 3, has also required temperature data. Since the PV installation under study has not been provided with temperature sensors, measurements have been taken from a neighbor PV-field. This is located about 200 meters farther and is fitted with 3 temperature sensors: two of them keep trace of the panels temperature on both surfaces while the third one collects the air temperature measurements. All these data are uploaded onto a cloud storage in the same way as the irradiance data and are available every day within a time frame ranging from 5 am to 10 pm. A picture of the air temperature sensors from which the data have been retrieved is shown in Figure 26.

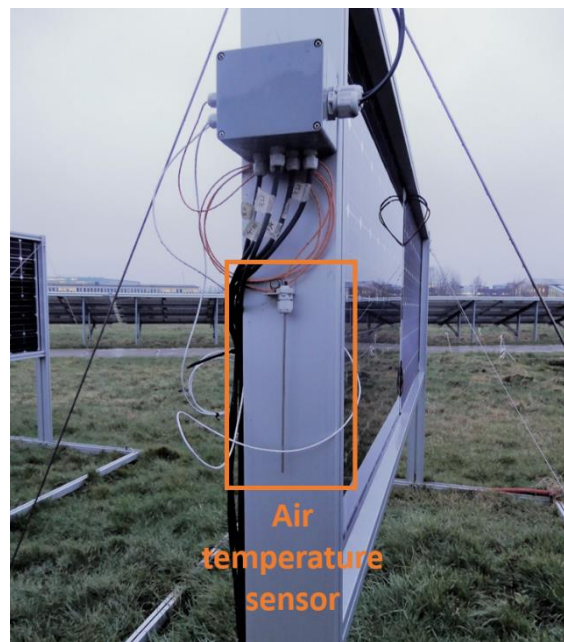


Fig. 26 – Picture of the air temperature sensor at a neighbor PV installation

# Chapter 3

## Model of the PV panels

### 3.1 Aim of the modelling

For an in-depth study of the possibilities of PtG, the Micro-Grid Lab research is focused on collecting appropriate data from all kinds of resources installed on site through the related measurement equipment. These data can further be processed and used to implement models aimed at investigating hydrogen production-renewable sources interactions. In particular, proper Simulink models are intended to be obtained for integration into big scale power grid simulations, with the final purpose to investigate the behavior of the “global prosumer” as well as its influences on the grid.

In the context of this work, the modelling has been focused on two elements of the configuration for hydrogen-electricity integration: electrolyser (energy storage) and PV panels (energy source). These models will eventually be added to a large-scale power grid model under design, scaled up and merged with other components to create the desired “global prosumer”.

Before moving on, it is important to mention that both the electrolyser and PV panels are intended to be represented into the complete Simulink model of the grid by means of the SimScape block named *Three-Phase Dynamic Load*. Full details on this block can be found at [29]. Now, it is important to note that this component allows to implement a three-phase load with active and reactive power controlled by external input. In this way, the electrolyser is modeled as a common positive load (power withdrawn from the grid) while the PV panels are modeled as negative loads (power injected into the grid). It follows that the laboratory measurements performed on electrolyser and PV panels should be aimed at obtaining the active power (together with the reactive) consumed by the former and produced by the latter, to be given as input values to the mentioned block.

The following Chapters provide a detailed description of the construction of the model for each element separately. The description starts in this Chapter with the PV panels model, that, being the simpler, has been the first one implemented. On the same basis and proceeding with the same method the electrolyser model has been constructed and is presented in Chapter 4.

### 3.2 Concept of the PV panels model

The concept underlying the construction of the PV panels model is presented in Figure 27. The PV panels are measured by operating values, the most important of which are the amount of active (and reactive) power produced and delivered to the main grid. To make good mathematical models it is also required to measure and evaluate other electrical variables (voltage, current, power factors, frequency etc.), as well as parameters related to ambient conditions such as solar irradiance and temperature. Clearly, for a dynamic analysis, all these data have to be time-related.

After the measurements, the collected data are properly processed to obtain the final power profiles to be given as input to the *Three-Phase Dynamic Load* block.

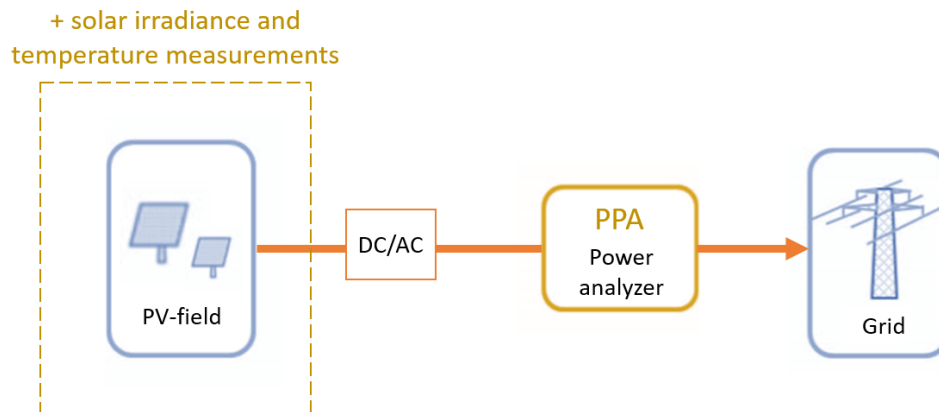


Fig. 27 – Scheme of the concept for the implementation of the PV panels model

### 3.3 Collecting the measurements

In order to build the PV panels model, the first step was to perform the following measurements:

- *The electrical variables related to the PV panels produced AC power (downstream of the inverter – DC/AC conversion) by means of the PPA power analyzer.*

In order to perform such a measurement, firstly, the physical connections had to be correctly arranged for this purpose. This was done by following the instructions reported in section D.1 of Appendix D. After that, the communication between power analyzer and DataLogger software had to be properly established. This was accomplished according to section A.1.1 of the short user's manual in Appendix A. Once the communication was up and running, the instrument settings could be edited through the related software by following the steps reported below (in reference to Appendix A):

- Click *READ PPA* to download the current instrument settings into the Configuration Control panel.
- Edit the Settings menu in such a way that, under *ACQU (Acquisition Control)* menu:  
Speed = Window  
Window = 5 s
- Click *SET UP PPA* to upload the changes to the instrument.
- Open the Multilog window through the *Multilog* button and choose the variables to be measured. For this experiment, they were in detail: active, reactive and apparent power, power factor, ph-to-ph voltage, RMS voltage, RMS current for each of the three phases and lastly, frequency<sup>9</sup>.

<sup>9</sup> Both the described settings configuration and the multiple parameters selection were saved for future use by means of the related options. This is useful to keep trace of the settings used for a certain experiment in case it has to be reproduced multiple times.



- Set the logging speed by selecting *Software Interval* mode and typing 5 (s) in the *Interval box*.
  - Set the measurement mode by choosing either *Direct Log to CSV* (the logged data are saved straight to a CSV file) or *Log Real Time Table* mode (the logged data are recorded and displayed by the software and can be subsequently exported either in Excel or CSV file format)<sup>10</sup>.
  - Start the logging through the *START/STOP* button.
- *The Solar irradiance by means of the pyranometer.*

The 24-hour solar irradiance data, measured by the pyranometer for each day (starting from 1<sup>st</sup> June 2017), are available on the Hanze's online database. The necessary data were accessed and downloaded through a private Hanze's account.

The chosen measured interval for both the instruments was equal to 24 h (starting on last 31<sup>st</sup> October at 10:32 and ending on 1<sup>st</sup> November at 10:32). The sampling time chosen for the PPA was 5 s, while the sampling time available for the pyranometer is 1 min (the minimum applicable to this instrument).

The mentioned data were imported to Excel, according to section A.2 of Appendix A, and the related graphs were built. The most significant results of active<sup>11</sup> and reactive power, together with solar irradiance, are represented in the following Figures 28, 29 and 30.

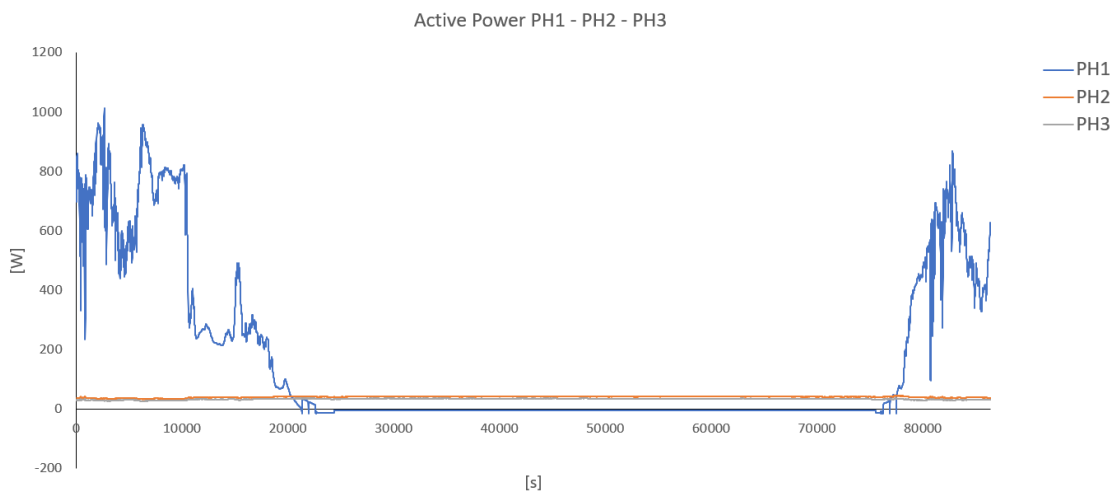


Fig. 28 – PPA measurements: active power

<sup>10</sup> The CSV format option within the Setting window was set to European (","),. This contributed to speed up the next CSV file import operation to Excel.

<sup>11</sup> Although the PPA measures the produced active power as negative power, in the graph it is represented as positive for the sake of clarity.

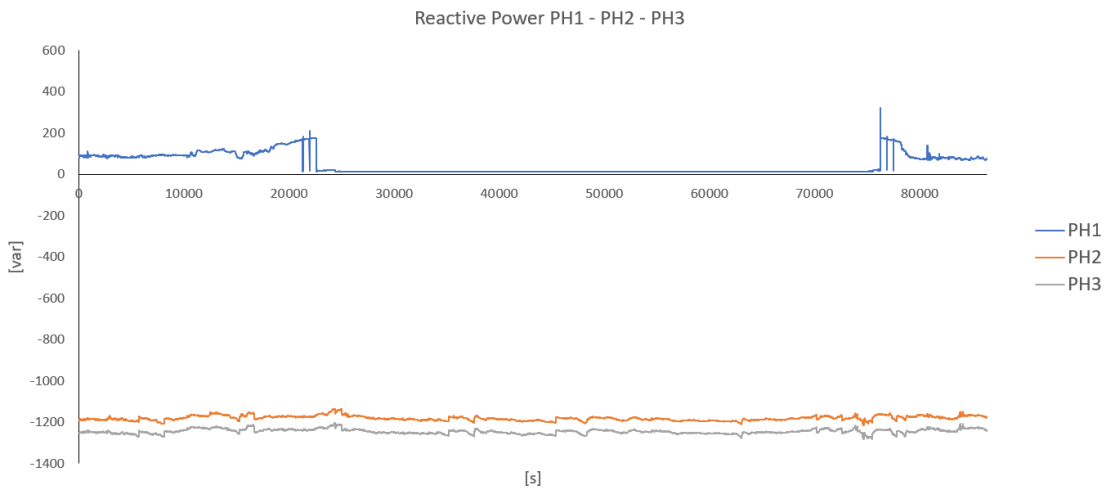


Fig. 29 – PPA measurements: reactive power

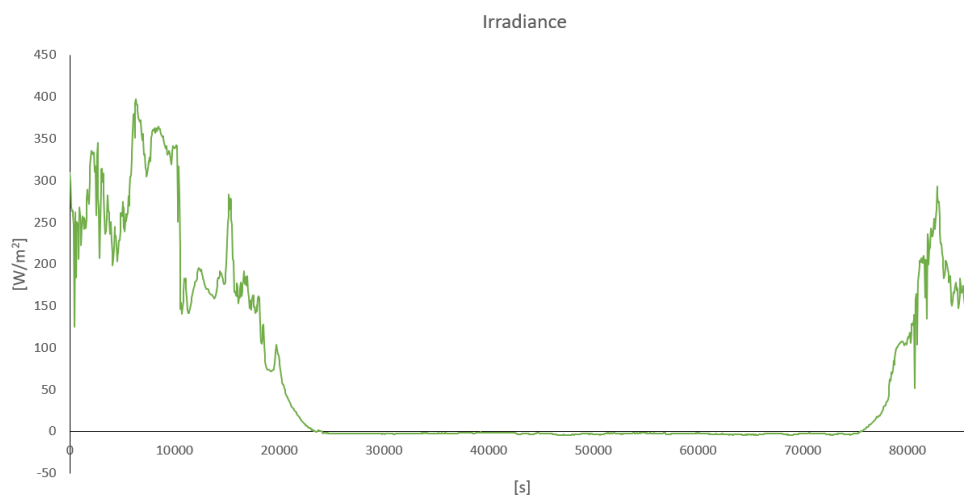


Fig. 30 – Pyranometer measurements: solar irradiance

In addition to these data, in order to build a good mathematical model in line with models already existing [30], also the temperature variable had to be taken into account. However, since no temperature measurements are available for the PV field under study, it was measured:

- *The air temperature by means of temperature sensors located on a neighbor PV installation.*

In the same way as the solar irradiance, the air temperature is measured by the associated sensors and automatically uploaded every day on the Hanze's online database. The temperature data can then be accessed and downloaded through a private Hanze's account.

The temperature measurements were retrieved within the interval in which all the other variables had already been measured (equal to 24 h, starting on last 31<sup>st</sup> October at 10:32 am and ending on 1<sup>st</sup> November at 10:32 am). Since the temperature sensors are preprogrammed to collect everyday measurements from 5:00 am to 10:00 pm, within the desired interval the data from 10:00 pm of 31<sup>st</sup> October to 5:00 am of the day after were missing. The temperature sensors sample time is set to 5 min.

The new temperature data were also imported into Excel files. The graphs showing the temperature profiles for each day from 5:00 am to 10:00 pm are plotted in Figure 31.

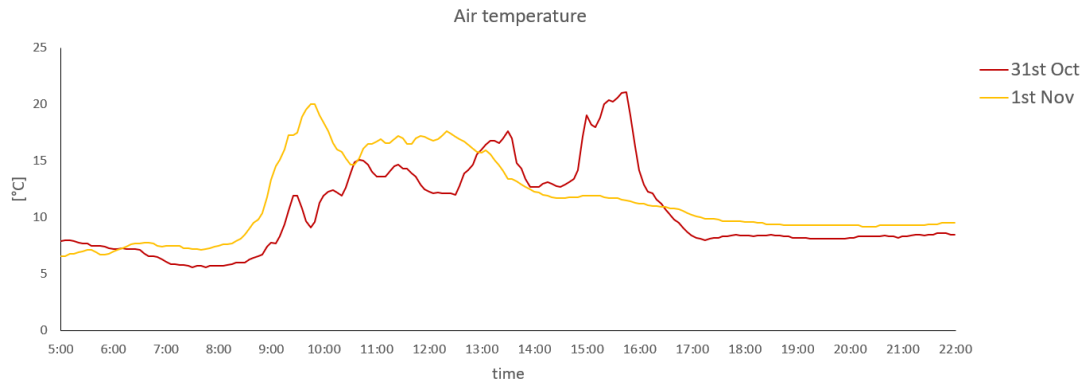


Fig. 31 – Temperature sensor measurements: air temperature

## 3.4 Processing the data

### 3.4.1 Active power, reactive power and solar irradiance

The measured data of active and reactive power as well as solar irradiance were moved to Matlab for data-processing operations and stored into two matrixes, named:

- *PQ\_real* – real measured electrical data;
- *Irrad\_real* – real measured irradiance data.

In particular, the matrix columns are organized as follows:

Tab. 8 – *PQ\_real* [17279x7]

(17279 intervals of roughly 5 s within 24 h, including data at time 0. 2 fewer data due to instrument imprecisions)

	Column 1	Column 2	Column 3	Column 4	Column 5	Column 6	Column 7
	Seconds from 0	P PH1 [W]	P PH2 [W]	P PH3 [W]	Q PH1 [var]	Q PH2 [var]	Q PH3 [var]
1.	Second 0	(convention: produced power marked as negative)					
2.	Second 4.931						
...	...						
17279.	Second 86401						

Tab. 9 – *Irrad\_real* [1441x2]

(1441 intervals of roughly 1 min within 24 h, including data at time 0. Non-uniform time steps due to instrument imprecisions)

	Column 1	Column 2
	Seconds from 0	Irradiance [W/m <sup>2</sup> ]
1.	Second 0	
...	...	
404.	Second 24199	
405.	Second 24260	
...	...	
1441.	Second 86400	

Since the pyranometer sample time could not be set equal to the PPA one, and furthermore, since the sample time for both the instruments turned out to be slightly imprecise, it was necessary to draw new estimated data from the real measured data. Because of the non-regularity of the time steps, this was done by a combination of linear interpolation and extrapolation. First, for each set of two known data points – represented by the coordinates  $(x_k, y_k)$  and  $(x_{k+1}, y_{k+1})$ , the straight line between them (so-called linear interpolant) needs to be constructed through the following formula:

$$\frac{(y - y_k)}{(x - x_k)} = \frac{(y_{k+1} - y_k)}{(x_{k+1} - x_k)} \quad (5)$$

In this way, a piecewise linear function is obtained. Then, the needed new data points – represented by the coordinates  $(x_n, y_n)$ , needs to be extrapolated from the straight line between the two known points – again given by the coordinates  $(x_k, y_k)$  and  $(x_{k+1}, y_{k+1})$ , through the following formula:

$$y_n = y_k + (x_n - x_k) \cdot \frac{(y_{k+1} - y_k)}{(x_{k+1} - x_k)} \quad (6)$$

In this case,  $x$  represents the time variable  $t$  (along the x-axis) whereas  $y$  represents any variables among active power, reactive power and irradiance (along the y-axis).

Because of the complexity of the analytical calculation, this process was carried out for all the measured variables by means of a Simulink model. Here, for each measured variable a *From Workspace* block reads out the real data values from the Matlab workspace in matrix format (time stamps in the first column and corresponding data samples in the second column) and linearly interpolates the discrete set of data. A *To Workspace* block writes the output to the Matlab workspace in *structure with time* format, by extrapolating the values with a sample time of 5 s.

This operation allowed to make the time step uniform for all the measured variables, and, at the same time, to get the same time step of 5 s for both electrical data and irradiance data. At last, for the sake of clearness, the resulting structures were recomposed into the original matrix format. The new matrixes are named:

- *PQ\_lin* – electrical data with uniform time step of 5 s obtained by linear interpolation;
- *Irrad\_lin* – irradiance data with uniform time step of 5 s obtained by linear interpolation.

The Matlab matrix dimensions are modified as reported below:

Tab. 10 – *PQ\_lin* [17281x7]

(17281 intervals of 5 s within 24 h, including data at time 0. Time steps precisely equal to 5 s)

	Column 1	Column 2	Column 3	Column 4	Column 5	Column 6	Column 7
1.	Second 0	P PH1 [W]	P PH2 [W]	P PH3 [W]	Q PH1 [var]	Q PH2 [var]	Q PH3 [var]
2.	Second 5						
...	...						
17281.	Second 86400						

Tab. 11 – *Irrad\_lin* [17281x2]

(17281 intervals of 5 s within 24 h, including data at time 0. Time steps precisely equal to 5 s)

	Column 1	Column 2
1.	Second 0	Irradiance [W/m <sup>2</sup> ]
2.	Second 5	
...	...	
17281.	Second 86400	

At this point, since the data of both powers and irradiance are energy quantities, the approach followed was in line with the pre-processing method described in [31]. According to this reference, in fact, when input data for power system studies are provided with different time steps or even with irregular timing, a pre-processing phase is needed to unify the representation within the same time step. Moreover, since most of the data considered in this context represent the average power in a given time step, the meaning the overall energy – integral of the considered pattern over the period of interest, has to be maintained in the processing. This condition is met by introducing a correction factor calculated as follows.

For the sake of notation,  $T$  is the total period of analysis;  
 $\tau_i$  is the initial irregular time step;  
 $\tau_o$  is the newly chosen regular time step;

thus,  $p_{T,\tau_i}$  represents the vector of initial values, each one with different formats and irregular time step;  
 $\tilde{p}_{T,\tau_o}$  represents the vector calculated from the one above on the basis of geometric considerations only;  
 $p_{T,\tau_o}$  represents the final vector of regularly distributed points at the chosen time step.

First, the total energies  $W_i$  and  $W_o$  are calculated by respectively integrating the patterns  $p_{T,\tau_i}$  and  $\tilde{p}_{T,\tau_o}$  over the period  $T$ . The correction factor  $\xi$  is then calculated as the energy ratio  $\xi = W_i/W_o$ . At last, the final pattern is obtained through the following relation:

$$p_{T,\tau_o} = \xi \cdot \tilde{p}_{T,\tau_o} \quad (7)$$

In this way, the total energy of the final pattern ( $W_o'$ ) is maintained equal to the initial one ( $W_i$ ).

This procedure was followed for the patterns of active power, reactive power and irradiance, where:

- The total period of analysis is:  $T = 24 \text{ h} = 86400 \text{ s}$
- The initial vectors with irregular time steps are the columns of the real data matrixes:

$$p1_{24h,\tau_i} = \text{Irrad\_real}(:,2) \rightarrow \text{irradiance}$$

Vector with 1441 rows and non-uniform time steps.

$p2_{24h,\tau_i} = PQ\_real(:,2) \rightarrow$  PH1 active power  
 $p3_{24h,\tau_i} = PQ\_real(:,3) \rightarrow$  PH2 active power  
 $p4_{24h,\tau_i} = PQ\_real(:,4) \rightarrow$  PH3 active power  
 $p5_{24h,\tau_i} = PQ\_real(:,5) \rightarrow$  PH1 reactive power  
 $p6_{24h,\tau_i} = PQ\_real(:,6) \rightarrow$  PH2 reactive power  
 $p7_{24h,\tau_i} = PQ\_real(:,7) \rightarrow$  PH3 reactive power

All vectors with 17279 rows and non-uniform time steps.

- The vectors with regular time steps are the ones obtained from the vectors above by linear interpolation:

$\tilde{p}1_{24h,\tau_o} = Irrad\_lin(:,2) \rightarrow$  irradiance  
 $\tilde{p}2_{24h,\tau_o} = PQ\_lin(:,2) \rightarrow$  PH1 active power  
 $\tilde{p}3_{24h,\tau_o} = PQ\_lin(:,3) \rightarrow$  PH2 active power  
 $\tilde{p}4_{24h,\tau_o} = PQ\_lin(:,4) \rightarrow$  PH3 active power  
 $\tilde{p}5_{24h,\tau_o} = PQ\_lin(:,5) \rightarrow$  PH1 reactive power  
 $\tilde{p}6_{24h,\tau_o} = PQ\_lin(:,6) \rightarrow$  PH2 reactive power  
 $\tilde{p}7_{24h,\tau_o} = PQ\_lin(:,7) \rightarrow$  PH3 reactive power

All vectors with 17281 rows and time steps precisely equal to 5 s.

The total energies  $Wk_i$  and  $Wk_o$  were calculated by respectively integrating the patterns  $pk_{24h,\tau_i}$  and  $\tilde{p}k_{24h,\tau_o}$ ,  $k = 1, \dots, 7$  over the period  $T^{12}$ . The correction factors were then computed through the ratio  $\xi k = Wk_i / Wk_o$ . Finally, the final vectors with regular time steps and preserved total energy were obtained through the following formula:

$$pk_{24h,\tau_o} = \xi k \cdot \tilde{p}k_{24h,\tau_o} \quad (8)$$

As a final check, the total energies  $Wk'_o$  were calculated by integrating the resulting patterns  $pk_{T,\tau_o}$ ,  $k = 1, \dots, 7$  and compared with  $Wk_i$ . The difference  $|Wk'_o - Wk_i|$  resulted  $<10^{-6}$  in the worst case, so that it was possible to state that the overall energy was preserved during the processing. At the end of the process, the resulting vectors were included in new matrixes, named:

- *PQ\_Econs* – electrical data with uniform time step of 5 s and energy conserved;
- *Irrad\_Econs* – irradiance data with uniform time step of 5 s and energy conserved.

<sup>12</sup> At first, this was done both by explicitly implementing the sum of trapezoidal areas underlying the patterns and by means of the Matlab function *trapz*. In details, the command  $A = trapz(X,Y)$  performs the trapezoidal numerical integration of  $Y$  with respect to the x-axis coordinates specified by  $X$ . Since by comparing the results in the two cases the difference between them ended up being every time  $<10^{-7}$ , the two methods were proved to be roughly equivalent. The explicit integration was at last chosen for the energy calculations.

As a graphical example, these matrixes are schematized below:

Tab. 12 – **PQ\_Econs** [17281x7]

	Column 1	Column 2	Column 3	Column 4	Column 5	Column 6	Column 7
1. 2.	Second 0 Second 5	$p2_{24h,\tau_o}$	$p3_{24h,\tau_o}$	$p4_{24h,\tau_o}$	$p5_{24h,\tau_o}$	$p6_{24h,\tau_o}$	$p7_{24h,\tau_o}$
...	...	(P PH1 [W])	(P PH2 [W])	(P PH3 [W])	(Q PH1 [var])	(Q PH2 [var])	(Q PH3 [var])
17281.	Second 86400						

Tab. 13 – **Irrad\_Econs** [17281x2]

	Column 1	Column 2
1. 2.	Second 0 Second 5	$p1_{24h,\tau_o}$
...	...	(Irradiance [W/m <sup>2</sup> ])
17281.	Second 86400	

### 3.4.2 Air temperature

Moving to Matlab for data-processing operations, the temperature data were stored into two additional matrixes, called:

- $Ta_{31\_10}$  – air temperature for 31<sup>st</sup> October;
- $Ta_{01\_11}$  – air temperature for 1<sup>st</sup> November.

These new matrixes are schematized as follows:

Tab. 14 – **Ta<sub>31\_10</sub>** [205x2]

(205 intervals of 5 min from 5:00 am to 10:00 pm, including data at time 0. Time steps precisely equal to 5 min)

	Column 1	Column 2
1. 2.	5:00 5:05	Air temperature 31/10 [°C]
...	...	
204.	21:55	
205.	22:00	

Tab. 15 – **Ta<sub>01\_11</sub>** [205x2]

(205 intervals of 5 min from 5:00 am to 10:00 pm, including data at time 0. Time steps precisely equal to 5 min)

	Column 1	Column 2
1. 2.	5:00 5:05	Air temperature 01/11 [°C]
...	...	
204.	21:55	
205.	22:00	

In contrast to the previous linearization case, now the sample time is regular so that the needed new data points can be obtained within the discrete set of known data points by linear interpolation. Again, given two known points represented by the coordinates  $(x_k, y_k)$  and  $(x_{k+1}, y_{k+1})$ , the new data within this range – represented by the coordinates  $(x_n, y_n)$ , can be obtained through the previous formula (6). In this case,  $x$  is the time variable  $t$  (along the x-axis) whereas  $y$  represents the temperature variable  $T$  (along the y-axis). Specifically,

$$x_{k+1} - x_k = 5 \text{ min}, \quad x_n = x_k + n \cdot 5 \text{ s} \quad \text{with } n = 1, \dots, 59$$

In this way, new data with the desired sample time of 5 s were obtained within each range of 5 min<sup>13</sup>.

Afterwards, the data within the desired 24 h time frame were selected from the results of the linearization and copied into a unique matrix, named as:

- $Ta$  – air temperature, corresponding to an interval of 24 h with uniform time step of 5 s obtained by linear interpolation.

The cells corresponding to the overnight missing data (from 10:00 pm to 5:00 am) were set to 0<sup>14</sup>. The resulting matrix can be schematized as follows:

Tab. 16 –  $Ta$  [17281x2]

(17281 intervals of 5 s within 24 h, including data at time 0. Time steps precisely equal to 5 s)

	Column 1	Column 2
1.	Second 0	Air temperature 31/10 [°C]
2.	Second 5	
...	...	
8257.	Second 41280	----- 0
8258.	Second 41285	
...	...	
13296.	Second 66475	----- 0
13297.	Second 66480	
...	...	
17280.	Second 86395	Air temperature 11/10 [°C]
17281.	Second 86400	

### 3.5 Creation of the model

According to what stated in 3.2, the concept underlying the PV panels modelling was to provide the produced electrical power, both active and reactive, in order to control the dynamic load block. Moreover, the further idea was to estimate these values from irradiance

<sup>13</sup> It is worth to note that, since the temperature is not considered as an energy quantity, it was enough to draw the new data on the basis of geometric considerations only.

<sup>14</sup> It is important to point out that, since the overnight pyranometer data appeared to be negative (due to calibration inaccuracy), they were changed to 0 for the sake of precision.



and temperature data. In fact, since a complete database is available on the Hanze's online cloud, these quantities can be easily given as input to the overall model.

In order to estimate the generated active power starting from irradiance and temperature inputs, the model described in [30] and already used for the STORE&GO project in [32] was taken as reference. This model allows the irradiance profile ( $G$ , in  $[W/m^2]$ ) to be converted into power – in particular, into the ratio between the produced power on the AC side ( $P_{AC}$ , in  $[W]$ ) and the PV plant nominal power ( $P_{nom}$ , in  $[W_p]$ ), which represents the production profile (in pu). The air temperature ( $T_a$ , in  $[^\circ C]$ ) is used to calculate the solar cell temperature ( $T_c$ , in  $[^\circ C]$ ), which is then used to estimate the thermal efficiency ( $\eta_{th}$ ). This is useful to quantify the reduction of production due to the PV panels over-temperature losses. The corresponding formulas are:

$$T_c = T_a + \frac{NOCT - 20}{800} \cdot G \quad (9)$$

$$\eta_{th} = 1 - \alpha_{th} \cdot (T_c - 25) \quad (10)$$

$$\frac{P_{AC}}{P_{nom}} = \eta_{DC/AC} \cdot \frac{G}{1000} \cdot \eta_{th} \quad (11)$$

where,  $NOCT$  is the Nominal Operating Cell Temperature of the module;

$\alpha_{th}$  is the thermal coefficient of the PV module (dependent on the PV technology);

$\eta_{DC/AC}$  is the efficiency – affected by losses due to reflection, dirt, I-V characteristic mismatch, DC cables, DC/AC conversion, tolerance and so on.

Note:  $G_{STC} = 1000 W/m^2$  and  $T_{c,STC} = 25 ^\circ C$  define the STC;

$G_{NOCT} = 800 W/m^2$  and  $T_{a,NOCT} = 20 ^\circ C$  define the NOCT.

In this context, the model inputs are:

$$G = Irrad\_Econs(:,2)$$

$$T_a = Ta(:,2)$$

while the model constants are set as follows:

$NOCT = 44 ^\circ C$  (from the PV module datasheet [26], reported in Table 6)

$\alpha_{th} = 0.41\%/^\circ C$  (from the PV module datasheet [26], reported in Table 6)

$P_{nom} = 16 \cdot 260 W_p$  (16 modules, each one with nominal power of  $260 W_p$ ;  
from PV module datasheet [26], reported in Table 6)

$\eta_{DC/AC} = 0.59$  (estimated by trial, in such a way to minimize the difference between the  $P_{AC}$  output pattern and the actual power profile produced by the PV plant)


However, the analyzed model is only able to provide the generated active power, while both active and reactive powers are needed in order to control the mentioned dynamic load block.

In this regard, the developed idea was to estimate the reactive power from the active power already evaluated by means of a look-up table representing the function  $Q(P)$ .

For the purpose of constructing this function, the real measured data of active and reactive power had to be handled. The considered vectors were  $PQ\_Econs(:,2)$  (PH1 active power) and  $PQ\_Econs(:,5)$  (PH1 reactive power), obtained from the real ones by applying the described pre-processing method. Moreover, since the independent variable (active power) must be monolithically increasing, some further data processing was required to get the final result: at first, the elements of the active power vector were sorted in ascending order and the reactive power vector was rearranged accordingly; afterwards, the rows corresponding to repetitive active power values was deleted from both the active and reactive power vectors; at last, for the reactive power vector, the mean value of the set of detected rows was calculated and stored in the only cell in the group left. The applied criterion can be depicted as follows:


Tab. 17 – **P\_lookup** [17269x2]

	Column 1	Column 2
1.	Second 2655	-1012.9 W
2.	Second 2650	-1011.9 W
...	...	...
8637.	Second 42820	4.5105 W
8638.	Second 71520	4.5105 W
...	...	...
17269.	Second 76090	15.084 W



Tab. 18 – **Q\_lookup** [17269x2]

	Column 1	Column 2
1.	Second 2655	76.087 var
2.	Second 2650	76.620 var
...	...	...
8637.	Second 42820	12.171 var
8638.	Second 71520	12.285 var
...	...	...
17269.	Second 76090	23.745 var



At this point, the look-up table could be constructed by placing the active power array along the horizontal axis and the reactive power array along the vertical axis. The resulting function is plotted in Figure 32.

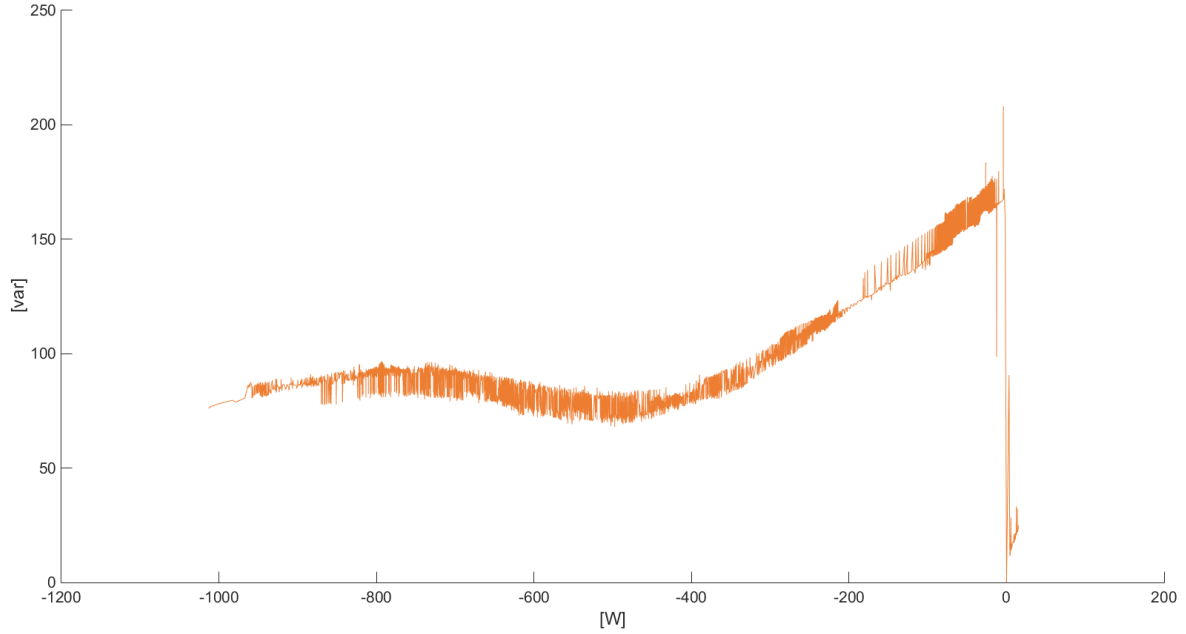


Fig. 32 – Function  $Q(P)$

In Figure 33 it can be observed the complete PV panels model. It is supplied by an ideal generator modeled through a *Three-Phase Source* block, while all the necessary electrical variables are measured through appropriate measurement blocks. It is worth to notice that this is only a default setup, used for the model final testing. Afterwards, the tested model can be included in a more general network simulation.

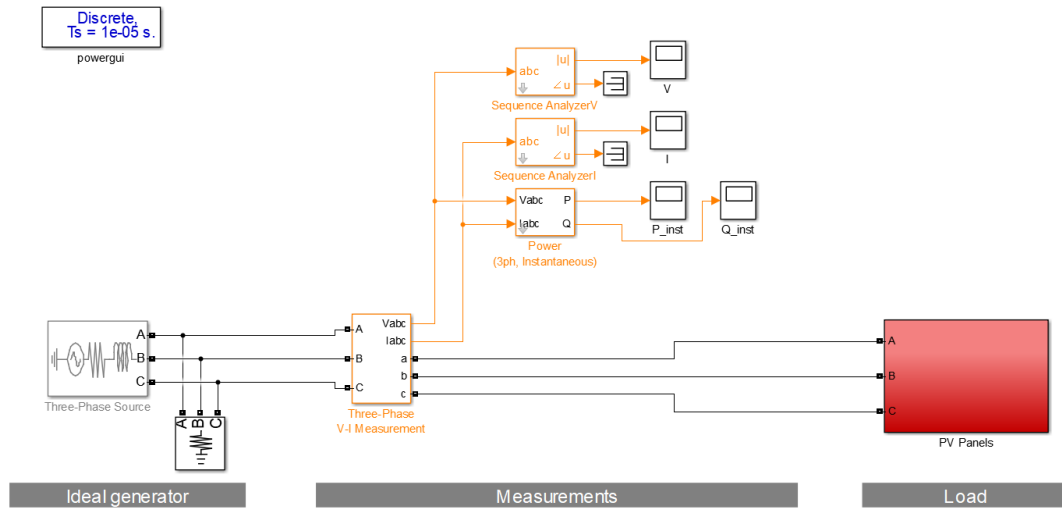


Fig. 33 – PV panels model

Figure 34 shows in detail the *PV Panels* subsystem. It includes a *Three-Phase Dynamic Load* block whose active and reactive power are externally controlled and received from the *PV\_model* subsystem. The inputs to this subsystem are the obtained vectors of solar irradiance (named *Irrad\_Econs*) and air temperature (named *Ta*), while the content of the subsystem itself is depicted in Figure 35. Here, the first blocks that appear on the left (indicated as  $G(t)$  and  $Ta(t)$ ) have been created in order to upload subsequent cells of the arrays, in synchrony with the clock implemented by the *Counter* subsystem as shown in Figure 36. Then, the central part corresponds to the graphical implementation of the formulas (9), (10) and (11), which



### 3.6 Validation of the model

In order to validate the model, power outputs from the simulation were compared with the real PV panels outputs (being  $-PQ\_real(:,2)$  – PH1<sup>15</sup> active power multiplied by -1 → produced power marked as positive<sup>16</sup>;  $PQ\_real(:,5)$  – PH1 reactive power). The resulting graphs are displayed in Figure 37 and 38.

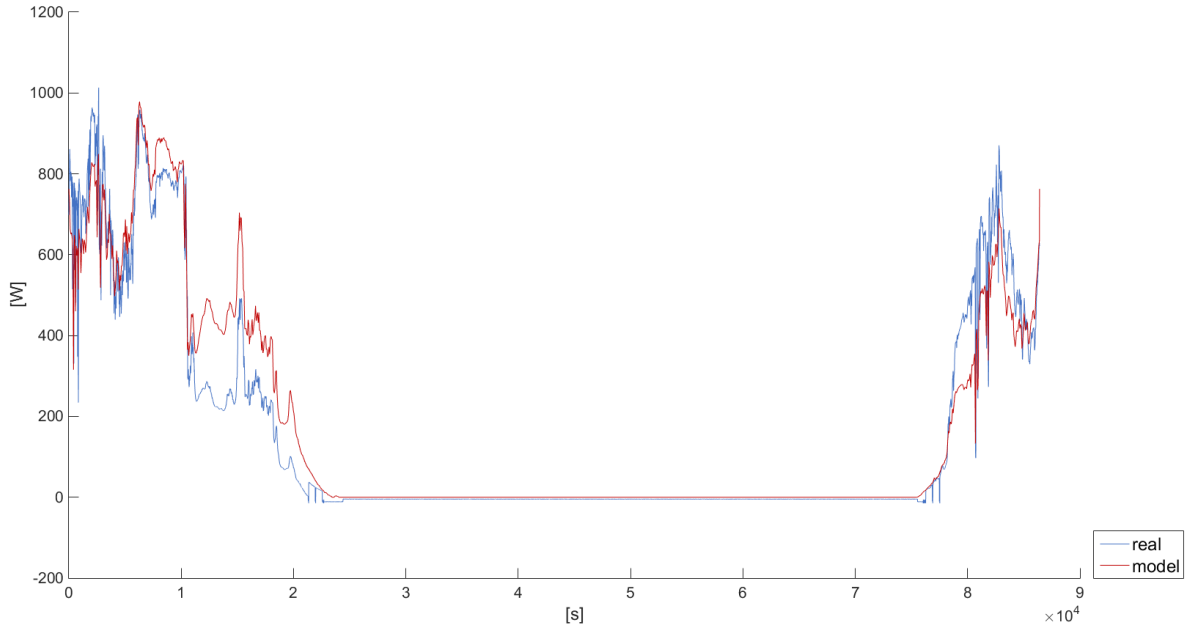


Fig. 37 – PV panels model: comparison between estimated and measured active power

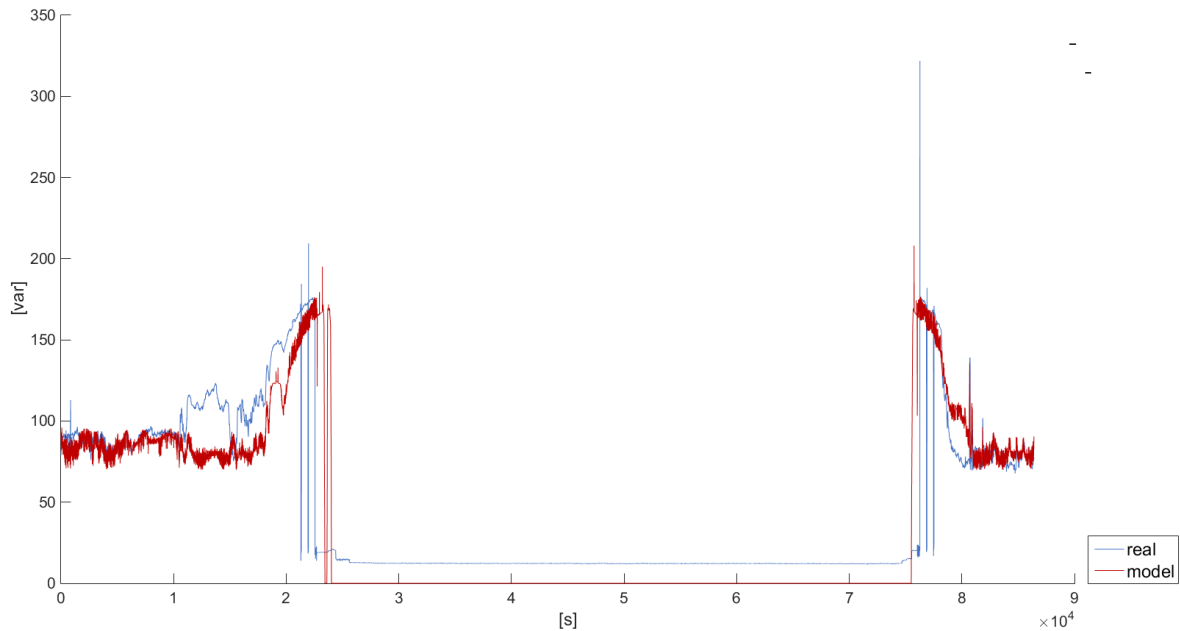


Fig. 38 – PV panels model: comparison between estimated and measured active power

<sup>15</sup> For this purpose, only the active power of phase 1 was considered. In fact, the active power of the other two phases, being roughly constant throughout the 24 h measurements, were proven to be constituted by electrical losses only. It means that the PV power conversion is operated only over one phase.

<sup>16</sup> Once again, the active power is represented as positive for the sake of clarity. This is despite the fact that the PPA measures the produced active power as negative and that the active power profile given as input to the Three-Phase Dynamic Load block has to be negative to represent a power generation.

It can be observed that the two active power profiles are very close to each other. Also the reactive power profiles have a similar trend, even if the simulated reactive power shows bigger variations than the respective real profile.

To conclude, it is possible to claim that the model appears as relatively accurate. However, improvements on the method to estimate the reactive power may be necessary in order to reduce the power variation (for example, by adding a filter to the  $Q(P)$  function). In order to prove the generality of the model, it will be necessary to give other temperature and irradiance profiles as input to the simulation and compare the results with the real power production. Given generic irradiance and temperature vectors, the model should return a power profile approximately similar to the real one, regardless of atmospheric conditions and time of the year.

# Chapter 4

## Model of the electrolyser

### 4.1 Concept of the electrolyser model

Taking the PV panels model as reference, the idea behind the electrolyser model is similarly schematized in Figure 39. The electrical behavior of the electrolyser is characterized by measuring the amount of active (and reactive) power consumed and withdrawn from the main grid. Moreover, other electrical variables (such as voltage, current, power factors, frequency etc.) are collected as well as hydrogen process parameters, the most important of which are hydrogen flow rate, stack voltage and stack current. Once collected, all the time-related data are processed following the data-processing method already used for the PV panels and the final power profiles are given as input to the *Three-Phase Dynamic Load* block.

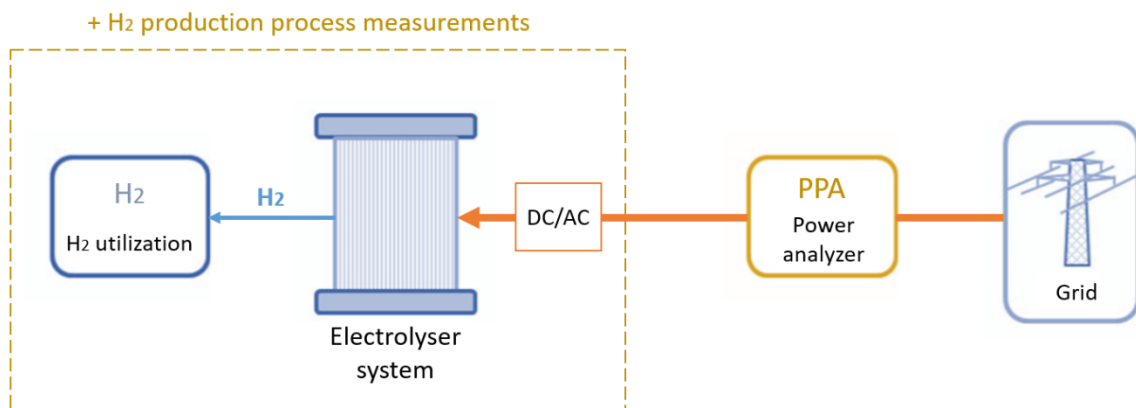


Fig. 39 – Scheme of the concept for the implementation of the electrolyser model

### 4.2 First approach: static

#### 4.2.1 Collecting the measurements

Similarly to the PV panels, also the first stage of the electrolyser modelling required to carry out a series of measurements. In particular, for the purpose of characterizing the electrolyser behavior, various experiments had to be performed under various load conditions, quantified as 25, 50, 75 and 100% of full-load. The idea was to simulate the H<sub>2</sub> load supply by operating the electrolyser in venting mode, and, in order to achieve the reduced load operation, to properly close the valves regulating the H<sub>2</sub> output flow. In fact, because of the almost linear relationship between H<sub>2</sub> output and stack current [6,22], a certain percentage of the maximum hydrogen flow rate roughly corresponds to the same percentage of maximum AC power consumption.

On this basis, the measurements performed can be listed as follows:

- *The electrical variables related to the electrolyser consumed AC power (upstream of the rectifier – AC/DC conversion) at 25, 50, 75 and 100% of full-load by means of the PPA power analyzer*

The first step of this procedure was to connect the electrolyser to the grid in order to receive power supply. This was done by following the instructions reported in section D.2 of Appendix D. After that, it was necessary to correctly start up the entire electrolyser system according to the manual available in Appendix B. Once the electrolyser was up and running, the valves placed on the tube leading the H<sub>2</sub> into the outside air were properly adjusted as shown in Appendix B in order to get an H<sub>2</sub> flow roughly equal to 25, 50, 75 and 100% of the maximum flow rate (averaged to 1.07 Nm<sup>3</sup>/h), depending on the case. At this point, after establishing the communication between power analyzer and DataLogger software as explained in section A.1.1 of Appendix A, two measurements were performed under each set load condition:

- Measurement of 2 h duration with 1 s time step

In this case, the procedure to set the instrument was the same as what reported for the PV panels in section 3.3, with the only differences represented by:

- Settings under instrument *ACQU* menu:  
Speed = Window  
Window = 1 s
- Logging speed in the *Interval box* set to 5 (s)

- Measurement of 30 s duration with 20 ms time step

In this second case, because of the very low logging time step, the option High-Speed Mode had to be selected through the associated button. In accordance, the instrument settings were changed as reported below (in reference to Appendix A):

- Settings under instrument *ACQU* menu:  
Speed = Window  
Window = 20 ms
- Selected parameters in the Multilog window: active power, apparent power, power factor, RMS voltage, RMS current for all three phases and then frequency.<sup>17</sup>
- Logging speed set by selecting *Instrument Interval* mode<sup>18</sup>
- Measurement mode set by choosing *Log Real Time Table* mode.<sup>17, 18</sup>

---

<sup>17</sup> Due to the high speed logging, PPA is not capable to log variables that require data processing, such as reactive power. All these are limitations due to High-Speed Mode (see Appendix A).

<sup>18</sup> Also for the electrolyser data, the CSV format was set to European (“;”) to make the CSV file import to Excel easier and all the described settings configuration were saved to allow the experiments to be reproduced in the same way.



These double measurements at each load condition were necessary to get electrical data for a long interval and as precise as possible while respecting the power analyzer specifications.

- *Hydrogen production process parameters at the various percentage of full-load by means of PLC and HOGEN40 software*

Under each load condition, all the hydrogen production process parameters listed in section 2.3.2.4 were logged by using both PLC and the electrolyser software as explained in Appendix C. In all cases, the selected sample times were the minimum handled by each method, respectively, 10 s for the PLC and 5 s for HOGEN40 software.

A special attention was payed to the synchronization of all logging operations during each performed experiment. At last, the entire set of retrieved data were imported into Excel, as indicated in section A.2 of Appendix A, and the associated graphs were built for data analysis.

When analyzing the power data at 1 s time step, a phase power imbalance was observed over the three phases. While the power consumption of phase 1 changes according to the load percentage, the other two phases always show roughly the same behavior independently of the load condition. This can be explained by the fact that, due to the small size of the electrolyser, the DC voltage required by the electrolysis process is rectified via a single phase only so that the power consumption over phase 2 and 3 only represent power dissipation. In addition, a huge gap in power consumption was observed between the AC and the DC side. This is again related to the small size of the unit and to its consequent low efficiency.

As an example, the most significant results of active and reactive power (on the AC side), DC power obtained by multiplying voltage and current of the stack (on the DC side) and hydrogen output flow are depicted in the following figures. Figure 40 and 41 show active and reactive power for all three phases at full-load. Phase 2 and 3 plotted therein follow nearly the same pattern at the other load percentages as well. On the contrary, the change in active and reactive power of phase 1 by varying the load is highlighted in Figure 42 and 43. By comparing the H<sub>2</sub> output flow in Figure 45 with the AC power in Figure 42, the approximately linear relationship between (the mean value of) these two quantities is demonstrated. At last, the comparison between the DC stack power in Figure 44 and the AC power in the previous Figure 42 shows the losses due to the AC/DC conversion.

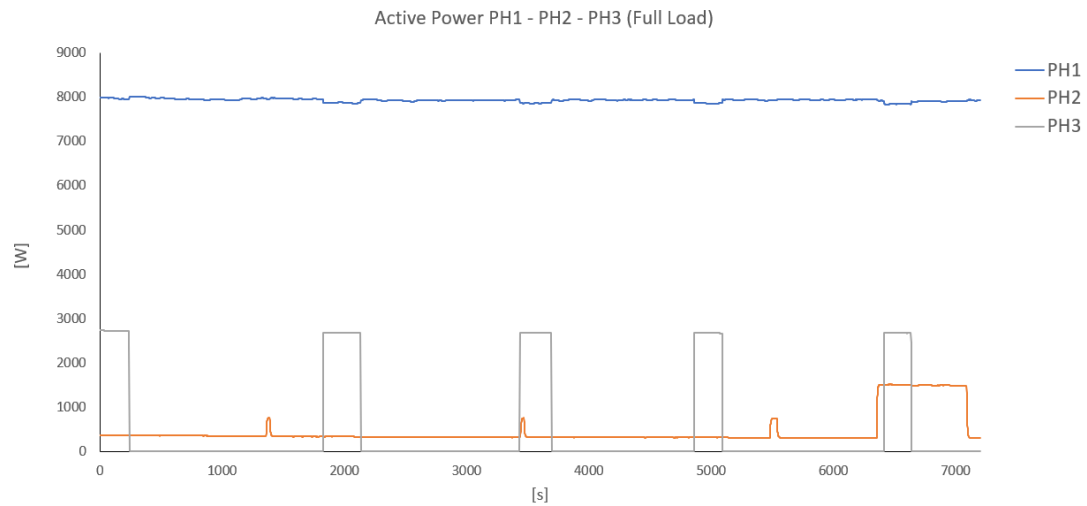


Fig. 40 – Three-phase active power at full-load

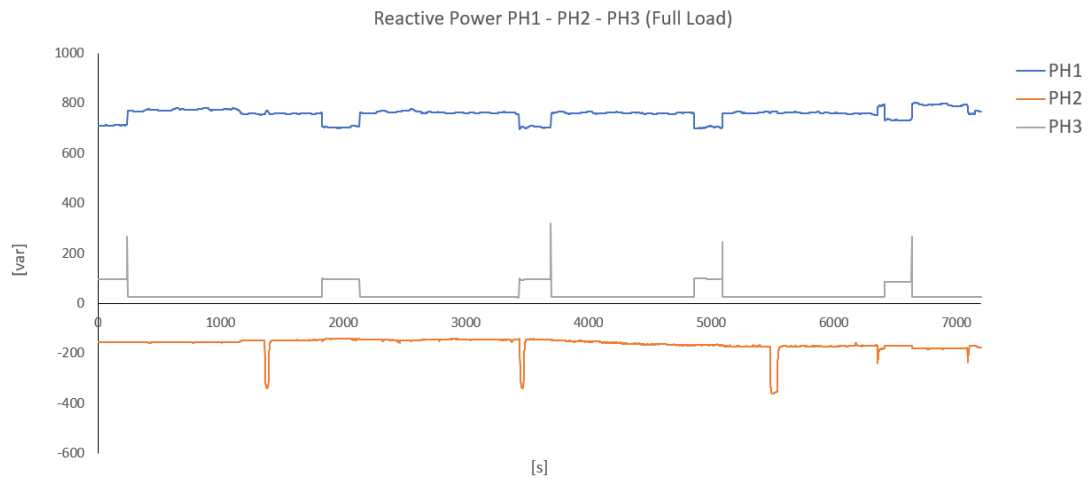


Fig. 41 – Three-phase reactive power at full-load

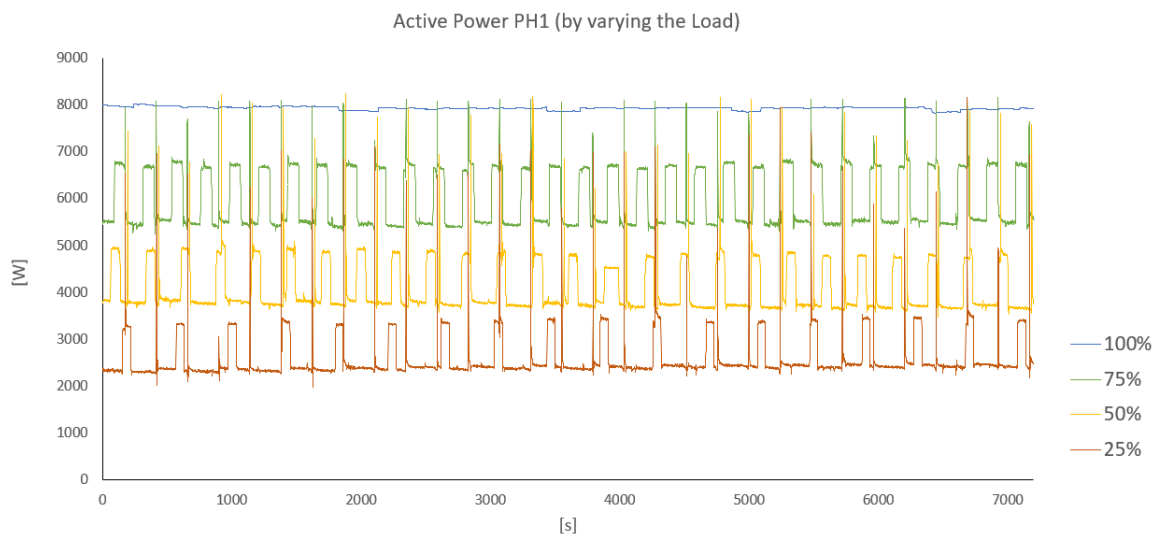


Fig. 42 – Active power of phase 1 by varying the load

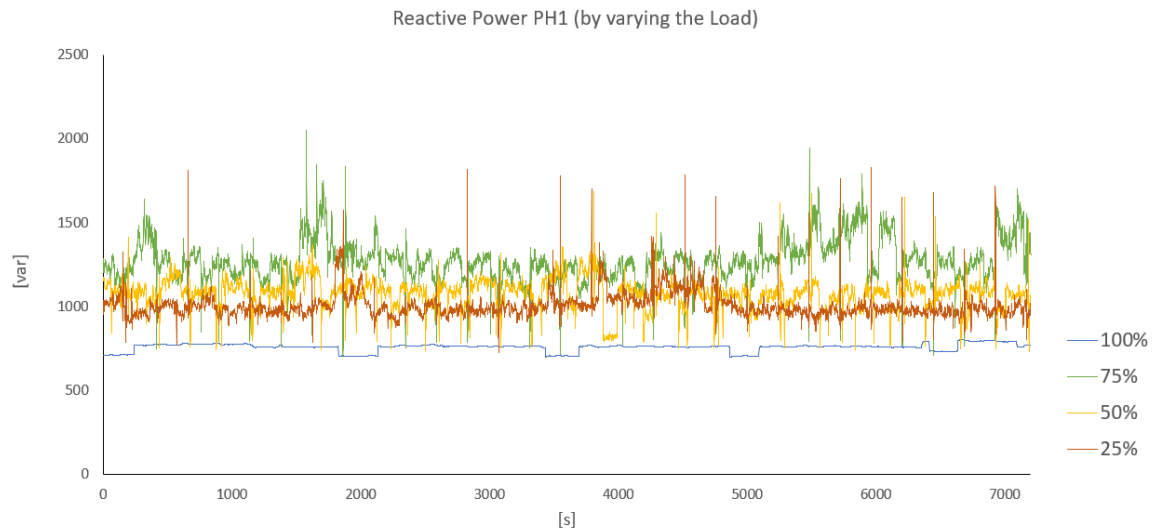


Fig. 43 – Reactive power of phase 1 by varying the load

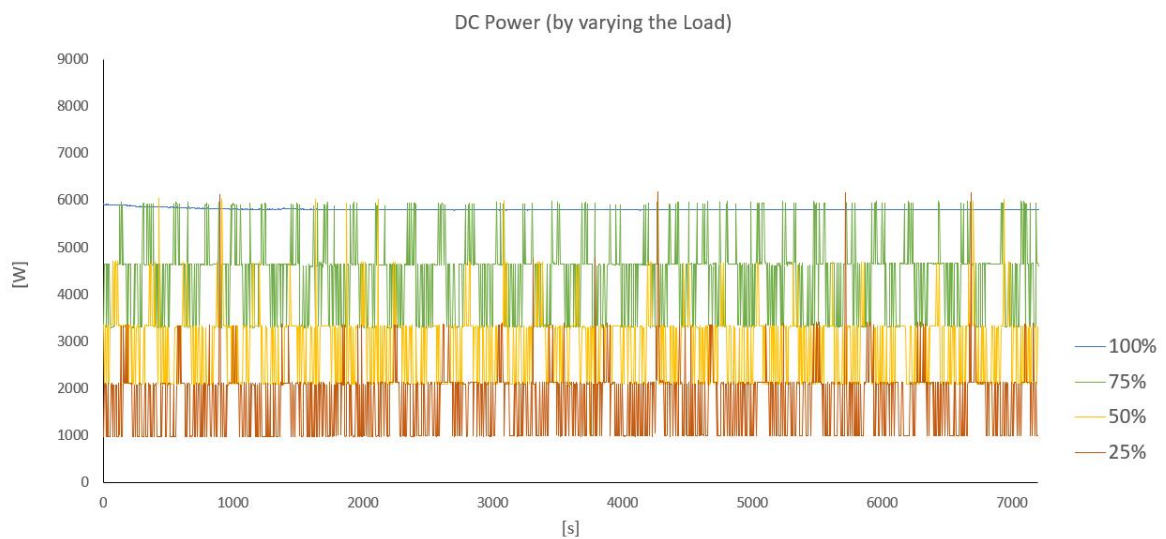


Fig. 44 – DC power by varying the load

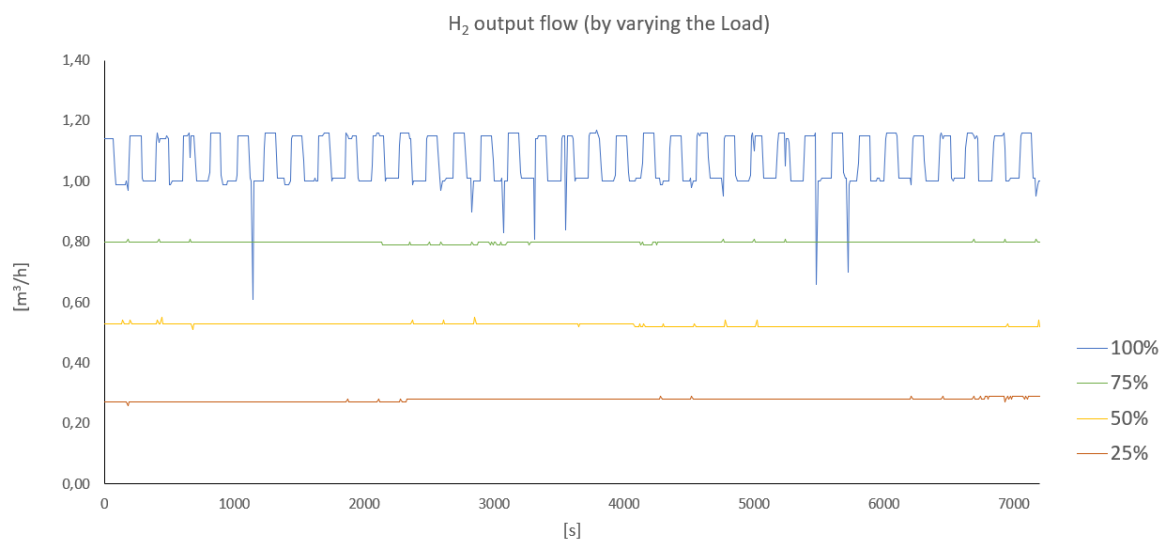


Fig. 45 – H<sub>2</sub> output flow by varying the load

Moreover, by analyzing the measured power at 20 ms time step, the active power of phase 1 for all the partial load conditions was observed to vary with a higher frequency and within a wider range than the respective waveforms measured at 1 s time step. This detail was made visible owing to the lower PPA sample time. Such huge and quick changes in power consumption at reduced load appear to be due to the way in which the control of the unit is built<sup>19</sup>.

As an illustration, Figure 46 shows the active power of all three phases measured during the 20 ms time step experiment at 25% of full-load. What said is proven by comparing these waveforms with the ones in Figure 47, representing the three-phase active power at the same percentage of full-load measured during the 1 s time step experiment. Finally, the comparison of the corresponding three-phase reactive power is possible by observing Figure 48 and 49.

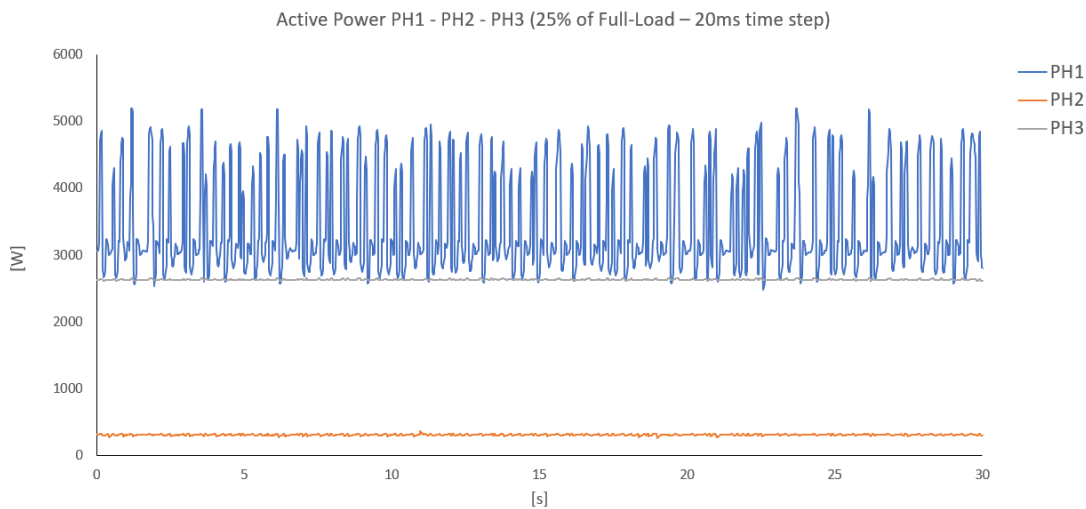


Fig. 46 – Three-phase active power at 25% of full-load and time step of 20 ms

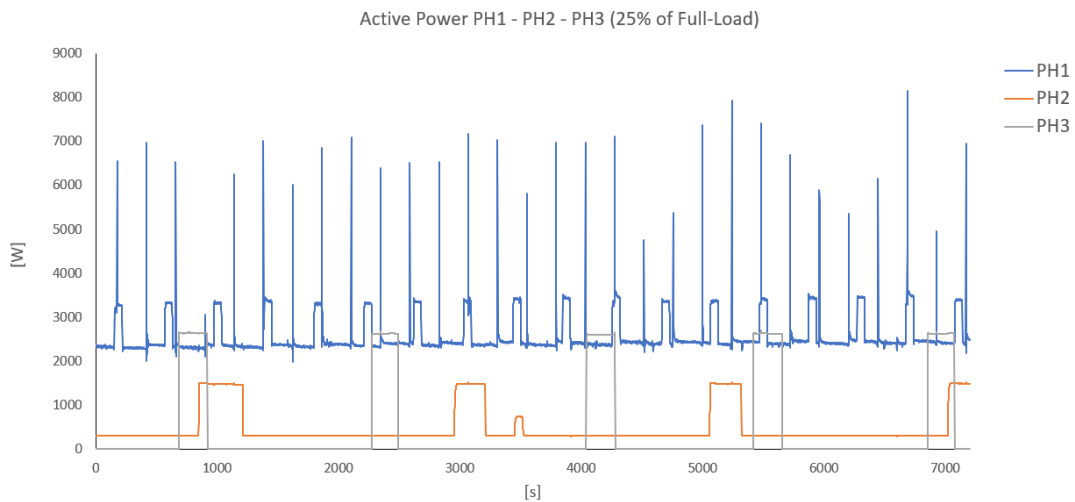


Fig. 47 – Three-phase active power at 25% of full-load and time step of 1 s

<sup>19</sup> Basically, the control is implemented in such a way to switch the supply of the stack in order to make the system pressure maintain a value around its setpoint.

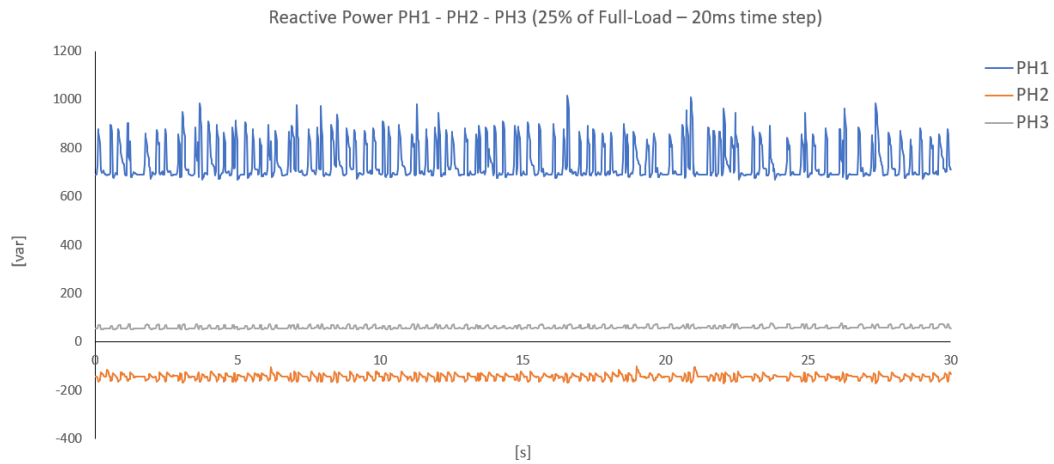


Fig. 48 – Three-phase reactive power at 25% of full-load and time step of 20 ms

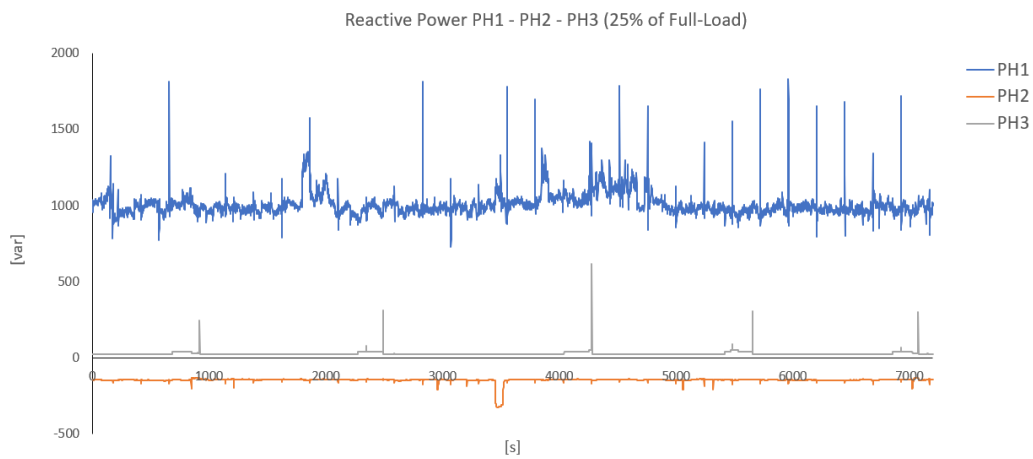


Fig. 49 – Three-phase reactive power at 25% of full-load and time step of 1 s

## 4.2.2 Processing the data

After both the measurements of 2 h and 30 s duration, the collected electrical data of active and reactive power were imported to Matlab for data-processing operations and stored into eight matrixes:

- $PQ\_x\_2h\_real$ , where  $x = 25, 50, 75, Full$  – P and Q at 25, 50, 75, 100% of full-load, measured during the experiment of 2 h duration and 1 s sample time;
- $PQ\_x\_30s\_real$ , where  $x = 25, 50, 75, Full$  – P and Q at 25, 50, 75, 100% of full-load, measured during the experiment of 30 s duration and 20 ms sample time.

As an example, a graphical representation of the matrix columns is provided as follows:

Tab. 19 – **PQ\_25\_2h\_real** [6910x7]

(6910 intervals of roughly 1 s within 2 h, including data at time 0. 291 fewer data due to instrument imprecisions)

	Column 1	Column 2	Column 3	Column 4	Column 5	Column 6	Column 7
	Seconds from 0	P PH1 [W]	P PH2 [W]	P PH3 [W]	Q PH1 [var]	Q PH2 [var]	Q PH3 [var]
1.	Second 0						
2.	Second 2.002						
3.	Second 3						
...	...						
6909.	Second 7199.3						
6910.	Second 7200.3						

Tab. 20 – **PQ\_25\_30s\_real** [1501x7]

(1501 intervals of roughly 20 ms within 30 s, including data at time 0. Non-uniform time steps due to instrument imprecisions)

	Column 1	Column 2	Column 3	Column 4	Column 5	Column 6	Column 7
	Seconds from 0	P PH1 [W]	P PH2 [W]	P PH3 [W]	Q PH1 [var]	Q PH2 [var]	Q PH3 [var]
1.	Second 0				Calculated from the PPA measured data through the formula: $Q_{abs,n} = \sqrt{S_n^2 - P_n^2}$ , where $n = 1, 2, 3^{20}$ Then $Q_1 = Q_{abs,1}$ , $Q_2 = -Q_{abs,2}$ , $Q_3 = Q_{abs,3}$		
2.	Second 0.021						
3.	Second 0.041						
...	...						
1501.	Second 30						

This schematic illustration is also representative of the other collected matrixes. Briefly, the instrument sample time appeared to be non-regular over the measured intervals, leading to fewer data than expected. It was then necessary to uniform the time step of all matrixes and, in order to do so, the same procedure of linear interpolation and extrapolation applied for the PV panels in section 3.4 was used. As a result, a uniform time step of 20 ms was obtained for all electrical variables measured during both the 2 h duration and 30 s duration experiments. In particular, the matrixes are identified as:

- **PQ\_x\_2h\_lin**, where  $x = 25, 50, 75, Full$  – P and Q at 25, 50, 75, 100% of full-load, corresponding to an interval of 2 h, with uniform time step of 20 ms obtained by linear interpolation;
- **PQ\_x\_30s\_lin**, where  $x = 25, 50, 75, Full$  – P and Q at 25, 50, 75, 100% of full-load, corresponding to an interval of 2 h, with uniform time step of 20 ms obtained by linear interpolation.

<sup>20</sup> The PPA does not measure reactive power in High-Speed Mode

An exemplification of the results at 25% of full-load is given below:

Tab. 21 – **PQ\_25\_2h\_lin** [360001x7]

(360001 intervals of 20 ms within 2 h, including data at time 0. Time steps precisely equal to 20 ms)

	Column 1	Column 2	Column 3	Column 4	Column 5	Column 6	Column 7
1.	Second 0	P PH1 [W]	P PH2 [W]	P PH3 [W]	Q PH1 [var]	Q PH2 [var]	Q PH3 [var]
2.	Second 0.02						
3.	Second 0.04						
...	...						
360001.	Second 7200						

Tab. 22 – **PQ\_25\_30s\_lin** [1501x7]

(1501 intervals of 20 ms within 30 s, including data at time 0. Time steps precisely equal to 20 ms)

	Column 1	Column 2	Column 3	Column 4	Column 5	Column 6	Column 7
1.	Second 0	P PH1 [W]	P PH2 [W]	P PH3 [W]	Q PH1 [var]	Q PH2 [var]	Q PH3 [var]
2.	Second 0.02						
3.	Second 0.04						
...	...						
1501.	Second 30						

At this point, according to [31], the process of unification of data within the same time step required a further operation to maintain the total energy of the final pattern equal to the initial one. This method has been already illustrated as part of the PV panels modelling in section 3.4. The same formulas were applied in this case to all the eight matrixes of active and reactive power. By reminding the already given notation, an exemplification of the procedure carried out for the 2 h experiment is presented below:

- $T$  represents the total period of analysis, equal to:  $T = 2 \text{ h} = 7200 \text{ s}$
- $p_{T,\tau_i}$  represents the vector of initial values, each one with different size and irregular time step, thus:

$$p_{1_{2h,\tau_i}} = PQ\_25\_2h\_real(:,2) \rightarrow \text{PH1 active power}$$

$$p_{2_{2h,\tau_i}} = PQ\_25\_2h\_real(:,3) \rightarrow \text{PH2 active power}$$

$$p_{3_{2h,\tau_i}} = PQ\_25\_2h\_real(:,4) \rightarrow \text{PH3 active power}$$

$$p_{4_{2h,\tau_i}} = PQ\_25\_2h\_real(:,5) \rightarrow \text{PH1 reactive power}$$

$$p_{5_{2h,\tau_i}} = PQ\_25\_2h\_real(:,6) \rightarrow \text{PH2 reactive power}$$

$$p_{6_{2h,\tau_i}} = PQ\_25\_2h\_real(:,7) \rightarrow \text{PH3 reactive power}$$

All vectors with 6910 rows and non-uniform time step.

- $\tilde{p}_{T,\tau_o}$  represents the vector calculated from the one above on the basis of geometric considerations only (linear interpolation in this case), thus:

$$\tilde{p}_{1_{2h,\tau_o}} = PQ\_25\_2h\_lin(:,2) \rightarrow \text{PH1 active power}$$

$$\tilde{p}_{2_{2h,\tau_o}} = PQ\_25\_2h\_lin(:,3) \rightarrow \text{PH2 active power}$$

$$\tilde{p}_{3_{2h,\tau_o}} = PQ\_25\_2h\_lin(:,4) \rightarrow \text{PH3 active power}$$

$$\tilde{p}_{4_{2h,\tau_o}} = PQ\_25\_2h\_lin(:,5) \rightarrow \text{PH1 reactive power}$$

$$\tilde{p}_{5_{2h,\tau_o}} = PQ\_25\_2h\_lin(:,6) \rightarrow \text{PH2 reactive power}$$

$$\tilde{p}_{6_{2h,\tau_o}} = PQ\_25\_2h\_lin(:,7) \rightarrow \text{PH3 reactive power}$$

All vectors with 360001 rows and time step precisely equal to 20 ms.

The total energies  $Wk_i$  and  $Wk_o$  were calculated by respectively integrating the patterns  $pk_{2h,\tau_i}$  and  $\tilde{p}k_{2h,\tau_o}$ ,  $k = 1, \dots, 6$  over the period  $T^{21}$ . The correction factors were then obtained through the ratio  $\xi_k = Wk_i/Wk_o$ . At last, the final vectors with regular time step of 1 s and conserved overall energy were computed through the formula:

$$pk_{2h,\tau_o} = \xi_k \cdot \tilde{p}k_{2h,\tau_o} \quad (12)$$

The final test was carried out by the integration of the new patterns  $pk_{2h,\tau_o}$ ,  $k = 1, \dots, 6$  and the comparison of the resulting total energies  $Wk'_o$  with the initial energies  $Wk_i$ . Since the maximum difference  $|Wk'_o - Wk_i|$  turned out to be  $<10^{-9}$ , it was proven that the overall energy was preserved throughout the processing.

The same procedure was applied also to the 30 s patterns for all the load operating conditions. At the end of the process, the resulting vectors  $pk_{2h,\tau_o}$  and  $pk_{30s,\tau_o}$ ,  $k = 1, \dots, 6$  were stored in matrixes, named:

- *PQ\_x\_2h\_Econs*, where  $x = 25, 50, 75, Full$  – P and Q at 25, 50, 75, 100% of full-load, corresponding to an interval of 2 h, with uniform time step of 20 ms and energy conserved;
- *PQ\_x\_30s\_Econs*, where  $x = 25, 50, 75, Full$  – P and Q at 25, 50, 75, 100% of full-load, corresponding to an interval of 30 s, with uniform time step of 20 ms and energy conserved;

A schematic example of the matrixes for both 2 h and 30 s experiments at 25% load is given below:

Tab. 23 – *PQ\_25\_2h\_Econs* [360001x7]

	Column 1	Column 2	Column 3	Column 4	Column 5	Column 6	Column 7
1.	Second 0	$p1_{2h,\tau_o}$	$p2_{2h,\tau_o}$	$p3_{2h,\tau_o}$	$p4_{2h,\tau_o}$	$p5_{2h,\tau_o}$	$p6_{2h,\tau_o}$
2.	Second 0.02	(P PH1 [W])	(P PH2 [W])	(P PH3 [W])	(Q PH1 [var])	(Q PH2 [var])	(Q PH3 [var])
...	...						
360001.	Second 7200						

Tab. 24 – *PQ\_25\_30s\_Econs* [1501x7]

	Column 1	Column 2	Column 3	Column 4	Column 5	Column 6	Column 7
1.	Second 0	$p1_{30s,\tau_o}$	$p2_{30s,\tau_o}$	$p3_{30s,\tau_o}$	$p4_{30s,\tau_o}$	$p5_{30s,\tau_o}$	$p6_{30s,\tau_o}$
2.	Second 0.02	(P PH1 [W])	(P PH2 [W])	(P PH3 [W])	(Q PH1 [var])	(Q PH2 [var])	(Q PH3 [var])
...	...						
1501.	Second 1500						

Therefore, at this point, two matrixes uniformed within the same time step of 20 ms are available for each load operating condition: *PQ\_x\_2h\_Econs* have an overall duration of 2 h (360001 values) and a lower resolution since the data were acquired by using a 1 s sample

<sup>21</sup> This calculation was implemented by means of the Matlab function  $A = \text{trapz}(X,Y)$ , where  $X$  is the time base, represented by the vector  $PQ\_25\_2h\_real(:,1)$  when integrating  $pk_{2h,\tau_i}$  and  $PQ\_25\_2h\_lin(:,1)$  when integrating  $\tilde{p}k_{2h,\tau_o}$ .



time; *PQ\_x\_30s\_Econs* have an overall duration of 30 s (1501 values) and a very high resolution since the data were acquired by using a sample time of 20 ms.

In order to get final patterns with the highest possible duration and resolution, the idea was then to overlay these two waveforms by treating the former as the mean value and the latter as the harmonic component. In details, the process consisted in: averaging the 30 s vector and subtracting the obtained mean value to the 30 s waveform, replicating this pattern multiple times to fit the length of the 2 h waveform, adding the resulting pattern to the 2 h waveform. This was done for both active and reactive power, for all three phases and at each loading condition.

The results were stored into four new matrixes, named:

*PQ\_x\_overlay*, where  $x = 25, 50, 75, \text{Full}$  – P and Q at 25, 50, 75, 100% of full-load, obtained by overlaying *PQ\_x\_2h\_Econs* and *PQ\_x\_30s\_Econs*.

For the sake of consistency, the representation of the resulting active and reactive power of phase 1 at 25% of full-load is provided in Figure 50 and 51. From this graph, it is possible to see that the mean value of the final pattern follows the initial 2 h waveform (Figure 47 and 49), while, by zooming in, the 30 s waveform behavior (Figure 46 and 48) is found.

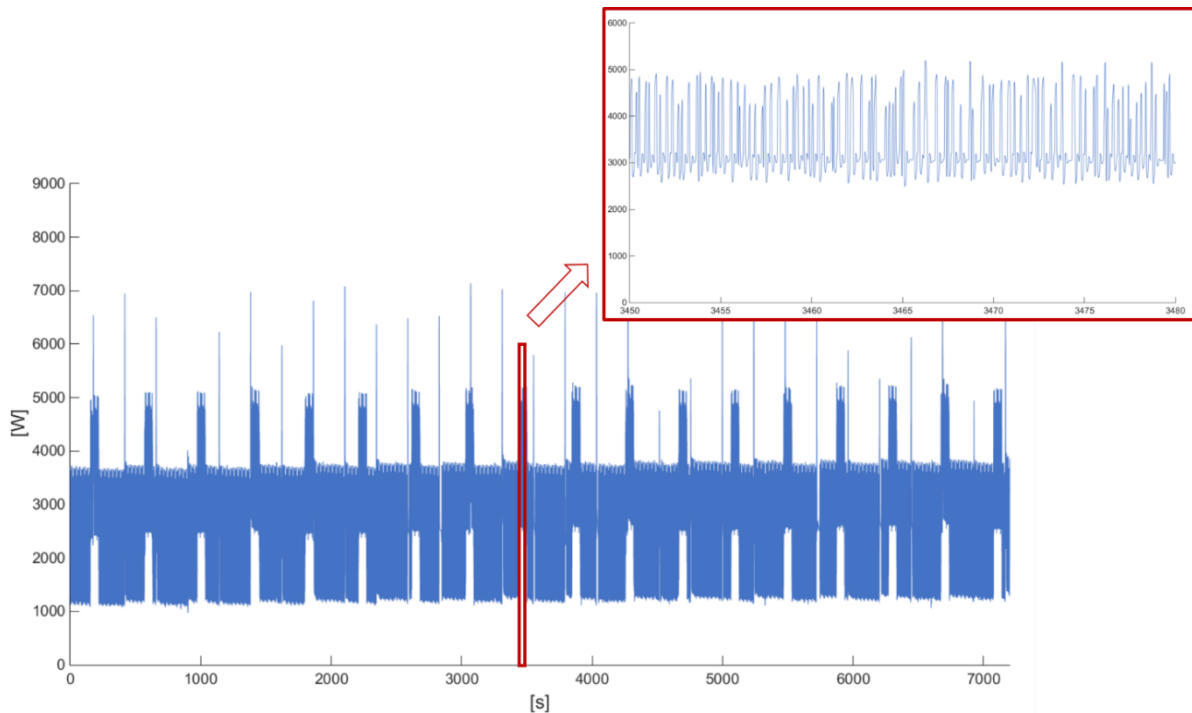


Fig. 50 – Active power of phase 1 at 25% of full-load after the overlaying process (with zoom)

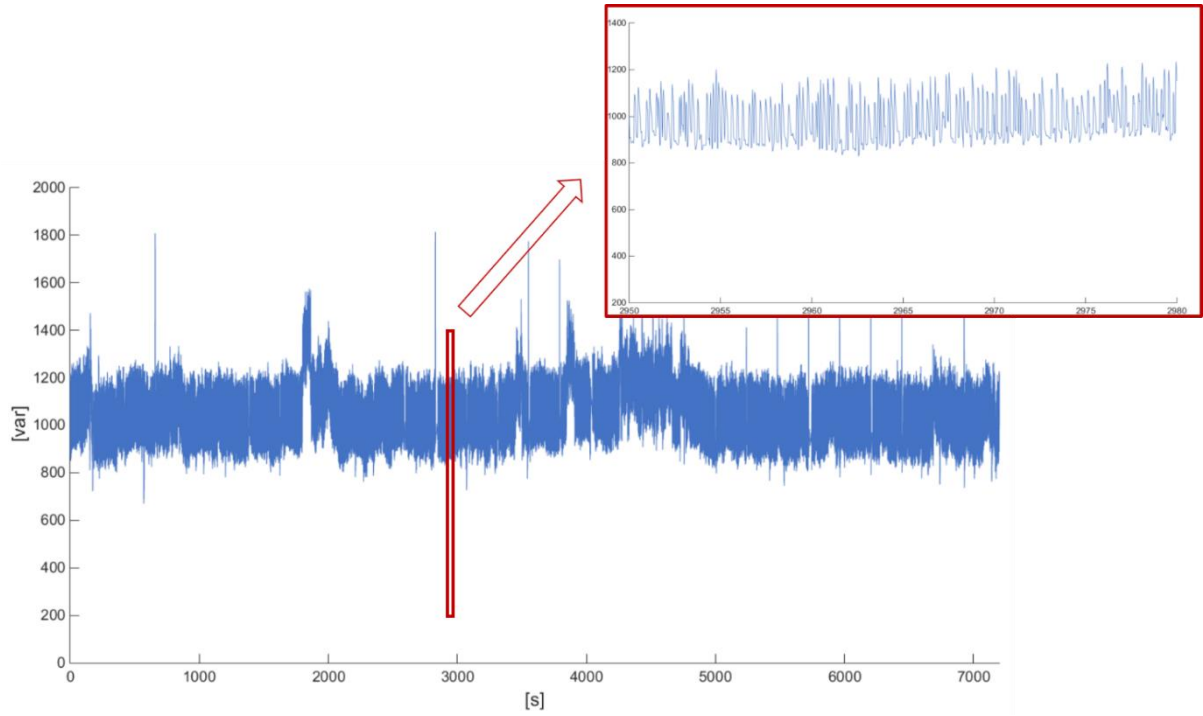


Fig. 51 – Reactive power of phase 1 at 25% of full-load after the overlaying process (with zoom)

The final step of the data processing was to make sure that the total energy of the newly obtained patterns preserved the total energy of the real measured ones. Once again, this operation was carried out with reference to the formulas in [31] and reported in the PV panels section 3.4. As an example, the calculation performed for the patterns at 25% of full-load is shown below by using the well-known notation:

- The total period of analysis is:  $T = 2 \text{ h} = 7200 \text{ s}$
- The initial vectors with irregular time steps are still represented by the real measured data:
  - $p1_{2h,\tau_i} = PQ\_25\_2h\_real(:,2) \rightarrow \text{PH1 active power}$
  - $p2_{2h,\tau_i} = PQ\_25\_2h\_real(:,3) \rightarrow \text{PH2 active power}$
  - $p3_{2h,\tau_i} = PQ\_25\_2h\_real(:,4) \rightarrow \text{PH3 active power}$
  - $p4_{2h,\tau_i} = PQ\_25\_2h\_real(:,5) \rightarrow \text{PH1 reactive power}$
  - $p5_{2h,\tau_i} = PQ\_25\_2h\_real(:,6) \rightarrow \text{PH2 reactive power}$
  - $p6_{2h,\tau_i} = PQ\_25\_2h\_real(:,7) \rightarrow \text{PH3 reactive power}$
- The vectors with regular time steps obtained from the ones above by geometric considerations (overlaying of waveforms) are the columns of the newly obtained matrixes:
  - $\tilde{p}1_{2h,\tau_o} = PQ\_25\_overlay(:,2) \rightarrow \text{PH1 active power}$
  - $\tilde{p}2_{2h,\tau_o} = PQ\_25\_overlay(:,3) \rightarrow \text{PH2 active power}$
  - $\tilde{p}3_{2h,\tau_o} = PQ\_25\_overlay(:,4) \rightarrow \text{PH3 active power}$
  - $\tilde{p}4_{2h,\tau_o} = PQ\_25\_overlay(:,5) \rightarrow \text{PH1 reactive power}$
  - $\tilde{p}5_{2h,\tau_o} = PQ\_25\_overlay(:,6) \rightarrow \text{PH2 reactive power}$
  - $\tilde{p}6_{2h,\tau_o} = PQ\_25\_overlay(:,7) \rightarrow \text{PH3 reactive power}$

As done before, the total energies  $Wk_i$  and  $Wk_o$  corresponding to the integral of the patterns  $pk_{T,\tau_i}$  and  $\tilde{p}k_{T,\tau_o}, k = 1, \dots, 6$  over the period  $T$  were calculated<sup>22</sup>, as well as the correction factor  $\xi_k = Wk_i/Wk_o$ . Finally, the ultimate vectors with preserved overall energy were computed through the well-known formula (12). The final check consisting in the comparison  $|Wk'_o - Wk_i|$  between the total energy  $Wk'_o$  resulting from the patterns  $pk_{T,\tau_o}, k = 1, \dots, 6$  and the known  $Wk_i$  resulted  $<10^{-9}$  in the worst case, which means that overall energy was actually preserved throughout the entire processing.

As the ultimate step, the resulting vectors were included in the final matrixes, named:

$PQ\_x\_Econs\_final$ , where  $x = 25, 50, 75, \text{Full}$  – final P and Q at 25, 50, 75, 100% of full-load, with energy conserved.

The matrix for the 25% case is schematized below:

Tab. 25 –  $PQ\_25\_Econs\_final$  [360001x7]

	Column 1	Column 2	Column 3	Column 4	Column 5	Column 6	Column 7
1.	Second 0	$p1_{2h,\tau_o}$	$p2_{2h,\tau_o}$	$p3_{2h,\tau_o}$	$p4_{2h,\tau_o}$	$p5_{2h,\tau_o}$	$p6_{2h,\tau_o}$
2.	Second 0.02						
...	...	(P PH1 [W])	(P PH2 [W])	(P PH3 [W])	(Q PH1 [var])	(Q PH2 [var])	(Q PH3 [var])
360001.	Second 7200						

Lastly, for all the analyzed load conditions, the patterns of active and reactive power of phase 1 resulting from the entire data-processing operation are depicted in Figure 52 and 53. These are particularly interesting if compared with the above Figure 42 and 43, representing the same parameters obtained by measurements.

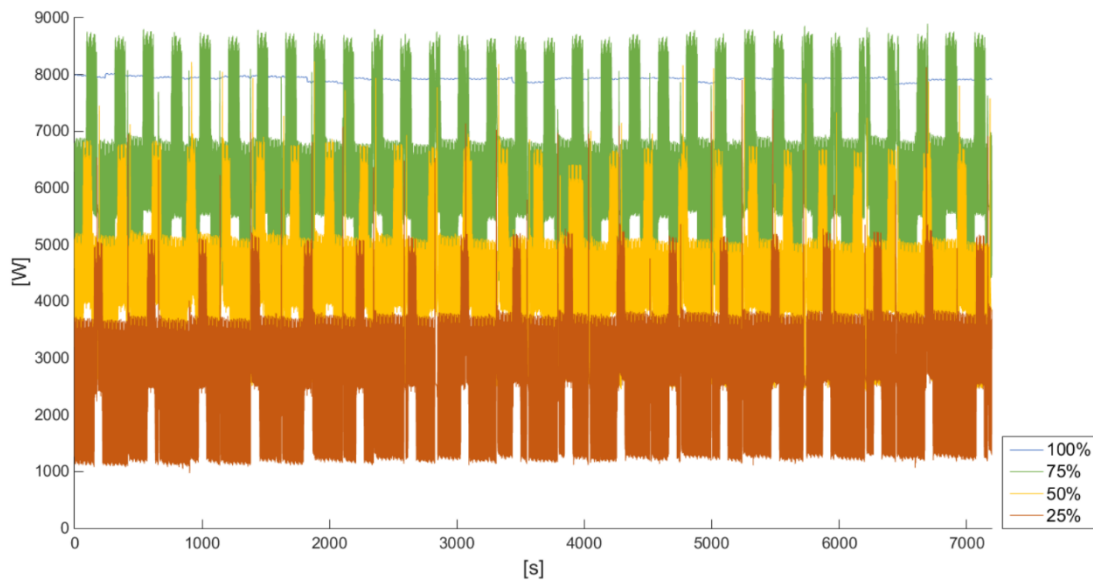


Fig. 52 – Result of the data processing: active power of phase 1 by varying the load

<sup>22</sup> Again, the calculation was implemented by using the Matlab function  $A = \text{trapz}(X, Y)$ , where  $X$  is the time vector, thus  $PQ\_25\_2h\_real(:,1)$  for  $pk_{2h,\tau_i}$  and still  $PQ\_25\_2h\_lin(:,1)$  for  $\tilde{p}k_{2h,\tau_o}$ .

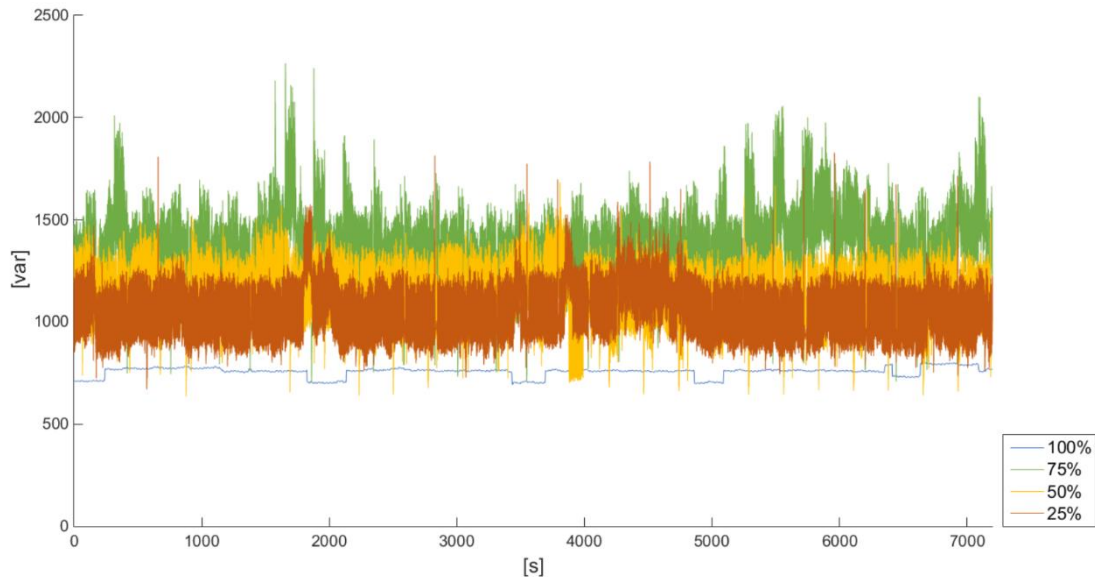


Fig. 53 – Result of the data processing: reactive power of phase 1 by varying the load

### 4.2.3 Creation of the model

By referring back to the concept presented in 4.1, the idea behind the measuring and following data processing was to provide both active and reactive power consumed at different loading conditions to be given as input to the *Three-Phase Dynamic Load* block. This block, along with the processed power profiles, was included in the complete electrolyser model which is depicted in Figure 54.

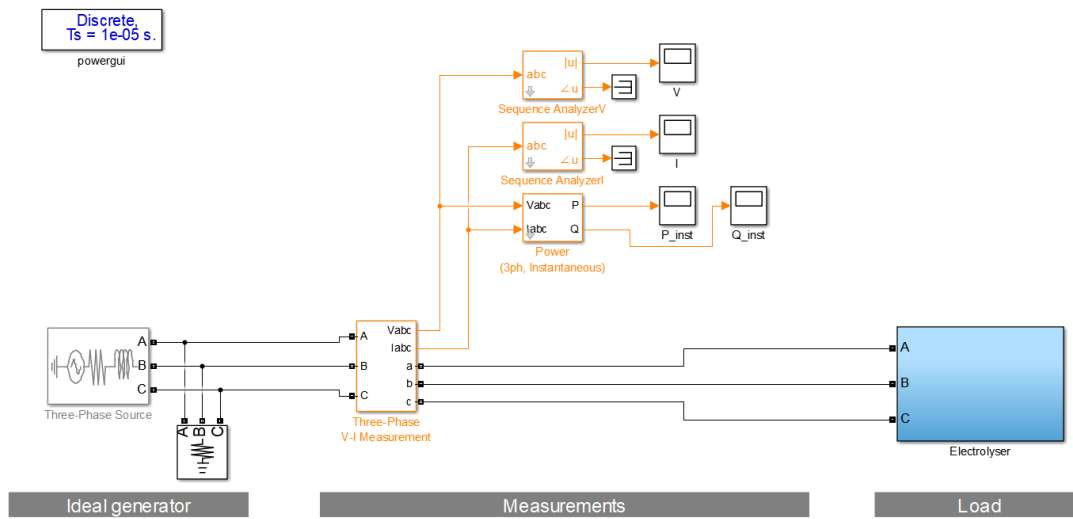


Fig. 54 – Electrolyser model

This view is conceptually similar to the one of the already illustrated PV panels model. An ideal generator modeled through a *Three-Phase Source* block simulates the power supply and proper measuring blocks monitor all the needed electrical variables. Once again, this only represents a basic test setup, after which the model can be added to a grid simulation of desired complexity.

Figure 55 shows in detail the *Electrolyser* subsystem. It contains a *Three-Phase Dynamic Load* block whose active and reactive power are externally controlled and received from the set of blocks on the left side. This group is formed by four subsystems, one for each percentage of

full-load and all with an identical layout, exemplified by the 25% case in Figure 56. Here, the subsystem *electrical\_data\_25* contains the columns of the above described matrixes of active and reactive power (named  $PQ\_x\_Econs\_final$ , where  $x = 25, 50, 75, \text{Full}$ ) in the form of constant vectors. The following blocks (indicated with  $f(t)$ ) are aimed at uploading subsequent cells of the arrays in synchrony with the clock implemented by the *Counter* subsystem. This has been already shown for the PV panels model in the previous Figure 36. The total active and reactive powers are then calculated by summing the values over the three phases at each time step. Moving back to the top view of Figure 55, a *Multiport Switch* and a *Constant* block allow to select the desired electrolyser load. The constant block can eventually be substituted with the desired control signal.

In addition, some useful  $H_2$  production process data have been included in the model as well. These are the profiles measured during the experiments explained in the previous section 4.2.1, further processed just with the purpose of unification within the chosen simulation time step of 20 ms. Specifically, the  $H_2$  flow profile can be used in case the  $H_2$  production at the current loading condition is needed, while the stack voltage and current profiles, if multiplied, can be used to monitor the power consumption on the DC side.

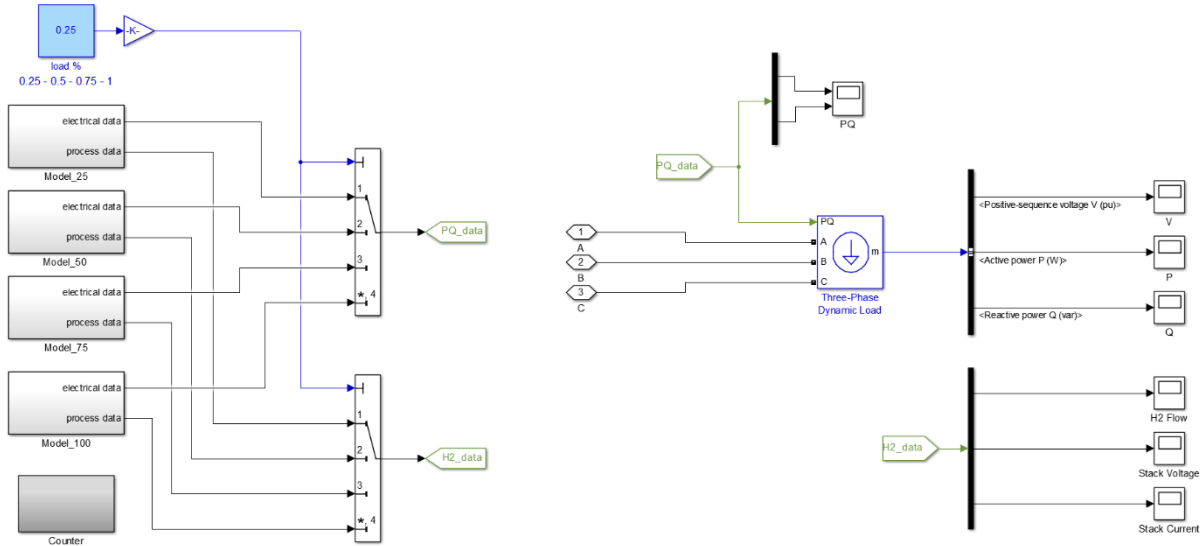


Fig. 55 – Electrolyser model: *Electrolyser* subsystem

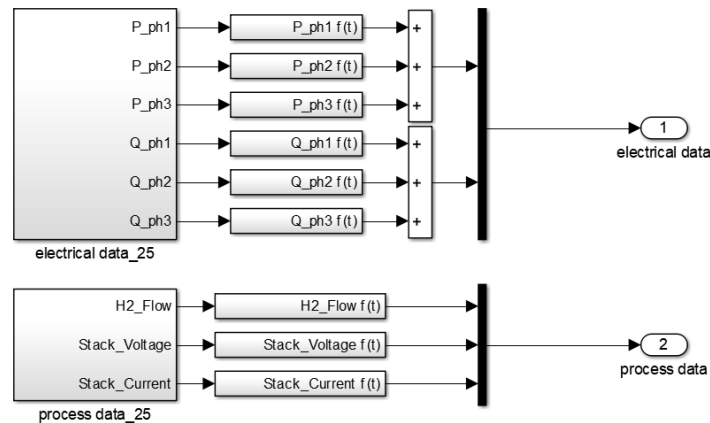


Fig. 56 – Electrolyser model: *electrical\_data\_25* subsystem

## 4.3 Second approach: dynamic

### 4.3.1 Collecting the measurements

In order to improve this static model, a second approach was intended to investigate the electrolyser dynamics, following the idea in [32]. This was possible by means of the new flow controller, which has been purchased and installed for the purpose of allowing studies on the electrolyser dynamic behavior. In fact, as confirmed during the first series of experiments, the hydrogen production rate can be considered proportional to the electrical current of the stack, this affecting the overall electrical consumption of the unit. It follows that a step change in the setpoint of hydrogen output flow produces a sudden and roughly proportional change of AC power consumption of the entire system. On this basis, the following operations were performed:

- *Control and measurement of the output hydrogen flow rate to realize step changes in the range 0-25%, 25-50%, 50-75%, 75-100% of full-load by means of the flow controller*

Four tests were performed by acting on the flow controller setpoint in such a way to get a step change of H<sub>2</sub> flow in the range 0-25%, 25-50%, 50-75% and 75-100% of the maximum flow rate. This was done by means of the software interface Modbus Tester and through a setpoint conversion necessary to fit the flow controller settings as explained in Appendix E. Considering that the electrolyser is not able to maintain the stand-by mode at zero load, the first experiment indicated as 0-25% was carried out from off-state. After properly arranging the electrolyser connection to the measured grid according to section D.2 of Appendix D, the electrolyser system was started by following the instructions given in Appendix B. The setpoint was set to 25% of the maximum flow rate before the start-up and kept constant throughout the measurement. For the following experiments referred to as 25-50%, 50-75% and 75-100%, the corresponding step change was given after 2 min from the beginning of the measurements.

Since the mentioned program only allows to set the H<sub>2</sub> flow setpoint (Modbus write) and monitor the H<sub>2</sub> output (Modbus read), the operations of data logging and saving were carried out for both setpoints and real signals by implementing a Matlab code on this purpose. This code, together with the related comments, is included in the section fully dedicated to the flow controller communication in Appendix E. Given that these experiments were aimed at dynamic studies, the sample time chosen for the logging was the minimum allowed by the communication flow controller-Matlab and equal to about 50 ms<sup>23</sup>.

- *Measurement of the electrical variables related to the electrolyser consumed AC power (upstream of the rectifier – AC/DC conversion) during the step changes by means of the PPA power analyzer.*

---

<sup>23</sup> The minimum sample time that can be handled by the flow controller is 30 ms and the Modbus Tester interface is able to monitor H<sub>2</sub> flow data by respecting this minimum value. However, the further communication layer introduced by Matlab adds a latency which rises the minimum sample time to 50 ms.

After connecting DataLogger software to the power analyzer according to section A.1.1 of Appendix A, the instrument was set by loading the same settings configuration already used during the static analysis for the measurements of 30 s duration and 20 ms time step. Accordingly, the sample time for each dynamic test was kept equal to 20 ms, which is the lowest that the power analyser is able to support. This was possible since the dynamic measurements had to last only few minutes (in any case less than 10 min), so that the duration limit for the power analyzer High-Speed Mode could be respected.

- *Measurement of the hydrogen production process parameters during the step changes by means of PLC and HOGEN40 software*

During each of the four dynamic experiments, all the hydrogen production process parameters illustrated in section 2.3.2.4 were logged by means of both PLC and the electrolyser software according to Appendix C. Once again, the sampling times were set to the minimum value supported by the programs. However, since these were respectively equal to 10 s for the PLC and 5 s for HOGEN40 software, the resulting data were meaningless for the purpose of dynamic analysis.

As usual, great care was taken in synchronizing all measuring devices during each performed experiment. Finally, the complete series of collected data were loaded into Excel files, as indicated in section A.2 of Appendix A, and the graphs were plot for the purpose of data analysis.

The results of all four dynamic experiments can be commented by looking at the graphs of three-phase active power and focusing on phase 1, which has been already said to be the only phase used for rectifying the DC voltage. From the graph of the 0-25% experiment shown in Figure 57 it is possible to observe the electrolyser start-up<sup>24</sup>. In particular, the various operating states described in section 2.3.2.2 are visible: the first part with a low power consumption of around 400 W corresponds to the generate-vent mode; then full power of 8 kW is applied to the stack in order to build up system pressure in correspondence of the pressurize storage state. At last, after the start-up phase, the power consumption drops and the steady-state at 25% of full-load is reached almost instantaneously. In this state, the power variates within a wide range around a mean value roughly equal to 25% of the maximum power (about 8 kW). This is made clear by plotting in the same graph the setpoint given to the flow controller, converted from percentage of full H<sub>2</sub> flow rate to percentage of full AC power consumption.

---

<sup>24</sup> The behavior of the electrolyser under study during the start-up, both hot and cold, has been already partially analyzed in [33].

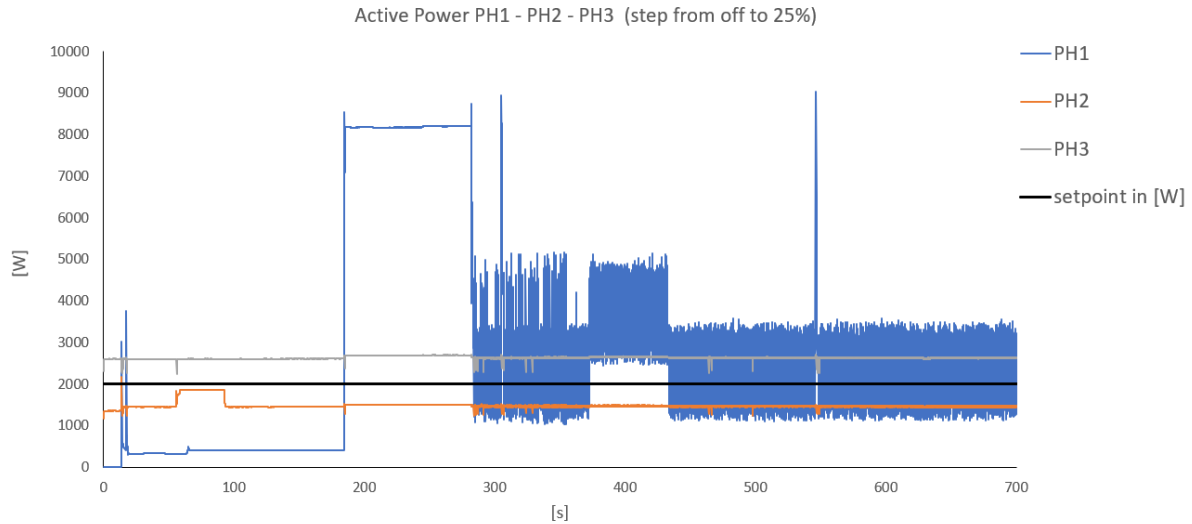


Fig. 57 – Active power of phase 1, 2 and 3 – start-up and step to 25% of full-load

From the graph of the 25-50% experiment presented in Figure 58 it is possible to see a sudden change from the steady-state at 25% of full-load to the next steady-state at 50% of full-load, both marked by the variation of power consumption around the line which represents the setpoint.

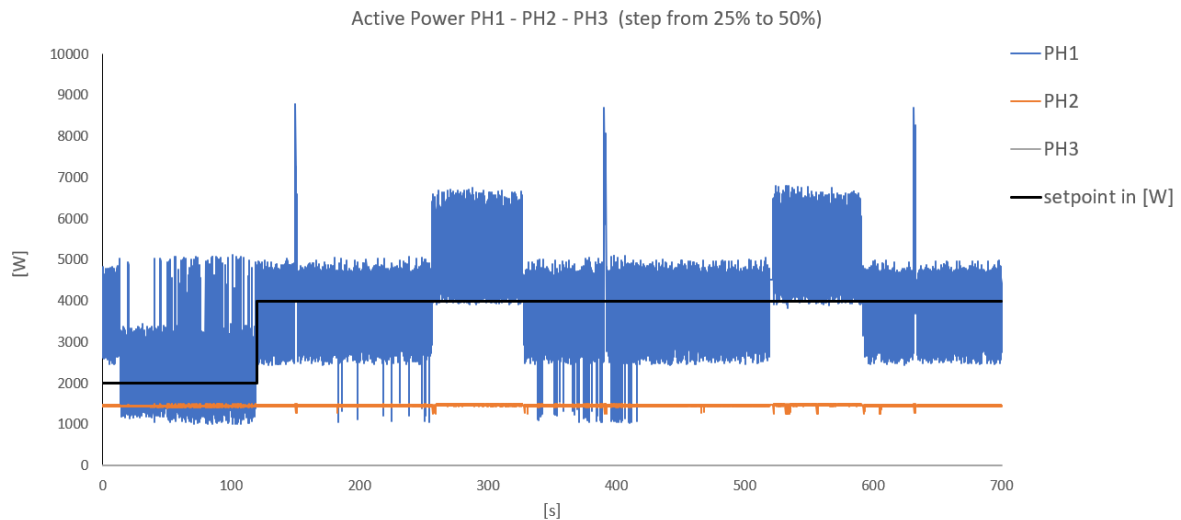


Fig. 58 – Active power of phase 1, 2 and 3 – step from 25 to 50% of full-load

The same behavior can be inferred also from the 50-75% and 75-100% experiments, whose graphs are shown in Figure 59 and 60. Basically, at a certain percentage of full  $H_2$  flow rate the active power variates approximately around the same percentage of maximum power consumption. Only at full  $H_2$  flow rate the power is roughly constant and exactly equal to the maximum power consumption. In any case, the dynamic of the change from one steady-state to another is almost absent.



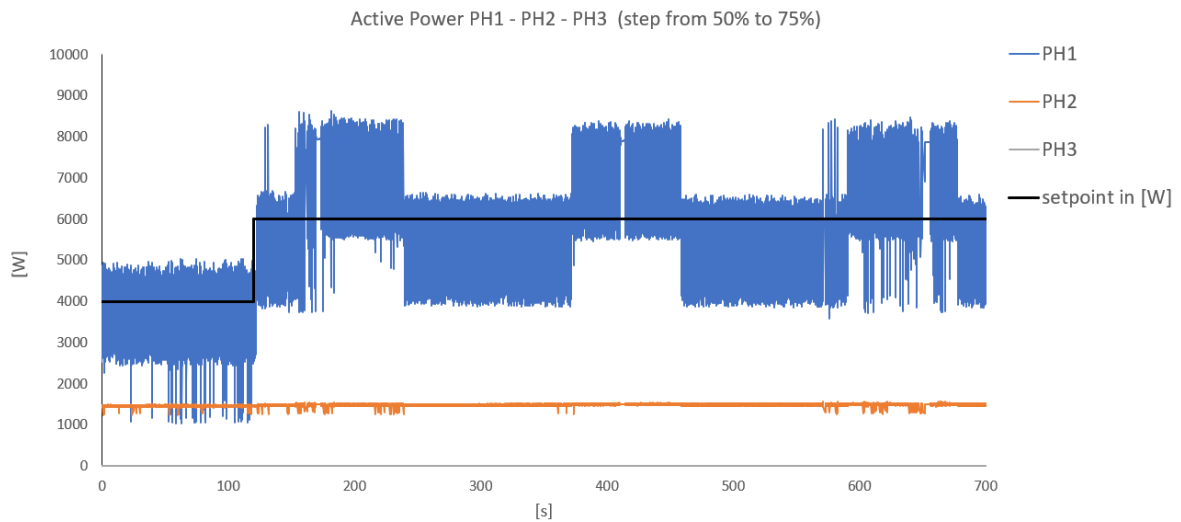


Fig. 59 – Active power of phase 1, 2 and 3 – step from 50 to 75% of full-load

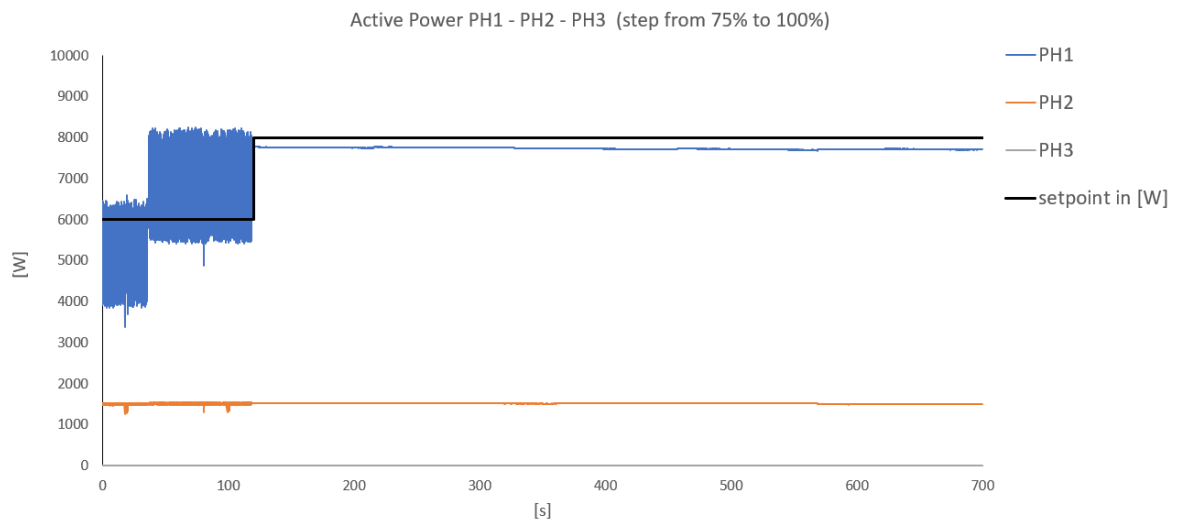


Fig. 60 – Active power of phase 1, 2 and 3 – step from 75 to 100% of full-load

Among the other measured variables, the only one that is worth to analyze is the  $H_2$  flow. In fact, since the change of  $H_2$  flow setpoint only affects the active power consumption, the reactive power is not relevant for the purpose of analyzing the electrolyser dynamic behavior. Also the DC power of the stack is not considered in this context because, on one hand, no dynamic is visible from the performed measurements due to the maximum sample time of the electrolyser software equal to 5 s; on the other hand, the power on the DC side must simply show the same dynamic behavior of the power measured on the AC side minus losses.

By looking at the graph in Figure 61, showing the  $H_2$  output flow for the 0-25% experiment, it can be observed that the dynamic lasts about 14 s. This is quite slow due to the fact that the start-up phase is still ongoing, thus the electrolyser unit is still building up pressure. In contrast, from the graph in Figure 62 which illustrates the  $H_2$  output flow for the 25-50% experiment, it is possible to see a very fast dynamic with less than 1 s duration. This case is also representative of the 50-75% and 75-100% experiments, in which the  $H_2$  output flow appears to change within the interval of 1 s as well.

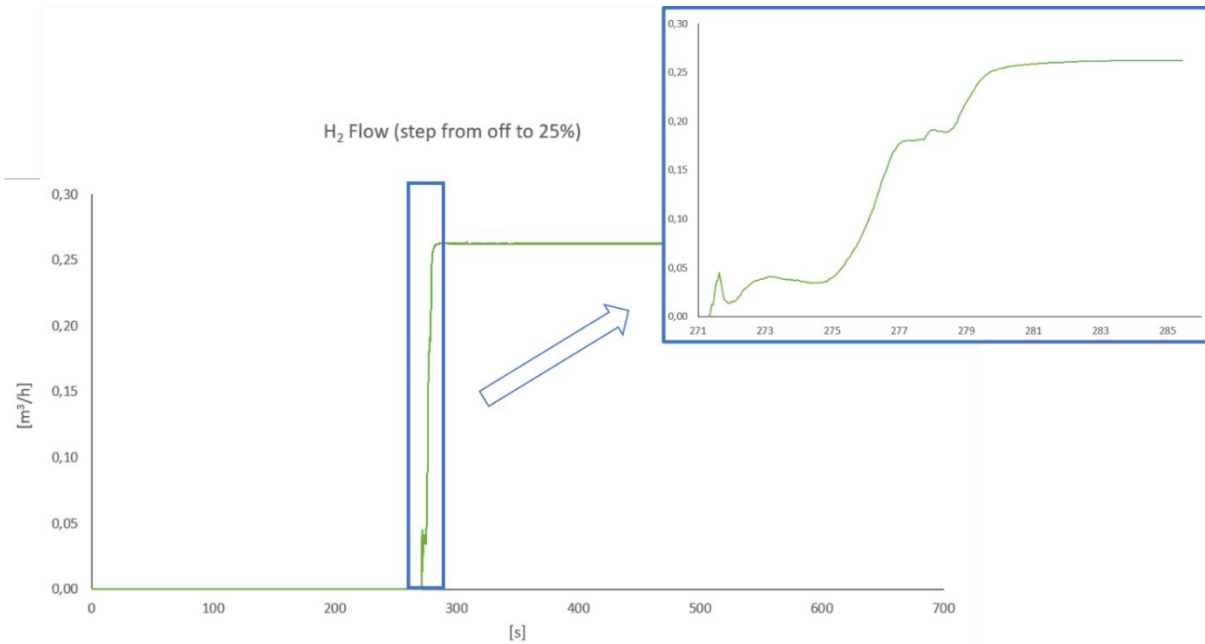


Fig. 61 – H<sub>2</sub> output flow - start-up and step to 25% of full-load (with zoom)

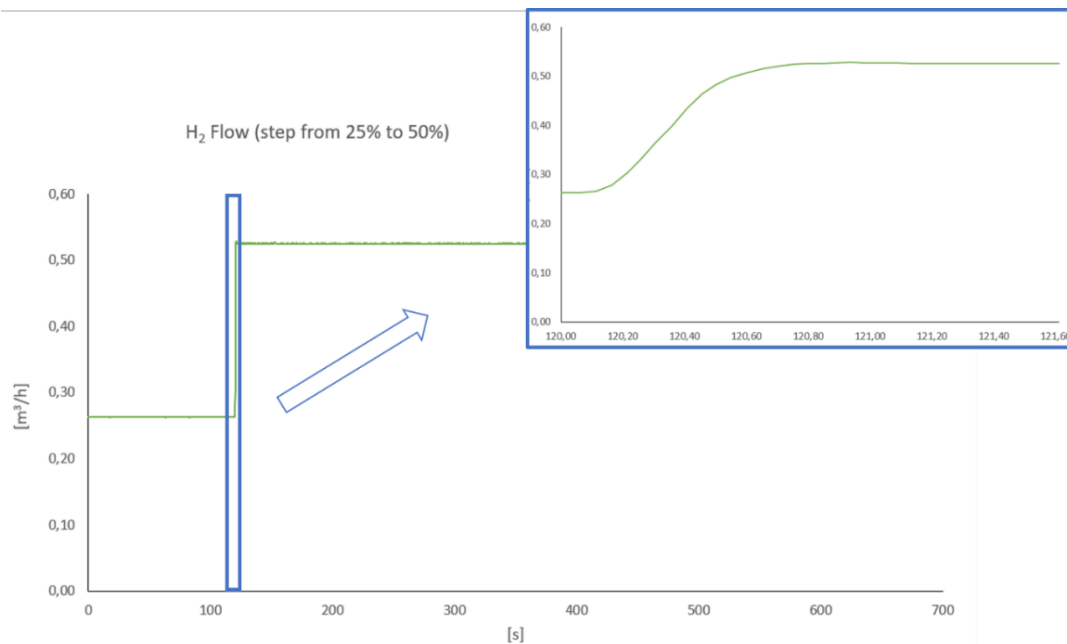


Fig. 62 – H<sub>2</sub> output flow - step from 25 to 50% of full-load (with zoom)

In conclusion, it is possible to state that the dynamic response of active power consumption is almost instantaneous. Therefore, the model constructed with the aim of mirroring the electrolyser electrical behavior through a static approach does not need to be modified, unless the start-up phase is needed to be introduced.

As a side comment, also the H<sub>2</sub> output flow shows a dynamic response very close to a step change when the electrolyser start-up has been completed. This means that, if the dynamic close to the start-up phase is not considered, the H<sub>2</sub> flow profile resulting from the switching between the waveforms included in the static version of the model is not too different from the real H<sub>2</sub> output flow.

### 4.3.2 Validation of the model

In order to demonstrate the validity of the model, the same four tests performed on the real electrolyser were carried out within the Simulink simulation and the results were compared. Basically, the H<sub>2</sub> flow setpoints given to the flow controller through the mentioned software interface were saved in Matlab by means of the implemented code. This code also allows the conversion of the setpoints from the range of values needed for the flow controller Modbus communication to the range 0.25-1 (meaning from 25% to 100% of full-load). These waveforms were then passed from Matlab to Simulink and given as input control signals to the electrolyser model. The *Electrolyser* subsystem previously shown in Figure 55 was modified as illustrated in Figure 63. Here, the *From Workspace* block stores the *flow\_setpoint* variable which case by case contains the described setpoint signal for each of the four step change experiments.

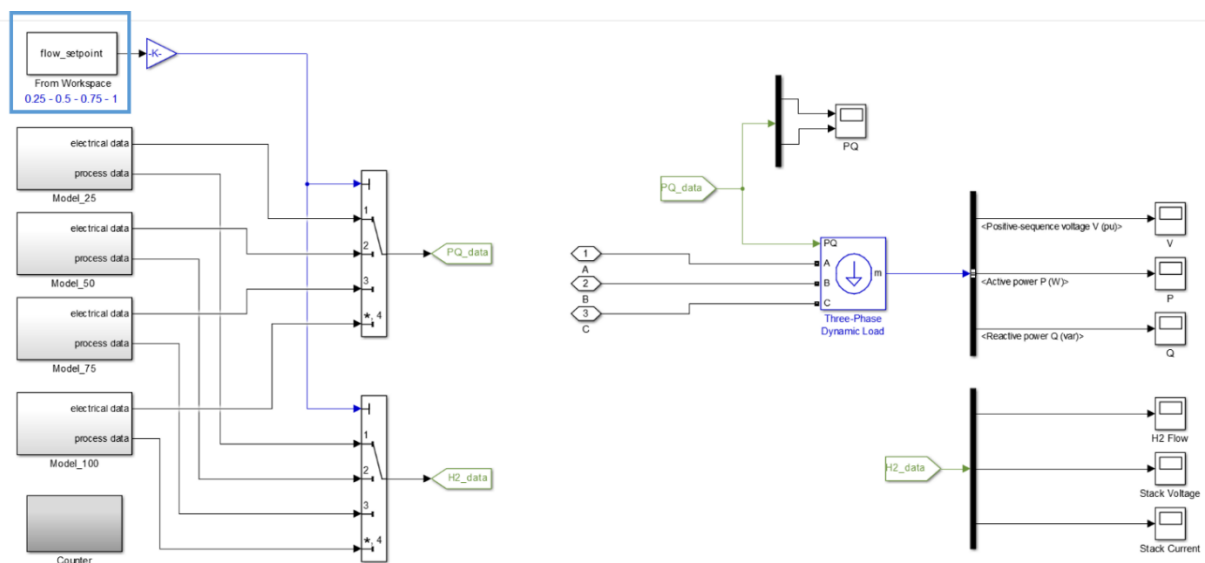


Fig. 63 – Electrolyser model: *Electrolyser* subsystem with *flow\_setpoint* control signal

For all the analyzed cases, the patterns of both active and reactive power of all three phases resulting from the simulation are depicted in Figures from 64 to 67. These are accompanied by the graphs of active power (already analyzed in the previous section) and reactive power, which together show the electrical behavior of the real electrolyser. In this way, it is possible to carry out a final comparison.

In the comparative analysis of the results, it is necessary to focus on the power profiles of phase 1 as the only one used by the converter to rectify the stack voltage. In this way, it is visible that the waveforms representing the active power consumption of the simulated electrolyser are only slightly shifted if compared to the real data. On this regard, it is worth to highlight that the real electrolyser behavior is not perfectly reproducible because shifts in the power consumption at a certain instant will anyway show up at different start-ups depending on the switching control initial instant. Another difference is represented by the start-up phase. This can be observed from the graph of the 0-25% real case (marked in yellow), while in the simulation it has not been considered. In conclusion, since the real and simulated data are generally comparable, it can be stated that the model built with the purpose to simulate the AC electrical behavior of the electrolyser (without considering the system start-up) is valid.

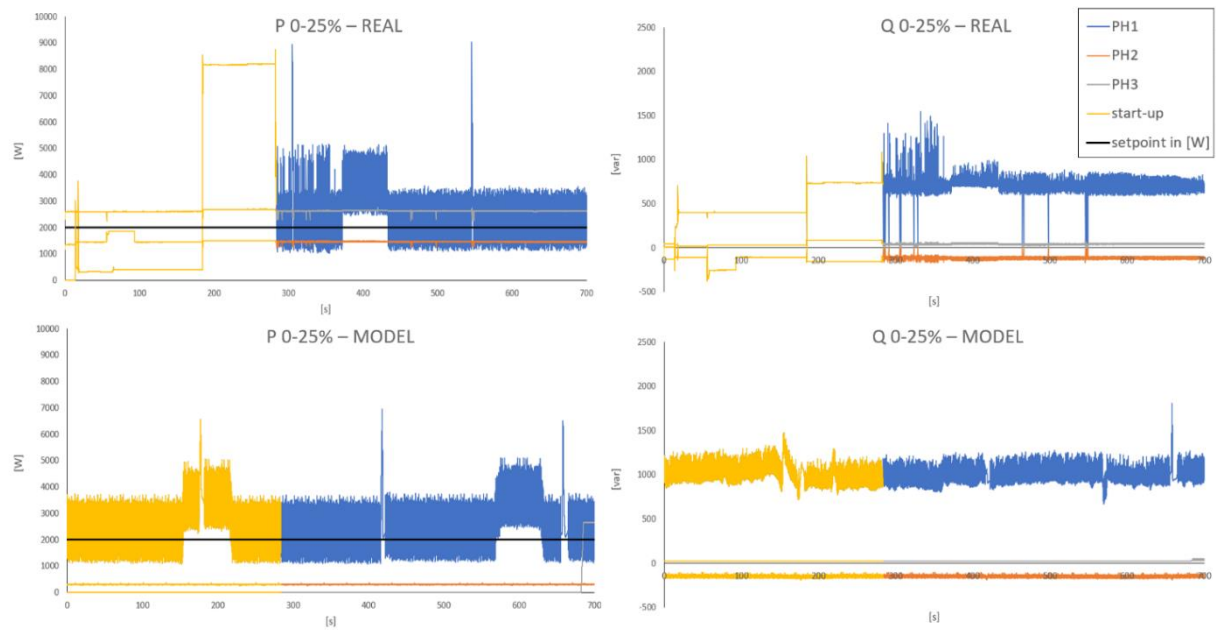


Fig. 64 – Electrolyzer model: comparison between real and simulated power profiles (case 0-25%)

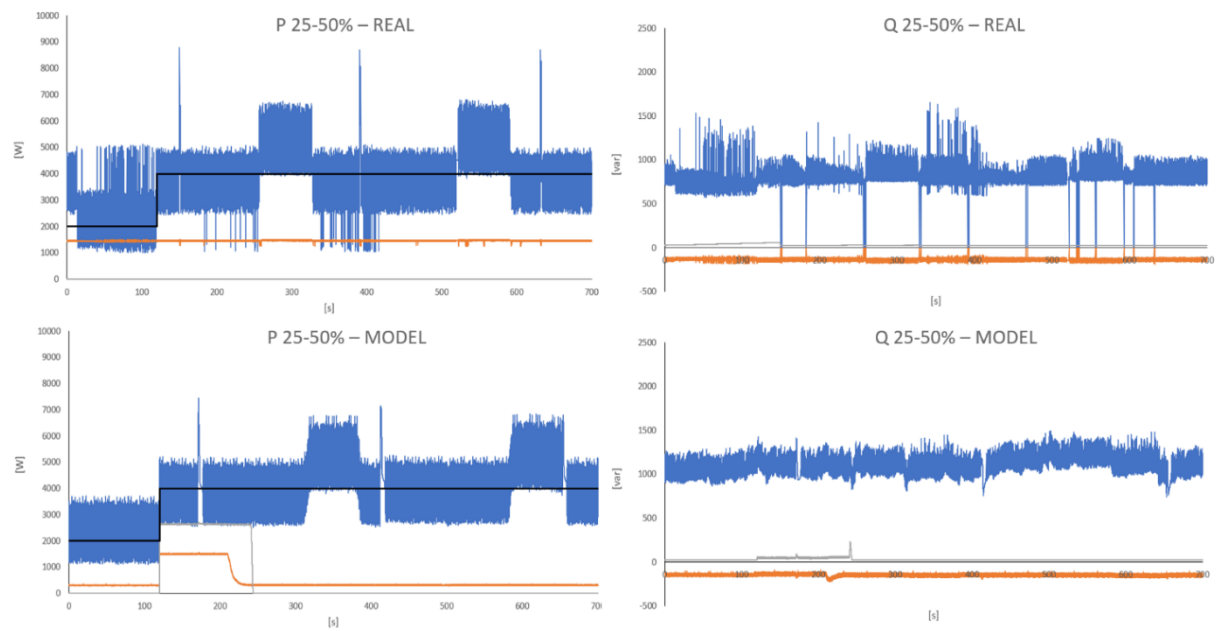


Fig. 65 – Electrolyzer model: comparison between real and simulated power profiles (case 25-50%)

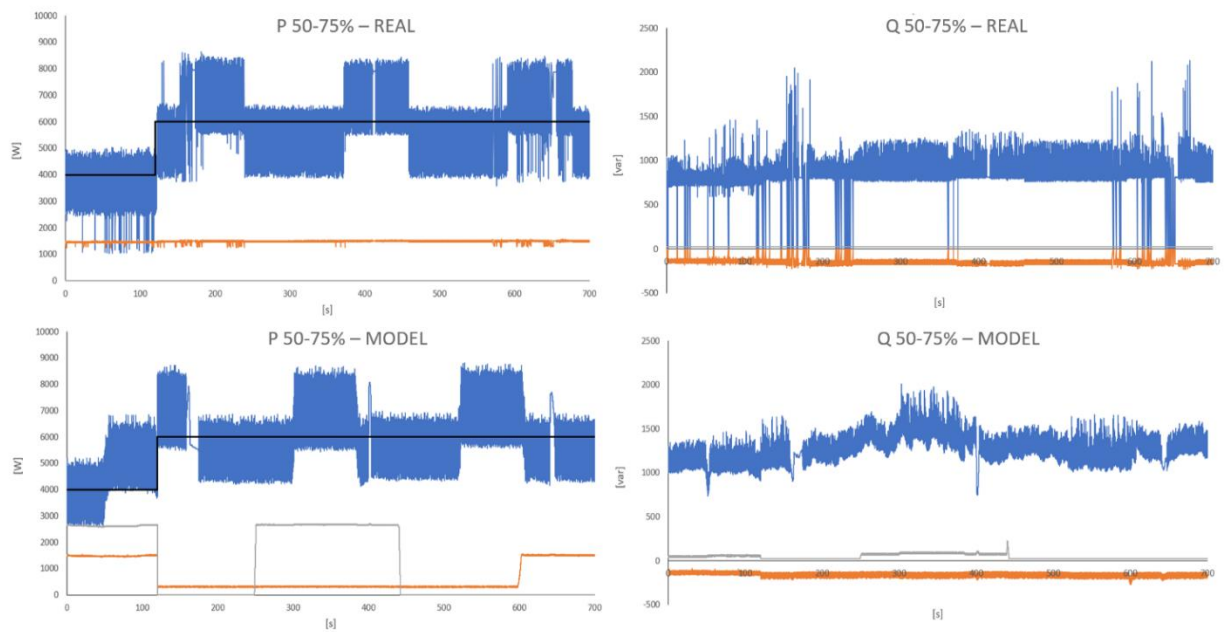


Fig. 66 – Electrolyser model: comparison between real and simulated power profiles (case 50-75%)

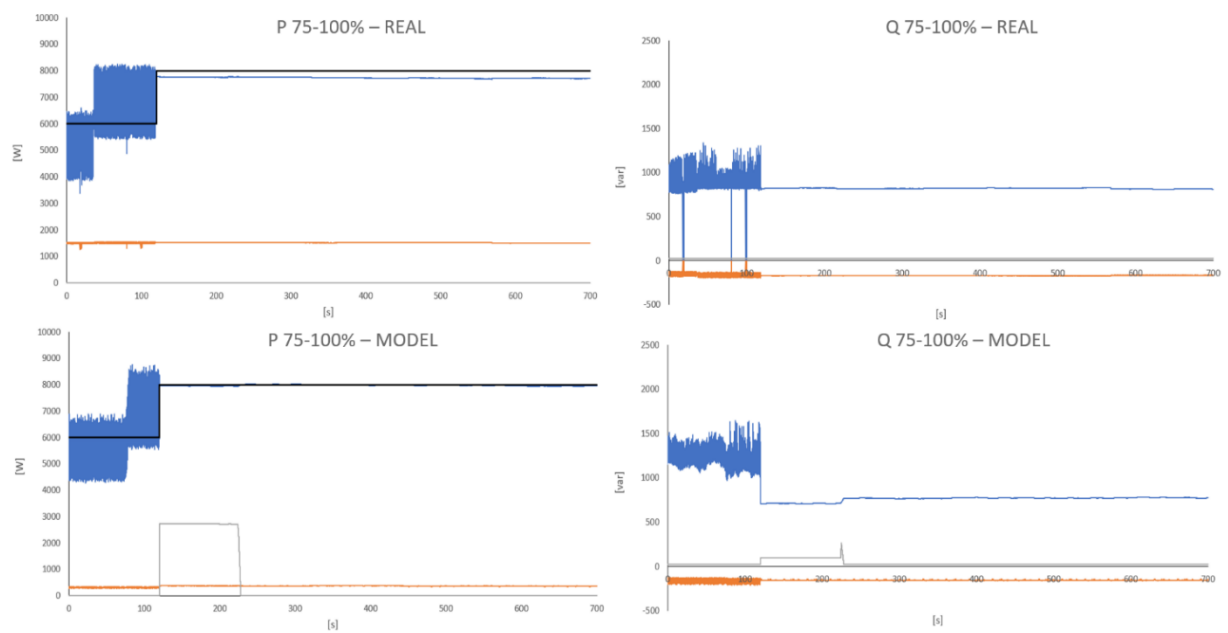


Fig. 67 – Electrolyser model: comparison between real and simulated power profiles (case 75-100%)

# Chapter 5

## Multi-site laboratory setup and remote simulation

### 5.1 Aim of the multi-site lab

The Micro-Grid Lab at the Hanze University of Applied Sciences and the G-RTSLab at the Politecnico di Torino co-operate within the project STORE&GO [34]. This project aims to sustain and promote the energy transition by investigating the role of PtG as a long term storage for the excess of RES production. In this context, the cooperation between the two labs is intended to give a contribution to the research on PtG technology, in regards of how to properly integrate electrolyzers into the electrical system and what are their characteristics in terms of performances and possible applications. Accordingly, a connection is established in order to join the two laboratories in a multi-site laboratory test setup and exploit the concepts of Remote Power Hardware-In-the-Loop (RPHIL) or, more specifically, “Internet-Distributed Hardware-In-the-Loop”.

### 5.2 Explanation of the Remote Power Hardware-In-the-Loop

#### 5.2.1 What is it?

Hardware-In-the-Loop (HIL) is a simulation methodology replicating real-world conditions for carrying out meaningful tests on device prototypes and new technologies proposed to be deployed in real energy systems. The aim is tuning, validating and verifying the system performances or collecting data with the purpose to create realistic device models – all this avoiding to deploy the device directly on the grid, which may be harmful for the grid itself or need uncommon situation that may be hard or unsafe to reproduce. In fact, while in real-world systems both hardware under test (HuT) and the grid are physical and naturally coupled, in the laboratory test environment the grid is replaced with its mathematical model, so-called rest of the system (RoS). In order to safely couple the HuT with this virtual system and to realistically simulate the behavior of the real system, the model has to be implemented on a robust target simulation platform and a Real-Time Simulation (RTS) has to be performed. This is a simulation solution able to follow the dynamic behavior of the system by respecting the timeline according to the wall clock. In this way it guarantees synchronization, accuracy, and stability of the overall system.

In case the HuT is a source (e.g. PV panels, wind turbines, synchronous generator, fuel cell, etc.) or a load (e.g. asynchronous motor, electrolyser, etc.) which respectively produces and consumes energy, the HIL solution takes the name of Power Hardware-In-the-Loop (PHIL). In this circumstance, a power interface consisting in a power amplifier and a set of sensors needs to be interposed between the HuT and the RTS to allow the power exchange with the RoS and to implement the simulation loop (Figure 68). Thanks to this, it is possible to make the HuT interact with the RTS [33].

Specifically, the control loop works as follows. The setpoint values of voltage or current are extracted from the simulated RoS to control the power amplifier, which acts as an energy source (generates power) or sink (absorbs power) depending on whether the HuT is respectively a load or a generator. At last, the real voltage or current signals from the HuT are monitored by means of sensors and sent as feedback to the RoS to close the loop.

An advanced and recently developed approach for deploying PHIL is to interconnect different distant laboratories in order to create an integrated laboratory for remote simulations and experiments, realizing the so-called Remote Power Hardware-In-the-Loop (RPHIL).

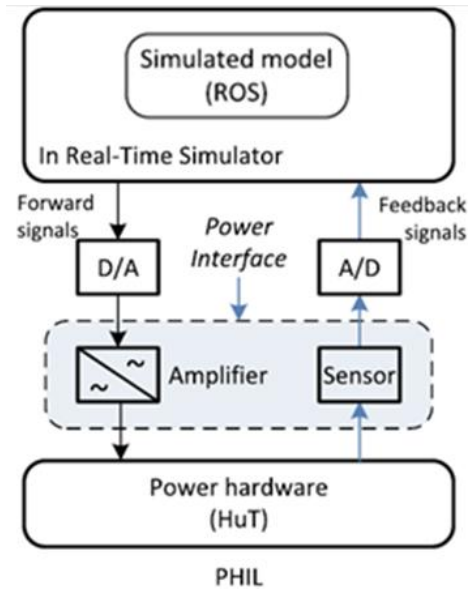


Fig. 68 – Power Hardware-In-the-Loop schematic

### 5.2.2 Why is it important?

RPHIL appears to be an effective approach especially for investigating new technologies for energy transition, with the purpose of solving the issues related to the introduction of new renewable energy sources into the electricity system (i.e. PtG). These technologies are making the overall energy systems to be investigated much more complex than the traditional ones, introducing new challenges to the research. In fact:

1. the newly integrated technologies deal with different energy vectors and sectors, thus requiring interoperability and multidisciplinary analysis;
2. the systems to be implemented are often large-scale energy systems, leading to enormously complicated simulation models;
3. the facilities for carrying out the experiments require huge investments as well as suitable areas where to be properly installed.

This may lead to the fact that a single laboratory with limited expertise, hardware/software facilities and available data has not the ability to provide satisfactory outcomes. The solution then lies in the share of existing research infrastructures by virtually joining different distant laboratories. The benefits that come with it are:

- Soft-sharing of expertise in a large knowledge-based virtual background

This allows interdisciplinary studies and interoperation among researchers belonging to different expertise areas, needed to ensure the correct exploitation of the performances of newly developed technologies (objective 1.).

- Soft-sharing of hardware and software resources

This enables to achieve two goals: improvement of simulation capabilities for large-scale systems by decoupling them into subsystems to be run on distant targets (objective 2.); avoidance of replication of already existing facilities by exploiting RHIL concept for testing remote devices (objective 3.).

Moreover, all the above mentioned objectives can be achieved while respecting another relevant point:

- The confidentiality of data, models and algorithms

The confidential information of one lab, whose sharing may either be not allowed or require long administrative authorization procedures, can be kept confidential by simulating models locally and exchanging with the partners only proper data and simulation results through the co-simulation medium.

### 5.2.3 How do we use it?

Within the context of the multi-site laboratory joining Hanze and PoliTo, the RPHIL concepts just outlined are applied to remotely test the PEM electrolyser installed at Hanze, with the aim of its characterization and the study of its dynamic behavior. The final goal will be the realization of a “geographically distributed real-time co-simulation” [35] for the purpose of grid impact analysis. On this regard, Figure 69<sup>25</sup> provides a general scheme illustrating the ongoing project of PHIL collaboration between Hanze and PoliTo, which is planned to be realized in subsequent steps:

Step (A) simply schematizes a local PHIL. The model implementing the RoS is run on the local RTT and the HuT is connected to it in PHIL through the power interface.

Step (B) shows the RPHIL. PoliTo’s lab is given the possibility to remotely access Hanze’s hardware and software setup to upload and execute the locally implemented model of the RoS on the remote RTT, to which the HuT is connected. This allows the researchers in PoliTo to run PHIL tests remotely on the electrolyser installed at Hanze.

Finally, in step (C) the concept of “Internet-Distributed Hardware-In-the-Loop” is illustrated. The vision of this methodology is not limited to only remote laboratory access but is extended to the implementation of the so-called “geographically distributed real-time co-simulation”. This means that the large-scale model of the RoS is decoupled into two subsystems to be simultaneously run in real-time on the simulators at the two distant locations.

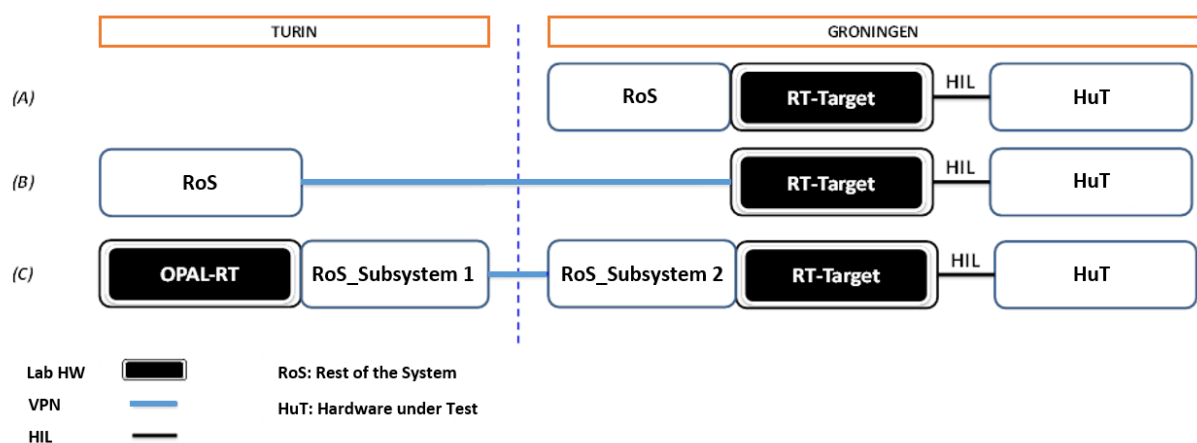


Fig. 69 – General scheme of the plan for PHIL collaboration between Hanze and PoliTo

<sup>25</sup> In this figure, the HuT represents the electrolyser unit; RT-Target [12,13] is the Real-Time computer located at Hanze, controlling the Triphase PM which acts as power interface; Opal-RT [36] is the name of the Real-Time simulator located at PoliTo.



## 5.3 Network connection

For the purpose of realizing the mentioned multi-site laboratory, the two physically separated laboratory LANs – one placed in Groningen and the other one in Turin, are merged into a single Ethernet segment via a bridge connection (Figure 70). As said, this communication link is based on the open source software OpenVPN, which enables to create a VPN tunnel between the two sites. This means that a completely decentralized virtual network is built over the Internet for a secure point-to-point data exchange, allowing to protect all forwarded data and installed equipment against undesired use.

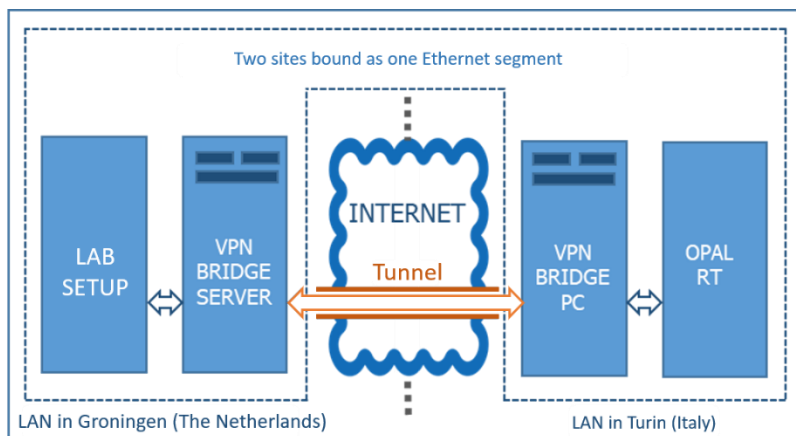


Fig. 70 – Schematic of the VPN communication between Hanze and PoliTo

In the test configuration, Groningen is the main LAN while Turin represents the sub-LAN. Therefore, the OpenVPN software is run on the VPN server that is part of the lab setup in Groningen and a virtual hub is created. In Turin, the computer connected to the same LAN of Opal-RT is equipped with a virtual VPN server and hub which is bridged to the server in Groningen. When a connection is initiated from Turin, a cascade connection is established between the two laboratory LANs. At this moment, the two separated network segments are converted into a single segment so that the devices on the two sides can communicate with each other as they belonged to the same network. It is worth to note that this is possible only in case each device over the two network segments is assigned an IP address belonging to a range identifying the same LAN. For more information about the computer networks, see [14].

In other words, after logging in on the VPN tunnel via OpenVPN software and through the proper IP address, the remote computer in Turin is capable of accessing the devices which are interconnected over Ethernet in the Micro-Grid Lab setup. Specifically, as shown in Figure 71, the remote user can control the Triphase PM by uploading Matlab/Simulink models onto the RTT as well as investigate the energy transition source which is connected to the power analyzer by reading and logging the instrument data. Furthermore, the recently built Ethernet connection from the electrolyser to the lab setup makes it possible for the remote user to autonomously start up the unit (once the manual operations have been completed), shut it down, monitor and log process variables. In the other way around, the local computer in Groningen is able to access the Opal-RT simulator which is part of the G-RTSLab setup in Turin.

Briefly, with this topology, the remote user can perform the same operations of the local user, acting as it was interconnected in the same LAN.

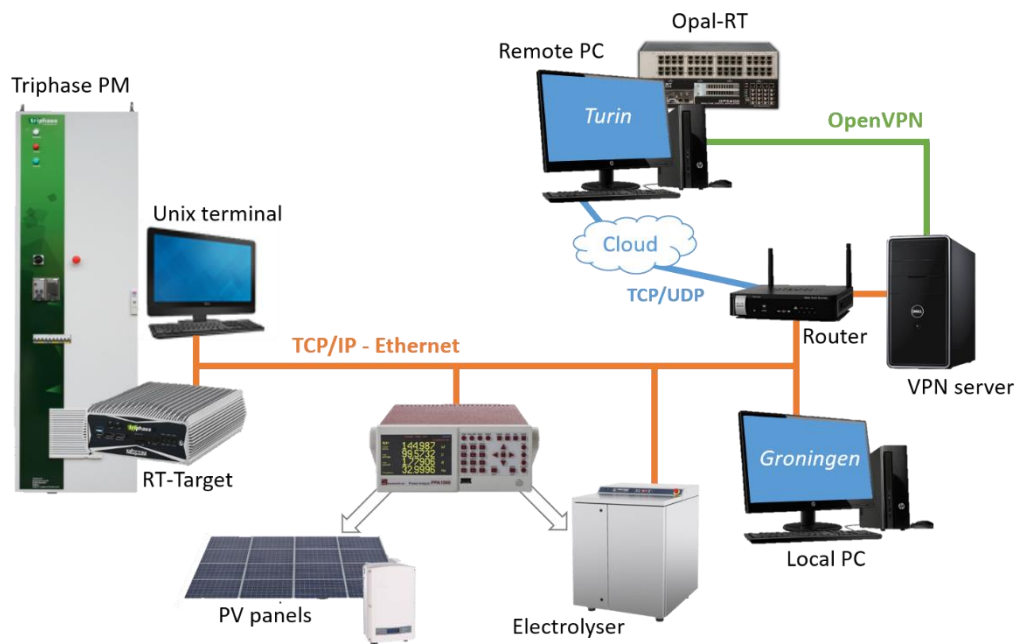


Fig. 71 – Multi-site lab network topology

Apart from the VPN, it is worth to say that another safety precaution against unauthorized use of the hardware in the lab is taken. Software and models for direct control of real-time facilities make use of a security method based on the MAC address or the ID number of the processor for identifying the computer which has installed the software or run the model. In this way, it can be ensured that a valid license for the installation of the software on a specific computer has been purchased. Moreover, as it happens in the Triphase PM control system, the identification of the workstation can be checked to make sure that only the user who uploaded and built a certain model can execute it.

In short, the currently realized network configuration allows the hardware installed on site to be fully and safely controllable from the remote side. With this setup and thanks to the interoperability of the Triphase PM, in the near future it will be possible to connect the electrolyser as HIL into remote running simulations, finally realizing the so-called distributed real-time co-simulation.

## 5.4 Test cases

As said, the implementation and use of the previously described connection:

- i) enables the remote access from PoliTo of the hardware and software resources located at Hanze, achieving the objective of the share of research infrastructures;
- ii) offers the possibility to remotely monitor and control the setup from within running simulations, which constitutes the first step towards a co-simulation involving RPHIL tests on the electrolyser.

The two experimental sets described in the following section were aimed at proving the feasibility of these two aspects.

### 5.4.1 First test set

The first experimental set was intended to demonstrate the functioning of the VPN communication for retrieving measurements from and sending control signals to the instruments, with a special attention paid to the data transmission delay. On these basis, two identical tests were performed by acting on the control and measurement equipment of the electrolyser, first locally from Groningen and then remotely from Turin. Specifically, the following operations were performed:

- *Control and measurement of the hydrogen flow rate (output) by means of the flow controller*

The setpoint given to the flow controller in both cases was as follows: the electrolyser was started up with the flow controller set to 25% of maximum flow rate and this value was kept constant for 7 minutes to make sure that the electrolyser had been correctly started and the steady-state had been reached; then 3 subsequent steps of 1 minute duration increased the setpoint of 25% at a time (1 minute at 50%, 1 minute at 75% and finally 1 minute at 100% of the maximum flow rate). The control was done by means of the software interface Modbus Tester, while the data logging and saving were possible for both setpoints and real signals by using the implemented Matlab code, commented in Appendix E.

- *Measurement of the active and reactive power (electrical input on the AC side) by means of the PPA power analyzer*

The electrical inputs to the electrolyser were measured by means of the power analyzer, interfaced with DataLogger software. The instrument was set by enabling High-Speed Mode and loading the same settings configuration already used during all the previous experiments at 20 ms time step.

In this way, by using the software programs provided with the measuring devices, it was possible to set the sample time of both the instruments to the lowest value that they are capable to handle. The most relevant results obtained are shown in the following figures.

Figure 72 illustrates the active power for all three phases obtained by measurements performed locally from Groningen. Figure 73 depicts the same parameters obtained by logging data in remote from Turin. By looking at the graphs and focusing on phase 1 (which is the most important as the only phase used for rectifying the DC voltage) no big differences are visible between the local and remote measurements. In both cases the electrical behavior of the electrolyser passing through the same operating states is captured: the generate-vent mode with a low power consumption (around 400 W); the pressurize-storage state during which full power is applied to the stack (8 kW); the steady-state at three partial load conditions (25, 50, 75%), in which the power profile variates around a mean value roughly equal to, respectively, 25, 50 or 75% of the maximum power consumption; at last, the steady-state at full-load, in which the power is maintained constant and equal to the maximum value (8 kW). This is the well-known dynamic behavior of the electrolyser: the simple visual comparison of the results has shown it can be captured from a remote location in the same way as on site.

In fact, the slight discrepancies emerging by comparing the two cases do not appear to be due to communication delays, but only to the fact that the electrolyser behavior is not perfectly reproducible at subsequent start-ups. (For instance, the generate-vent mode can last longer depending on the initial water quality, the waveforms representing the power consumption at a certain time can be shifted depending on the switching control initial instant and so on.)

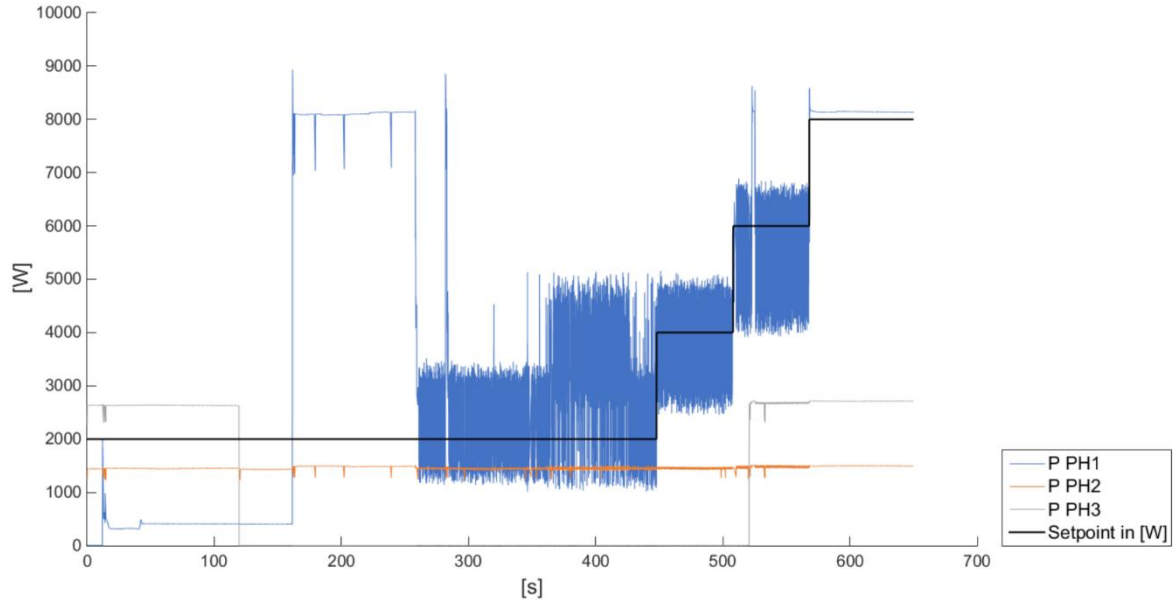


Fig. 72 – Active power withdrawn by the electrolyser - Local measurements

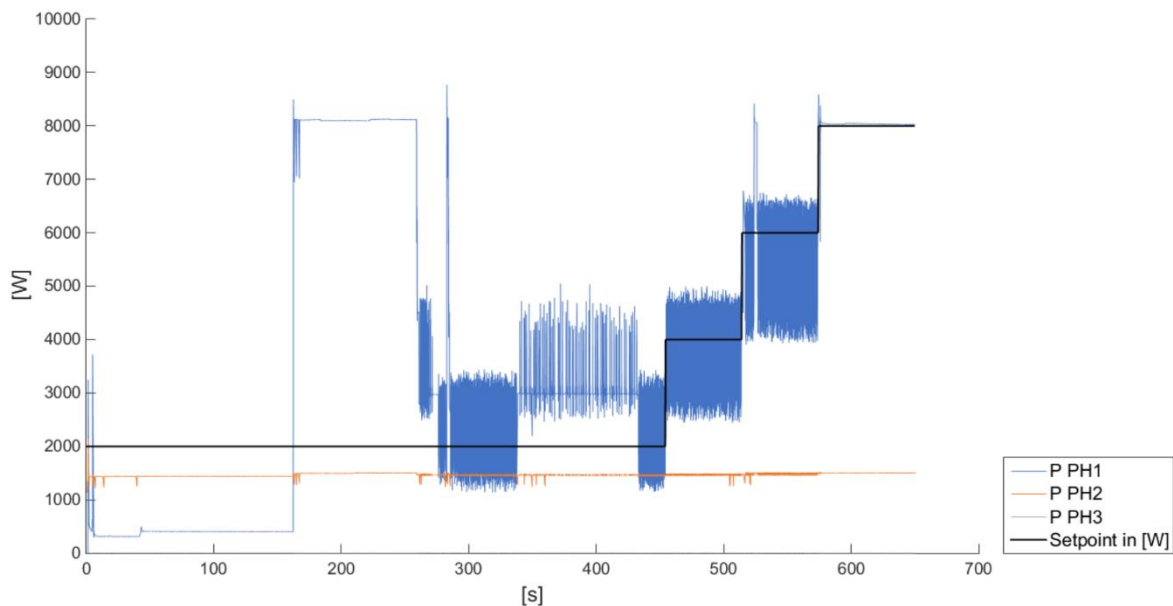


Fig. 73 – Active power withdrawn by the electrolyser - RHIL measurements

The  $H_2$  output flow measured from Groningen is presented in Figure 74, whereas the same parameter measured from Turin is shown in Figure 75. In both cases it can be seen the dynamic behavior of the flow passing through the steady-state at the four load conditions (25, 50, 75, 100% of the maximum output flow – averaged to  $1.05 \text{ m}^3/\text{h}$ ) with a dynamic between the steady-states that lasts no more than 1 s. Here again, it is possible to say that the two graphs are very similar, thus also the dynamic of the flow can be captured without any visible difference between the remote and the local measurements.

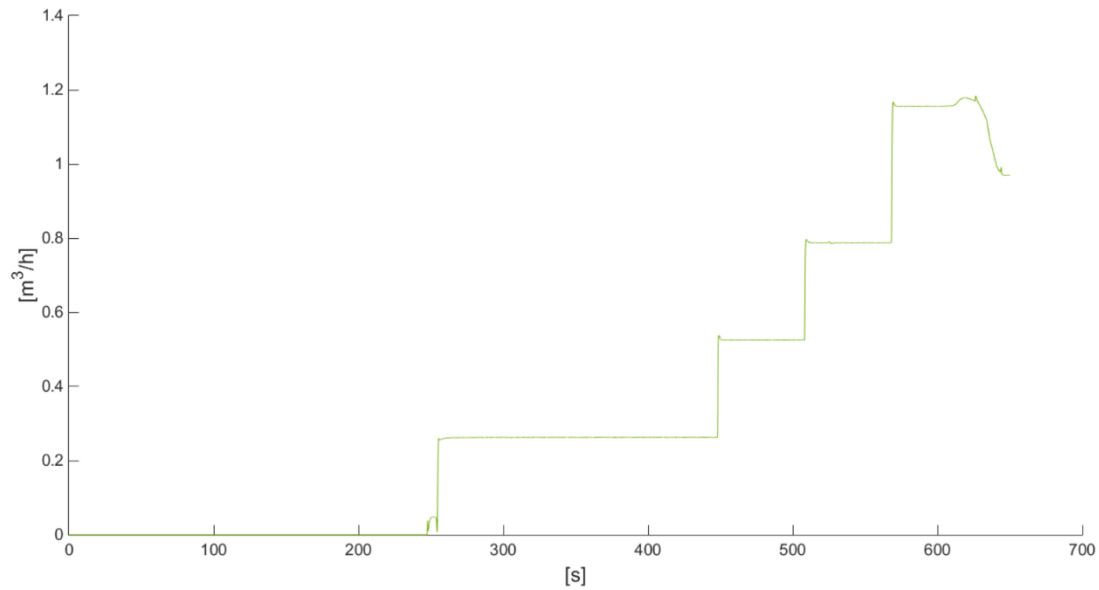


Fig. 74 – Production of H<sub>2</sub> - Local measurements

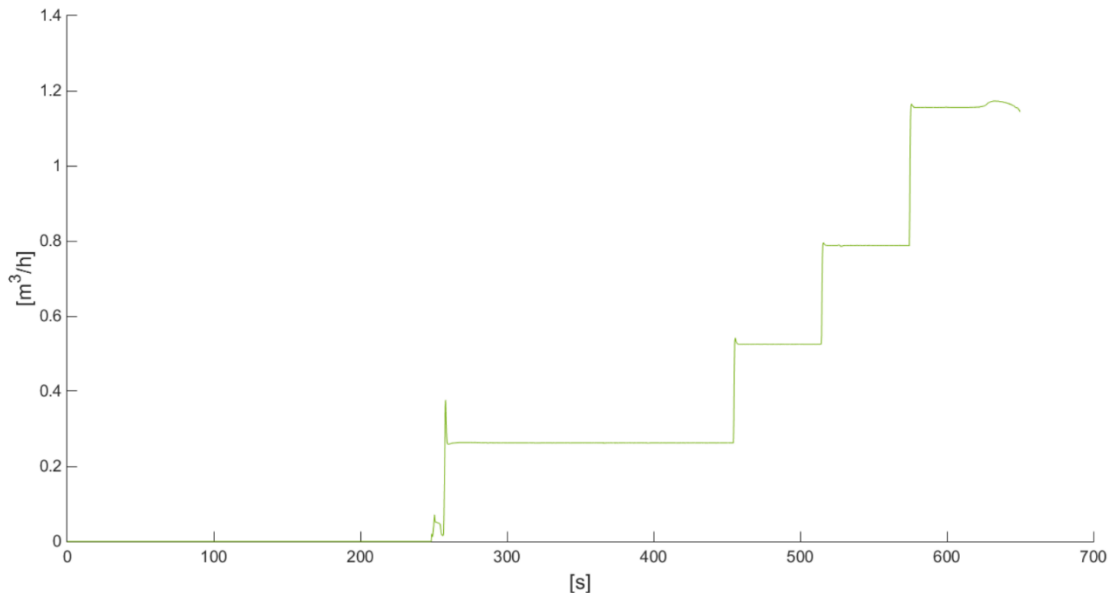


Fig. 75 – Production of H<sub>2</sub> - RHIL measurements

Since the delay due to the data transmission between the two laboratories via VPN could not be inferred from a comparison of the graphs, it was necessary to pay attention to the logging time of the instruments and, for a further analysis, to look deeply into the packets exchange by using WireShark – software for network protocol analysis [37]. From such analysis, it emerged that:

- *Power analyzer*: the minimum sample time handled locally is 20 ms and it can be respected on average when the instrument is read in remote. This is due to the way in which the High-Speed measurement mode is implemented [17]: the power analyzer is able to sequentially send the data packets to the server PC without any need for query. It follows that, since the speed of the forwarded data is higher than the latency of the communication link, the packets are queued and then received at irregular intervals.

- *Flow controller*: the minimum transaction time for the control through Modbus Tester interface equals 30 ms from Groningen and rises to about 100 ms from Turin. The minimum sample times for the measurements through the implemented code in Matlab are 50 ms from Groningen and 140 ms from Turin<sup>26</sup>. This slight delay is due to the fact that the instrument communication is based on a normal Modbus TCP/IP protocol [14,24], so that the query from the remote PC must be received before the instrument could send back the reply.

In conclusion, the latency introduced by the VPN communication only slightly affects the remote measurements in terms of regularity of the time step for the power analyzer and minimum sample time for the flow controller. Also the transaction time for the remote control of the flow controller setpoint is marginally influenced. Nevertheless, the delays introduced in the entire control chain are minimal and do not prevent the use of the multi-site setup for research purposes.

### 5.4.2 Second test set

The second series of experiments was aimed at carrying out the control and measurement of electrolyser data from within a Matlab Simulink environment, both locally and remotely. The objective was to demonstrate the possibility of integrating the hydrogen production unit into co-simulations on the basis of RHIL and “Internet-Distributed Hardware-In-the-Loop” concepts. A Simulink model was created for this purpose, which is composed of three different conceptual parts:

- Flow controller Modbus writing: used to write the setpoint of H<sub>2</sub> flow to the flow controller;
- Flow controller Modbus reading: used to read the measured data of H<sub>2</sub> flow from the flow controller;
- Power analyzer TCP reading: used to read the three-phase active and reactive power from the power analyzer.

Each part contains *Matlab Function* blocks implemented on purpose either for writing or reading the data of the respective instrument, taking into account the protocol requirements and also the necessary translations (may be ASCII, binary, decimal or hexadecimal). The three component parts of the Simulink model are shown in Figures from 76 to 78 and all the codes included therein are reported and commented in Appendix E. Useful information for the implementation of these codes were retrieved from [14,24,38,39,40,41].

---

<sup>26</sup> When the code is only used to log the measured data. Otherwise, if the code is used to log both setpoint and measured data, the minimum sample time equals 80 ms from Groningen and 280 ms from Turin.

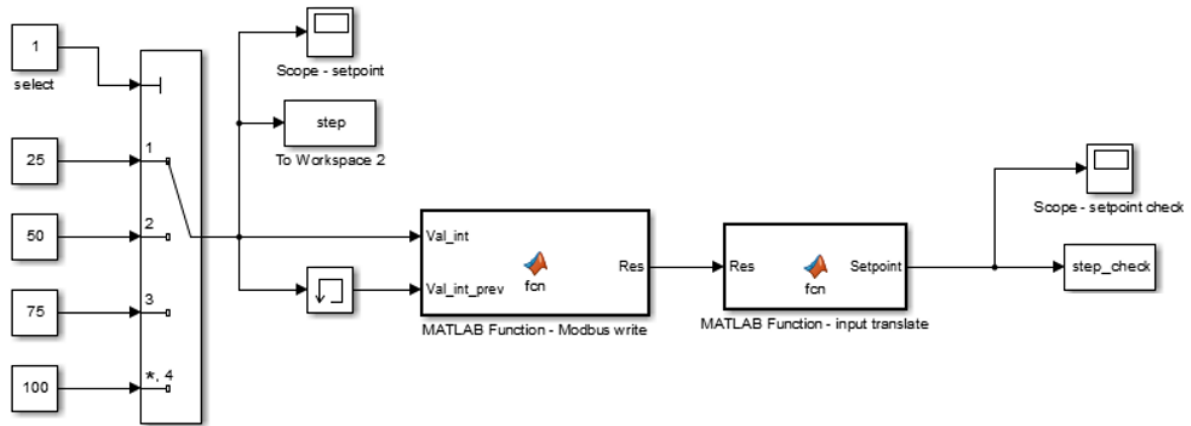


Fig. 76 – Simulink model subsystem: Flow controller Modbus writing

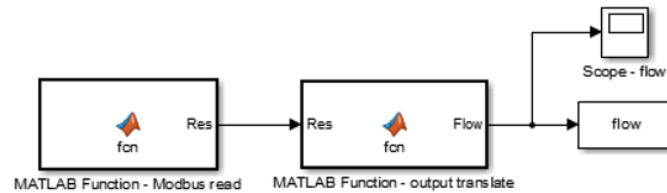


Fig. 77 – Simulink model subsystem: Flow controller Modbus reading

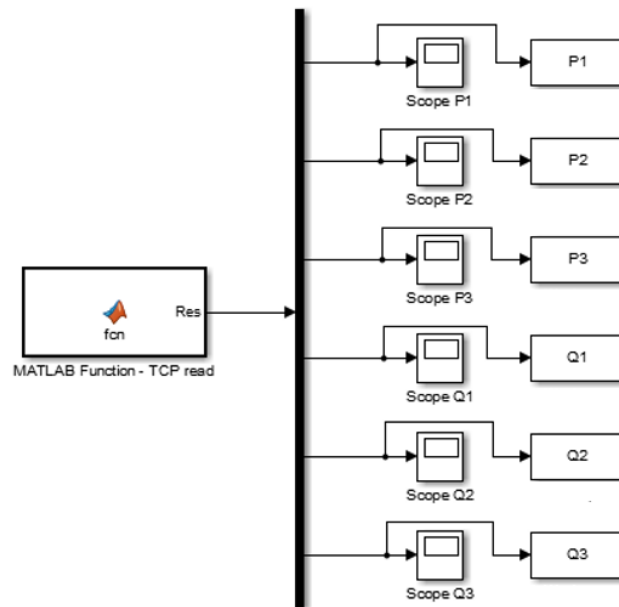


Fig. 78 – Simulink model subsystem: Power analyzer TCP reading

With this model, two identical tests were performed by giving the flow controller the same setpoint already described in the previous section, first locally from Groningen and then remotely from Turin.

The results obtained for the three-phase active power are shown in Figure 79 (model run from Groningen), and in Figure 80 (model run from Turin). All the considerations on the electrolyser dynamic behavior presented in the above section are still valid here. From both graphs, by focusing of phase 1, it can be observed: the electrolyser start-up phase comprising generate-vent and pressurize-storage states; then the steady-states at 25, 50, 75 and 100% of full-load, with a very fast dynamic from one steady-state to the next one. The only main difference highlighted in these cases is that the ranges of power variation are consistently reduced if compared with the results of the previous experimental set. The measured values at each time step appear to be only an average of the real data within the considered interval.

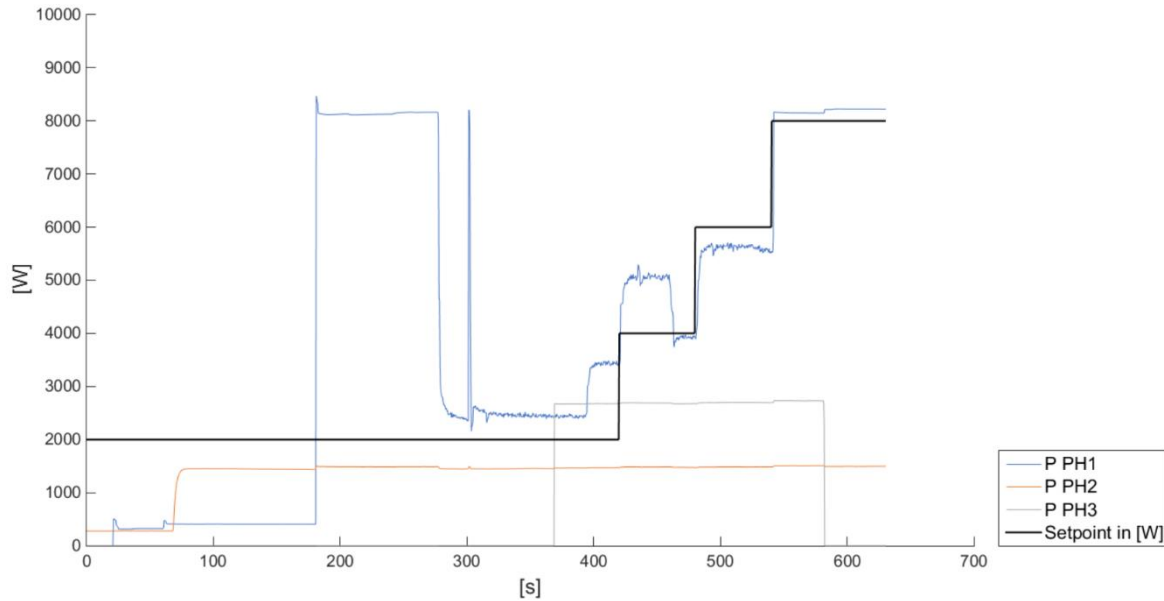


Fig. 79 – Active power withdrawn by the electrolyser - Local measurements (from Simulink)

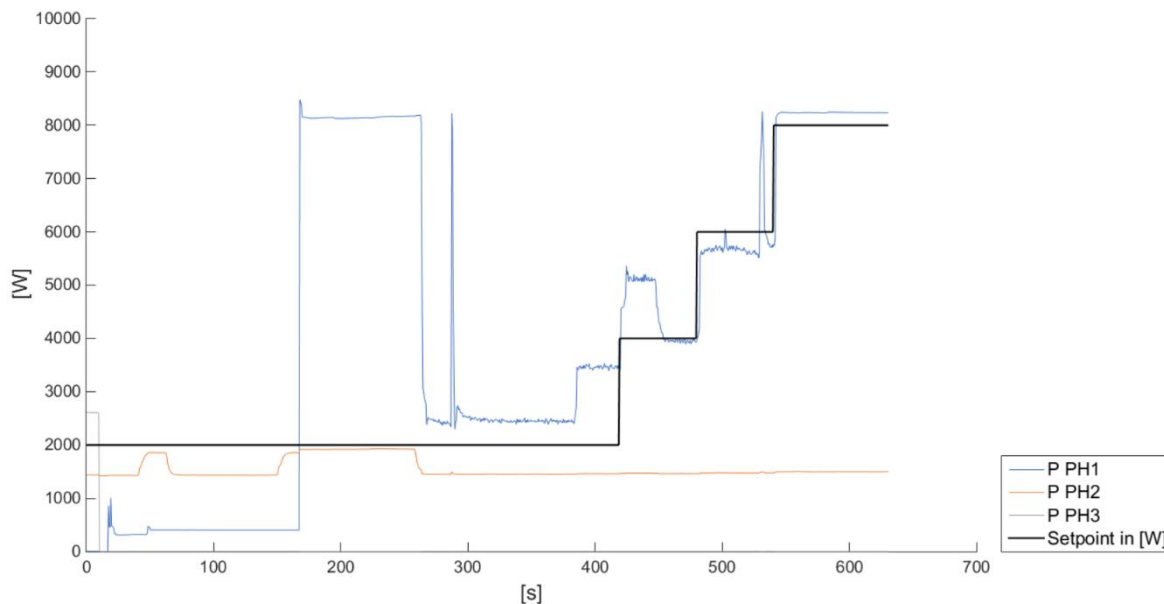


Fig. 80 – Active power withdrawn by the electrolyser - RHIL measurements (from Simulink)

This is due to the fact that, within the Simulink environment, the instruments cannot be read at the minimum sample time available as in the previous cases, but this has to be necessarily higher because of the further latency introduced by the simulation. In fact, it is worth to notice



that the Simulink block *Matlab Function* works by interacting with Matlab while running the simulation. At each simulation time step the model is momentarily paused, the *Matlab Function* blocks interface with the respective Matlab file and this runs the code to read/write data from and to the instruments. Finally, when the data replies are received, they are transferred from Matlab to Simulink and the simulation starts again moving to the subsequent time step.

This interaction increased the minimum simulation time step to 400 ms when the model was run from Groningen. When the same model was run from Turin, the latency due to the communication Matlab-Simulink in addition to the delay due to the VPN communication further raised the minimum simulation time step to 600 ms<sup>27</sup>. In both cases, this is the minimum fixed-step time it was possible to set. In fact, since the simulation time step also identifies the time period in which new values are requested and received from the instruments, a lower value would create too much data traffic which would slow down the communication and eventually lead to failure in the instruments and simulation crash.

At last, the measurements of H<sub>2</sub> output flow are presented in Figure 81 (model run from Groningen) and in Figure 82 (model run from Turin). The two graphs are barely distinguishable from the respective graphs obtained during the previous test case. In fact, unlike the power read from the power analyzer, the H<sub>2</sub> flow measured by the flow controller is generally not influenced by the huge increment in time step due to the simulation latency. This is because the flow is constant during the steady-states and does not present the variation typically analyzed in the power behavior. Only the accuracy in capturing the flow dynamic, lasting less than 1 s, might be influenced by the higher time step.

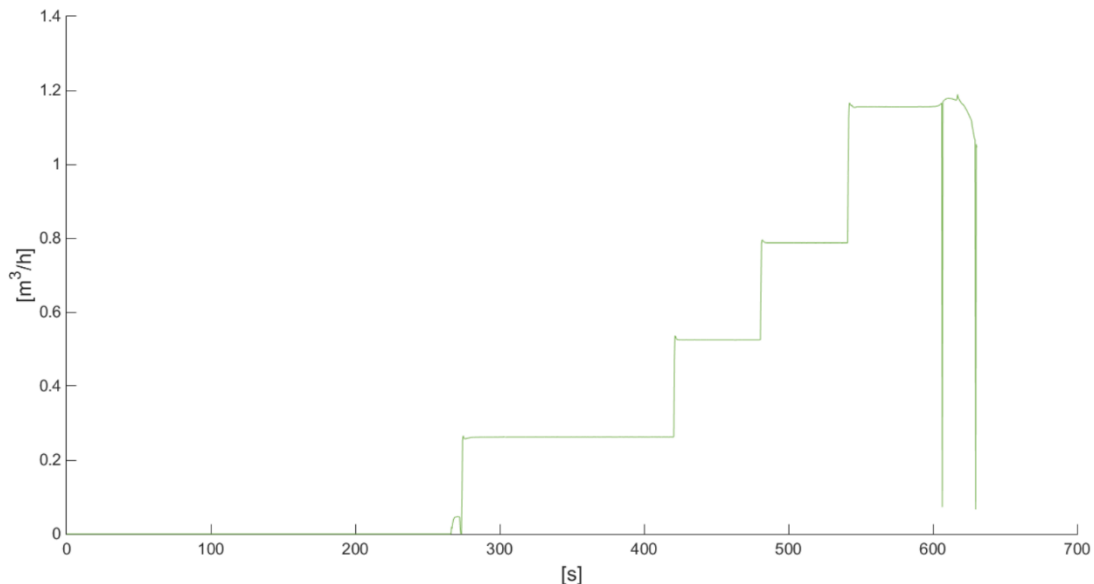


Fig. 81 – Production of H<sub>2</sub> - Local measurements (from Simulink)

<sup>27</sup> The simulation was performed as a normal non-real-time simulation, with the simulation time step set to 25 ms. The simulation duration was timed and the time step scaled up to real-time by multiplying for the conversion factor.

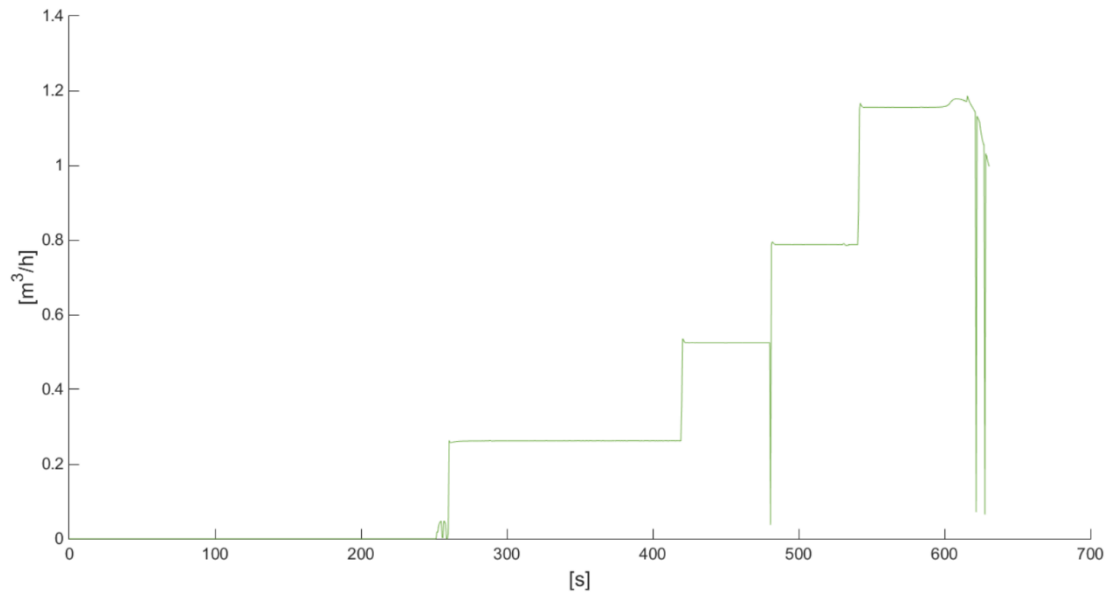


Fig. 82 – Production of H<sub>2</sub> - RHIL measurements (from Simulink)

In conclusion, it is possible to manage the measurement and control chain of the electrolyser from within a simulation running locally and – what is more important, remotely, but this leads to limits in terms of minimum sample time for reading the instruments and minimum simulation time step. In particular, this influences the accuracy in reading the power from the power analyzer, whereas the reading of the flow controller is only marginally affected with regard to the capture of the flow dynamics. Improvements in the method of integrating the measuring and control devices into Simulink may lead to a lower simulation time step (for example by developing appropriate Simulink *S-function* blocks for interacting with the instruments without any need to interface with the Matlab environment).

# Conclusion and future work

This thesis work explained in detail all the technical aspects concerning the creation of a multi-site laboratory setup for measuring and control of energy transition sources for PtG investigations, both from local and remote locations. The activities involved the installation and test of the different infrastructure parts, as well as their connections. In particular, the main systems developed so far count in:

- Local electrical grid, which can be managed either connected to the main grid or in island. This infrastructure aims to replicate a micro-grid environment and allows the connection of different components, considering both loads and generation.
- Energy transition sources, comprising a PV-field (energy source) of total nominal power equal to 4.16 kW and a PEM electrolyser (load – energy storage) of maximum power equal to 8 kW.
- Measurement infrastructure, mainly composed of power analyser, able to properly measure with high sampling rate electrical variables (i.e., active and reactive power, current, voltage and so on), to capture the dynamic behavior of the connected resource. Furthermore, proper sensors are available to monitor the hydrogen production process parameters, whereas temperature sensors and a pyranometer exist for monitoring weather conditions surrounding the PV-field.
- Control system, up to now consisting only in the flow controller, that allows to modify the hydrogen production of the electrolyser which in turn affects the unit power consumption. In the future, the control will be possible also by directly acting on the system electrical inputs (AC side) through a power amplifier, which is able to replicate the network conditions given manually as setpoints or simulated in another platform (i.e., Real-Time Simulator).
- Communication infrastructure, based on high-speed Ethernet and Real-Time network, interconnecting the various measuring and regulation devices for receiving the collected measurements and sending the control signals to change the operating conditions of the electrolyser in quasi real-time.
- VPN connection, joining the two distant laboratories in a multi-site laboratory layout, with the purpose of sharing existing facilities and expertise for interdisciplinary studies carried out by means of remote tests on local resources.

The test field developed was applied to build experimental-based models of PV panels and electrolyser. Appropriate data were collected from the resources installed on site through the related measurement equipment. These data were further processed by maintaining the meaning of the overall energy and finally used to implement Simulink models suitable for integration into big scale power grid simulations.

The overall communication infrastructure was tested to demonstrate the possibility to send control signals and collect measurements over the VPN connection. The control and measuring devices of the electrolyser were integrated into a simulation and the model obtained was run both locally and remotely by giving the same setpoints. Despite slight delays

introduced by the connection latency, the electrolyser dynamic behavior was captured in the same way from both the approaches. This opens the possibility to use the entire communication chain and the collected data for research purposes.

The next steps will be focused on the implementation of the Simulink model of a large-scale power grid, running on the Real-Time Simulator. This will be eventually decoupled into subsystems to run on different Real-Time Targets in order to realize a “geographically distributed real-time co-simulation”. The setpoints will be used to control the electrical variables of the electrolyser through the power amplifier, already installed in the lab setup and for which a model is under design. Proper tests will be carried out by employing the entire multi-site infrastructure in Remote Power Hardware-In-the-Loop.

# Appendix A

The aim of this appendix is providing some helpful instructions on how to use the PPA1500 power analyzer and DataLogger software that comes with it. In particular, individual features and options of this software which have been useful during the performed experiments are illustrated.

First of all, it is worth to say that DataLogger is able to connect to the power analyzer via RS232, USB and LAN. The program comprises all measurement modes which reflect instrument operating options. It also allows to export text files in CSV format or directly to Microsoft Excel.

## A.1 How to get started with DataLogger software

### A.1.1 Connection

Before establishing the communication between the software and the power analyzer, the instrument has to be properly prepared to accept it. First, the device must be powered on and the cables correctly connected in accordance to the selected kind of interface (RS232, USB or LAN). Then, the instrument must be set up correspondingly. This is done by accessing the *REMOTE* menu on the device itself and selecting the chosen interface under the *Interface* drop-down menu (Figure 83). Note that, for LAN interface, also a valid IP address needs to be assigned to the instrument (Figure 84).

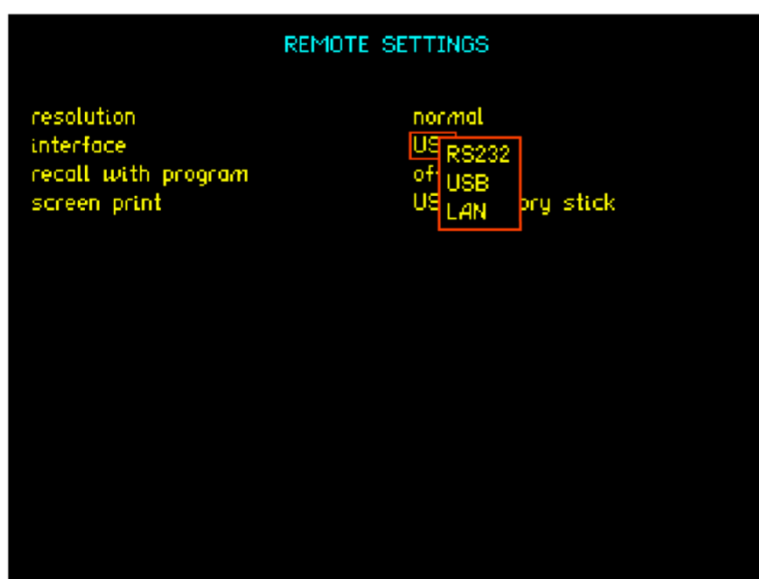


Fig. 83 – PPA REMOTE menu



Fig. 84 – PPA REMOTE menu - detail

After setting up the instrument properly, the communication can be established via software. The Communications window can be accessed by opening the drop-down menu *Configure* and selecting *Connection...* (Figure 85).

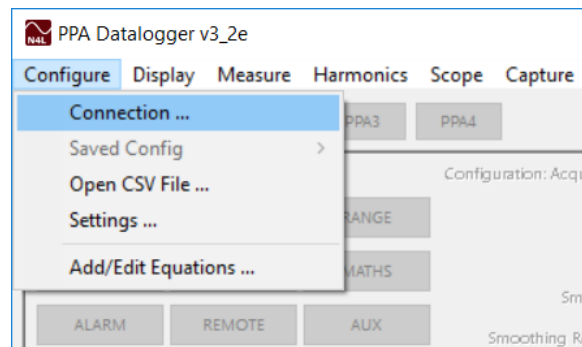


Fig. 85 – Configure PPA connection

In the Communications window, it is possible to set up the number of instruments to connect and the interface used for each one (Figure 86). Of course, for the purpose of this thesis, only one instrument has been used, thus *Connect to 1 PPA* has been selected. The chosen communication method has been either USB or LAN, depending on the kind of operation performed (in short, either USB or LAN indifferently for the local experiments, certainly LAN for the remote experiments). Note that, when USB is selected, an additional information to be provided is the COM port assigned to the cable by the PC operating system (see Appendix C for how to look up for this information). Furthermore, when LAN is selected, the same IP address assigned to the instrument needs to be entered. By pressing the *Test* button, the connection settings are verified. If the software fails to connect an error message will pop up, while if it succeeds a message showing the instrument info will appear. By pressing *Save as Default*, the software will remember the current settings. Once *Connect* is pressed, the communication will be established and the device configuration settings downloaded by the program.

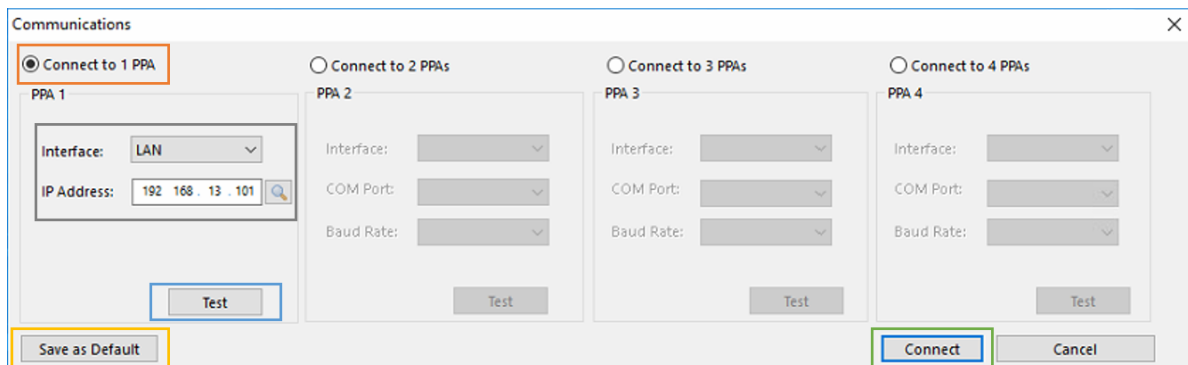


Fig. 86 – Communications window

## A.1.2 Software main screen

After the communication has been established, it is necessary to set up the instrument settings in accordance to the measurement to perform. In what follows, the layout of the software main window is presented, together with the measurement options included therein utilized during the experiments (Figure 87).

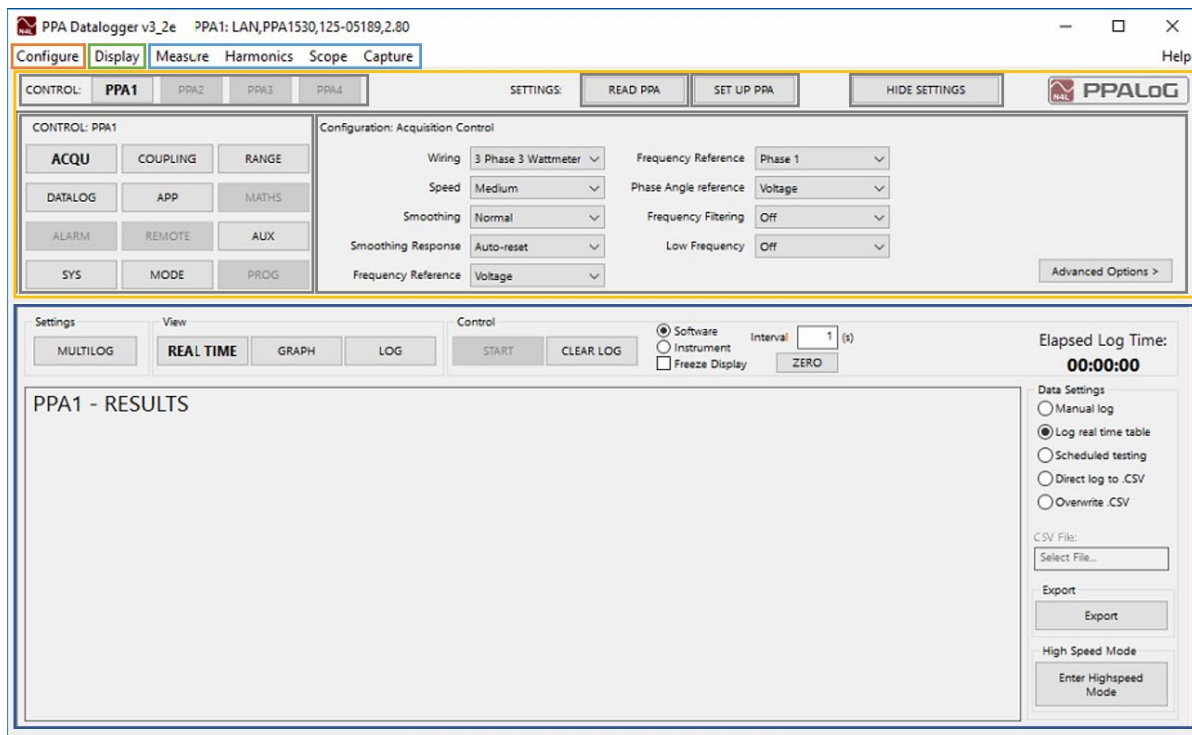


Fig. 87 – Datalogger Software main screen

## CONFIGURE MENU

Besides the already mentioned Communications window, under the drop-down menu *Configure* the Settings window is available by selecting *Settings...* (Figure 85). Here, it is possible to change some of the general software settings. One of the most useful is *CSV File Format*, which allows to set the decimal format of the numbers exported to CSV files by choosing between Standard (".") and European (","). Through this choice it will be possible to make the CSV file import operation to Matlab or Excel much easier.

## CONFIGURATION PANEL

This panel stores and let the user edit the settings of the connected instrument:

- *READ PPA* button enables the program to download the device settings, in such a way that the information displayed reflect the ones on the instrument front panel.
- The *Settings* menu are the same present on the instrument front panel. It is possible to look at and edit the desired menu by clicking on the related icon. The menu contents are displayed in the *Configuration Control* panel. For detailed information on each single menu refer to the user's manual [18].
- *SET UP PPA* button enables to communicate the changes to the instrument.
- *HIDE SETTINGS/SHOW SETTINGS* allows to hide or show the whole *Configuration* panel.

Additionally, it is possible to save, load, import or export settings configurations through the options available under *Saved Config* in the *Configure* drop-down menu (Figure 85).

## DISPLAY MENU

The drop-down menu *Display* can be used to save the displayed numerical and graphical results as pictures.

## MEASURE, HARMONICS, SCOPE AND CAPTURE MENU

The other menu in the upper side of the screen allow to set up the power analyzer measuring mode. They are respectively the *Measure*, *Harmonics*, *Scope* and *Capture* mode.

## RESULTS PANEL

Once the mode is selected, the view in the Results panel will change accordingly.

### A.1.3 Measure Mode

The measuring mode used during the performed experiments is the *Measure* one. Therefore, this will be the only one analyzed in the following section. In particular, in this mode, the power analyzer has the ability to log a high number of parameters (up to 60) with many different methods of data logging. It is entered by pressing the associated menu button in the upper side of the main screen so that the Results panel is adjusted accordingly. In what follows, the steps needed to perform a measurement in *Measure* mode are presented (Figure 88).

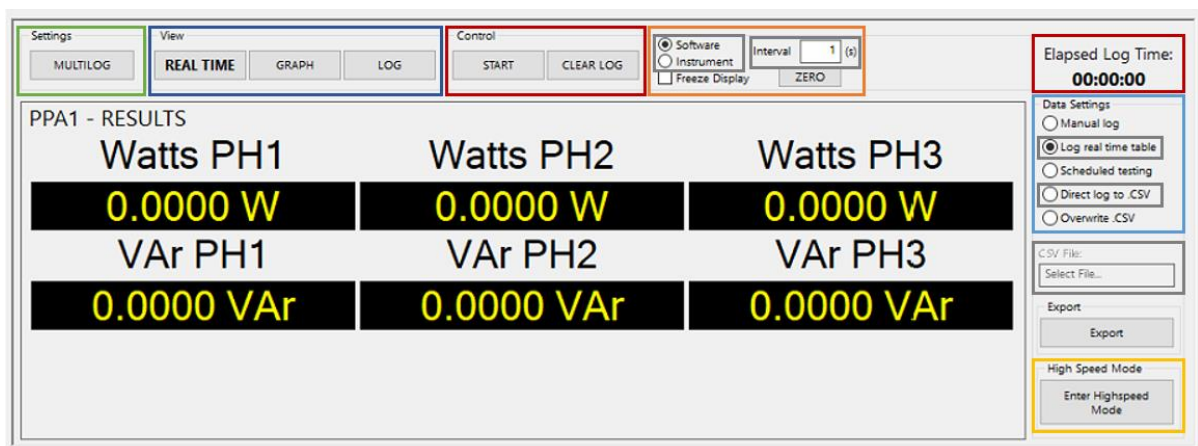


Fig. 88 – Results panel in Measure mode

## MEASUREMENT SPEED

First of all, it is necessary to set the measurement speed by choosing between two speed setting modes: *Software Interval* and *Instrument Interval*. In *Software Interval* mode, the software requests data to the instrument at the rate set in the *Interval box*, independently from the instrument settings. Although the minimum valid interval specified by the manual is 1 ms, it has been found that the minimum interval which gives correct results is 20 ms (see High-Speed Mode below). On the other hand, in *Instrument Interval* mode, the software requests results to the instrument synchronously with the speed specified in the instrument settings (under *Speed* in the *Acquisition Control* menu accessible through the Configuration Control panel (Figure 87)).



## HIGH-SPEED MODE

High-Speed Mode is the measurement mode which allows to read data reliably at high speeds by recording them directly to the PC RAM. It is recommended to enter this mode when measuring with sample times lower than 100 ms. However, some limitations are inevitable at such high speeds and the software will make the user aware of them after entering this mode through the proper button. Specifically, High-Speed Mode works only if the measurement setting *Log Real Time Table* is selected, reads data only from one power analyzer, reduces the number and the choice of parameters that can be logged and requires the *Instrument Interval* logging mode. Therefore, the instrument settings need to be set up properly. At last, it is necessary to be aware that it is not advisable to log in this mode for longer than 10 minutes.

## MULTILOG SETTINGS

Secondly, after setting the measurement speed, it is necessary to choose the variables to be measured. This can be done by opening the Multilog window through the *Multilog* button. The button is only available when the instrument is correctly connected. The parameters listed in this window are color coded (Figure 89).

The screenshot shows the 'PPA1 Multi Log Selection' window. At the top, there's a 'STORE / RECORD SELECTION' button. Below it, a tab labeled 'PPA1' is active. The main area is a grid for selecting parameters across six phases (1-6) and two sets of SUM and NEU columns. The parameters are listed on the left and are color-coded: blue for basic measurements, green for advanced measurements, and orange for integrated/average measurements. The 'Selected Items' list on the right shows 'Watts' for PH1, PH2, and PH3, and 'VAr' for PH1, PH2, and PH3. Buttons for 'UP', 'CLEAR', 'REMOVE', 'DOWN', 'Maths', 'Add ADI Input', 'Add ADI Output', and 'Remove' are present. An 'OK' button is highlighted with a green box.

Fig. 89 – Multilog window

By clicking the tick boxes, the corresponding parameter will be added in the Selected Items list. It is possible to edit this list by removing items, clearing them all at once and rearranging their order through the associated buttons. By pressing *Ok* the selected parameters will appear in the Result panel. Lastly, it is possible to save or load multiple parameters selections by the *STORE/RECORD SELECTION* menu.

## DATA SETTINGS

This box includes 5 measurement settings. Only two of them have been used to perform the measurements during the experiments: *Log Real Time* entered in High-Speed Mode, and *Direct log to CSV* entered at normal speed logging. In *Log Real Time* mode, the data are read from the instrument and recorded by the software which displays them in the **LOG view**. Once the logging has been completed, the *Export* button can be pressed to export the results either in Excel or CSV file format. In *Direct Log to CSV* mode, instead, the data are saved straight to a CSV file, whose name and location are assigned by means of the *CSV File* box.

In both cases, the logging can be started and stopped by pressing the **START/STOP** button. While logging, the **Elapsed Log Time** is updated every time a new reading is recorded and the **REAL TIME** and **GRAPH views** can be used to display the numerical and graphical results respectively. Finally, the logged data can be cleared with the **CLEAR LOG** button.

## A.2 Importing CSV files into Excel

CSV files obtained from the power analyzer can be imported into Excel. Once opened a new Excel file, the spreadsheet can be created from the text file by means of the *From Text* button under *Data* tab. After properly editing the data format in the wizard, the logged parameters will be included in the Excel sheet separated by columns.

# Appendix B

The aim of this appendix is providing a user's manual for operating the electrolysis system. In this case, detailed instructions on how to utilize the hydrogen production unit are of fundamental importance. Users must be aware and follow such rules for making the unit function correctly. They must also respect all safety requirements for avoiding any risks related to the handling of hydrogen.

## B.1 Electrolyser operating manual

### B.1.1 Hydrogen risks and safety measures

- Hydrogen is odorless, tasteless and colorless. Even if it is non-toxic, hydrogen can act as an asphyxiant gas by reducing the oxygen amount in air. When a person is exposed to such oxygen deficiency, the common effects can be rapid breathing, fatigue, reduced mental alertness, diminished muscular coordination and defective judgement, ending up in nausea, vomiting and loss of consciousness in the worst cases.  
→ Avoid overexposure to hydrogen
- Hydrogen is highly flammable in the presence of oxygen, with a lower explosive limit of 4% by volume in air [2]. Gas leaks may have high temperatures and therefore constitute a risk for fire and skin burnings. → In case of leakage that does not represent hazard, try to stop the gas flow and cool down the area with water. If fire occurs, do not try to extinguish the flame but allow it to burn out.

### B.1.2 How to start up the electrolyser system

In order to turn the system on, the different processes must be started in the following order:

- 1) Starting up of the water demineralizing process – situated in the room on one side of the container;
- 2) Starting up of the hydrogen production unit – situated in the room on the opposite side.

Note: the water used for electrolysis has to go through a demineralizing process before bringing the electrolyser into operation. The demineralizing process allow the mineral concentration in the water, quantified by the water conductivity parameter, to be reduced and the result is called demi water (the higher the water conductivity the higher the concentration of mineral in the water) [2]. In order to make the system function properly and avoid damages, the conductivity of the demi water flowing to the unit must be below 0.5  $\mu\text{S}/\text{cm}$  [21].

As already illustrated in section 2.3.2.2 (Figure 20), in the first room the demineralization is carried out by means of two units containing ion exchange resins and a RO unit. Here are the steps to follow:

1. Check the main valve of the tap water feed tube on the left hand side of the room and open it if necessary (Figure 90).



Fig. 90 – First room detail: main valve of the feedwater tube

2. Open the valve (marked with an orange circle in Figure 91(a)). In this way the water will flow out from the demineralization process if the RO unit is on. If it does not turn automatically on from stand-by mode once the valve has been opened, push the unit ON/OFF button (encircled in green in Figure 91(b)). If the display shows the process parameters without any error, press the enter button (indicated with a blue circle in Figure 91(b)) to start up the pump. Now the water will flow out of the tube downstream of the open valve and the conductivity on the ion exchange filters display will slowly decrease.

(a)



(b)



Fig. 91 – First room details: (a) two ion exchange units; (b) RO unit and pump control panel

After opening the valve, the pressure of the tap water in the supply tube upstream of the RO unit may suddenly drop. In this case, adjust the pressure reduction valve on the left hand side of the room to meet a pressure value over 1.5 bar, but not exceeding 2 bar!

3. Close the valve again when the conductivity displayed on both ion exchange unit is below the limit of  $0.5 \mu\text{S}/\text{cm}$ .

If the system has not been operated for a certain period, the conductivity may be considerably high at the beginning. If the conductivity does not decrease after the above indicated valve has been open for a while, the ion exchange resins are likely to be saturated

with minerals, thus the units need to be replaced. It may also be that the pressure of the pump in the RO unit is too high. If it reaches a value above 13 bar, an error will occur and the pump will shut off. It will then be necessary to restart the process by shutting off the RO unit, closing the water supply valve, reopening it after few seconds and starting up the unit again. If the pressure keeps being too high these steps must be repeated. If this method does not work the unit filters certainly need to be replaced!

As already depicted in section 2.3.2.2 (Figure 21), in the second room the electrolyser performs the electrolysis process and two 5L tanks are available to store the produced hydrogen. This unit can be started up after the demineralizing process has been made work properly. The tanks can be filled during hydrogen production and then emptied at last by blowing off the hydrogen in the outside air. Alternatively, instead of filling the tanks, the hydrogen can be directly vented while produced. Here are the instructions to follow:

4. Choose either to store the hydrogen into the tanks or to directly blow it off outside.  
If producing in tanks filling mode, close valve BV-09 (encircled in green in Figure 92) and open valve BV-04 (encircled in blue). Otherwise, if producing in venting mode, do the opposite, which means to close valve BV-04 and to open valve BV-09.

jThe valve is said to be open when its handle is aligned with the tube on which the valve is placed. It is defined as closed when its handle is perpendicular to the tube!  
jIf tanks filling mode has been chosen, it is advisable to empty both the tanks before starting the hydrogen production. In order to blow the hydrogen off the tanks, open valve BV-09 and BV-04 as indicated above. Close valve BV-09 again when the manometers just above the tanks show the tanks pressure being around 0 bar!

Note: For the purpose of characterizing the electrolyser load, the experiments analysed in Chapter 4 were performed in venting mode. However, the produced gas blow-off had to be carried out in a different way. This is because the aim of the experiments was to measure the input/output process variables under various load conditions, quantified as percentage of full-load. In order to achieve the reduced load operation, which means a reduced hydrogen production, the valves placed on the tube leading the hydrogen into the outside air had to be adjusted in such a way to get the desired hydrogen flow.



Fig. 92 – Second room details: valves. BV-09 in green, BV-04 in blue, BV-013 in orange, PCV-01 in yellow

The valve BV-04 was found not to be sensitive enough for carrying out this operation precisely. The only option then was to let the hydrogen flow through the lower tubes (indicated by an arrow). Along this way, the hydrogen flow passes through a fully rotating valve, called back pressure regulator PCV-01 (encircled in yellow). This one is much more sensitive, so that a quite wide rotation corresponds to a load reduction of few percent of the full-load. Therefore, the test setup can be described as follows: valve BV-04 closed, valve BV-09 closed, valve BV-

013 (marked in orange) partially open, back pressure regulator properly adjusted depending on the analysed case.

- 5.1 Turn the main switch, located on the electrolyser back side, to the ON position (Figure 93(a)). In this way, the electrolyser will move automatically into the PRE-START mode (fully described in section 2.3.2.2) during which a dashed line will flash on the display (Figure 94).

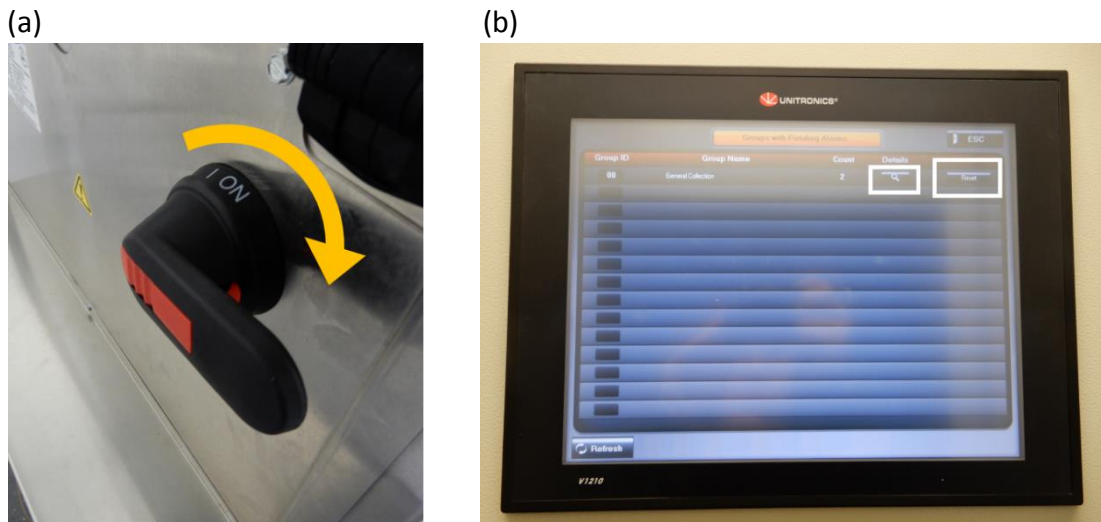


Fig. 93 – Second room details: (a) electrolyser main switch; (b) PLC display

- 5.2 If the main switch is on already (for instance, because it has been left on since the last operation), act on the PLC on the other side of the cabin to bring the electrolyser into PRE-START mode. Check the errors that appear under the *Alarm* menu on the PLC display (Figure 93(b)). If an error categorized as *General collection* shows up, press the *details* button to find out more details. In case the error codes *ID 002: 072 H2 STATUS* and *ID 012: GEEN H2 TIJDENS PROCEDURE* are listed, it is safe to press the *Reset* button. After this, the electrolyser will go to the PRE-START mode.

It is safe to leave the main switch on over a single or few days if the unit is going to be operated frequently!

Tab. 26 – Electrolyser display details

Letter	Details
A	Product pressure
B	System pressure
C	Display scroll keys
D	Start button
E	H <sub>2</sub> production indicator
F	Units toggle
G	Stop/Reset button
H	Screen

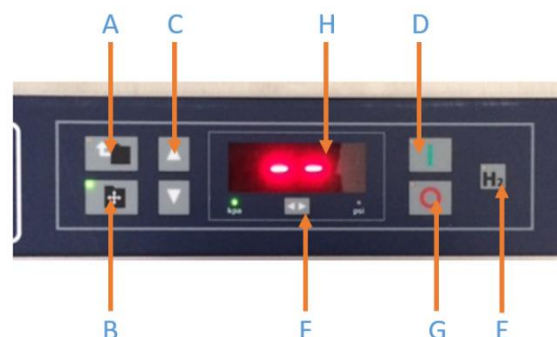


Fig. 94 – Electrolyser display



6. Wait till the start button light begins to flash, which indicates that the PRE-START operation has been completed, then press this button. After this, the electrolyser will go into GENERATE-VENT mode and the H<sub>2</sub> production indicator will light up. If all the needed process conditions are met, the system will move into PRESSURIZE-STORAGE mode and then, after reaching the system pressure, into STEADY-STATE operation during which the hydrogen will start to flow out from the unit (all of these states have been described in section 2.3.2.2 as well).

¡If the PRE-START operation does not start automatically passing through either step 5.1 or step 5.2, the electrolyser power supply may have been switched off as a consequence of a fault in the controller. Check on the PLC display under *Alarms* if any errors other than the above mentioned are listed. In such a case, more troubleshooting is necessary to make sure of the correct and safe functioning of the system!

7. Check the manometers indication (already visible in Figure 92) in order to detect if the hydrogen production is actually taking place and the STEADY-STATE operation has been achieved. Of course, the indicators to look at are different whether the hydrogen is produced in tanks filling mode (marked in yellow in Figure 95) or in venting mode (marked in blue) since the hydrogen follows a different pathway.

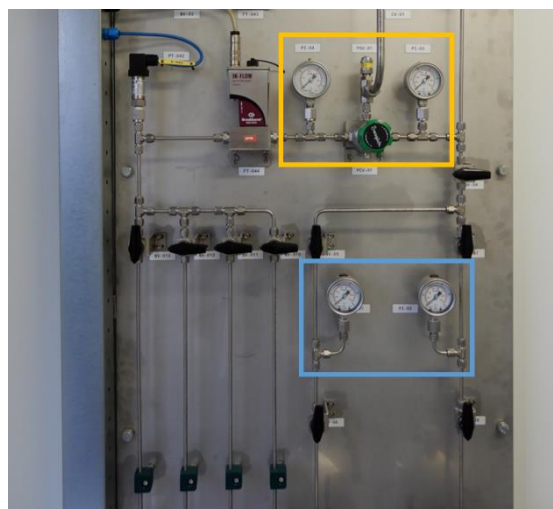


Fig. 95 – Second room details: manometers

### B.1.3 How to shut down the electrolyser system

1. Press the stop button on the electrolyser display to turn the unit off properly. The water circulation pump will continue to work for roughly one minute more. When all the auxiliaries are disconnected, an error code will show up on the PLC display.

¡Do not attempt to shut off the electrolyser by turning the main switch off. This must be done only in case of emergency!

¡It is strongly advisable not to shut off the system during GENERATE-VENT mode because this operation may cause flooding in the H<sub>2</sub>O/H<sub>2</sub> separators!

2. If the system was producing in tanks filling mode, it is necessary to discard the produced hydrogen stored in the tanks by venting it off. Assure that valve BV-04 is open and then slowly open valve BV-09. Close the latter when the tanks pressure indicators display pressure values closed to zero.
3. Turn off the demineralizing units by pressing the ON/OFF button of the RO device.
4. Close the main valve on the tap water feeding tube on the left side of the room.

As before, it is safe to leave the RO unit on and the main tap water valve open over a single or few days if the unit is going to be operated frequently. The demineralizing system will go automatically in stand-by mode if there is no water flowing to the electrolyser!



# Appendix C

The aim of this appendix is providing a user's manual for operating the electrolyser software packages. As already mentioned in section 2.3.2.4, the electrolyser process variables are measured by means of sensors and meters during hydrogen production. Some of these data can be logged and retrieved from the PLC, others from the electrolyser unit itself. The categorization has been provided in the PFD schematics in section 2.3.2.2. Here, few instructions on how to manage the needed software programs are given.

## C.1 Electrolyser software manual

### C.1.1 How to interface with the PLC

The electrolyser PLC works by logging data on a SD card plugged into it. It is possible to change the logging settings by pressing the *Settings Algemeen* button in the lower side of the PLC home view (Figure 96(a)). On this page, the current logging time step and the seconds left before the next log are displayed, as well as the IP address settings (Figure 96(b)). By pressing on the logging time box, it is possible to set the desired value in seconds, the minimum one being 10 seconds. Moreover, by clicking on the *Log nu* button, the logging can be performed manually so that the values can be logged by choice on a certain instant.

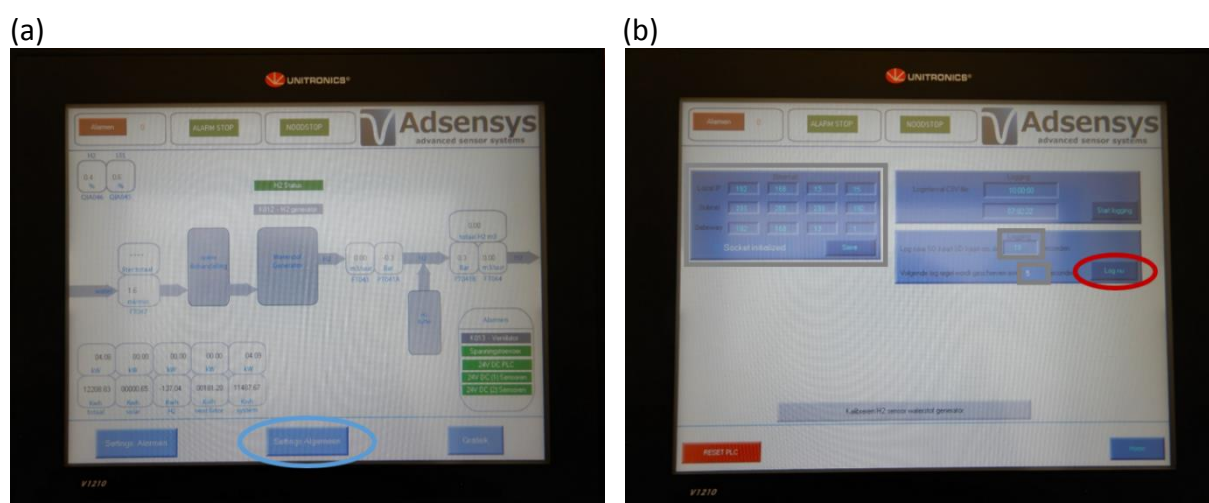


Fig. 96 – PLC display: (a) main screen; (b) general setting screen

The connection of the PLC device to the laboratory LAN via Ethernet has made it possible to interface with the PLC screen from a PC connected to the same LAN. In this way, all the above manual actions can now be performed remotely by means of the Unitronics' Remote Operator software.

### C.1.2 How to connect to the PLC in remote

In order to remotely connect to the PLC, after properly completing the installation of Remote Operator software on the PC in use, one should follow the instructions below:

1. Start up the Remote Operator program.
2. Click on the *Communication Settings* icon situated in the toolbar. The Communication Settings window will pop up (Figure 97).

3. Here, select the options showed in Figure 97:
  - Connection type: Ethernet (Call);
  - Target IP: same IP address assigned to the PLC from its own screen;
  - PLC Name: Adsensys (Pay attention! It is capital sensitive).
4. Press the **Check Connection** button to see if the connection to the PLC can be established. If the connection is successful, the PLC information will be displayed. Click **Ok** to close the window.
5. Click on the **Start/Stop** button located in the upper bar. The PLC screen should be displayed on the remote PC screen.

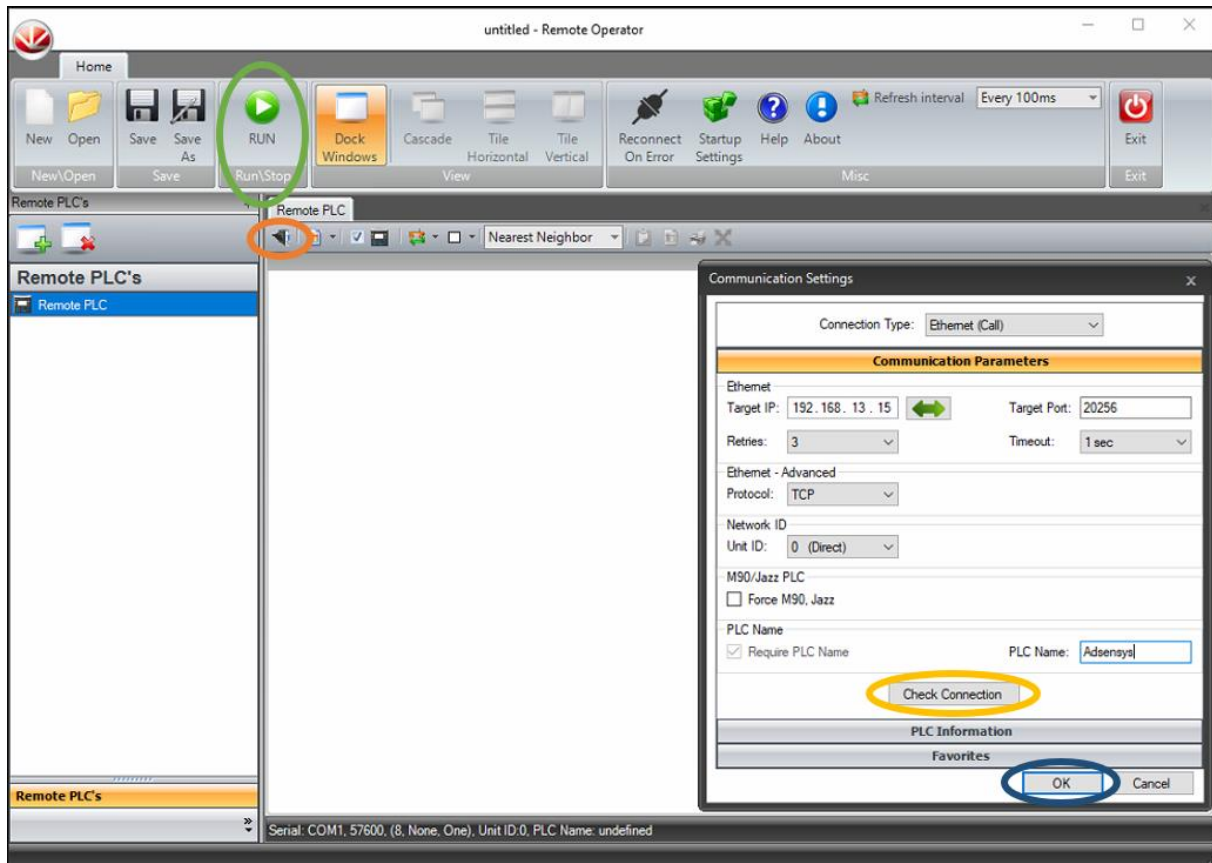


Fig. 97 – Remote Operator main screen

### C.1.3 How to retrieve the measured data from the electrolyser PLC

The data into the SD card can be read out once the logging process has been completed, meaning that in this way the measurements cannot be collected in real-time. There are two possibilities for retrieving the saved data on site:

- By connecting a PC to the PLC via miniUSB-USB cable;
- By pulling out the SD card and plugging it into a PC.

Since before pulling out the SD card the system has to be powered off, the second method is less preferable than the first one. In addition, a third option is available for retrieving data when the PC is connected in remote via Ethernet. In all three cases, the SD card content can be accessed by using the Unitronics' software called SD Card Suite. How to use this program depending on the chosen method will be described in what follows.

### C.1.3.1 Retrieving data by connecting a PC to the PLC via miniUSB-USB cable

In this case, before using the SD Card Suite software, a driver that can turn a USB-port into a COM-port needs to be installed on the PC. After completing the installation of SD Card Suite and the MiniUSB-R232 driver, one should follow the instructions below:

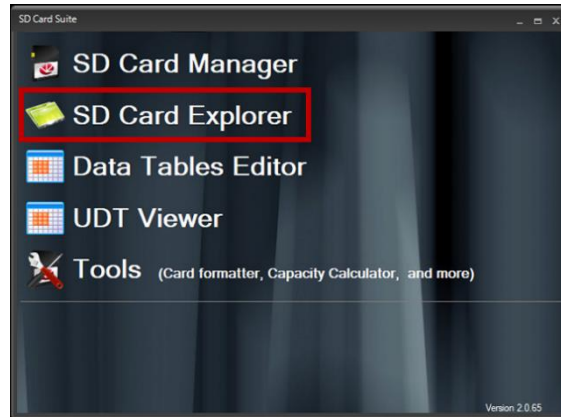


Fig. 98 – SD Card Explorer selection

1. Open the PLC enclosure with the proper key, connect the miniUSB-USB cable to the miniUSB port placed on the top of the PLC and to the USB port on the PC with the software previously installed.
2. Start up the SD Card Suite software and select the SD Card Explorer program (Figure 98).
3. Click on the **Settings** icon located in the top left corner. The Communication Settings window will pop up (Figure 99).
4. Here, select the options showed in Figure 99:
  - Connection type: Serial;
  - Baude rate: 115200;
  - PLC Name: Adsensys (Pay attention! It is capital sensitive).
5. In order to find out on which COM port the connected USB is working, check out the drop-down menu *Ports (COM & LPT)* in the device manager. It can be found on the PC in use by following the path: Windows>Control Panel>Device Manager.
6. Select the COM port in the Communication Settings window of the SD Card Explorer.
7. Press the **Check Connection** button to see if the connection to the PLC can be established. If the connection is successful, the PLC information will be displayed. Click **Ok** to close the window.
8. Click on the **Open** icon located in the top left corner to access the SD card. The files saved on the card should show up.

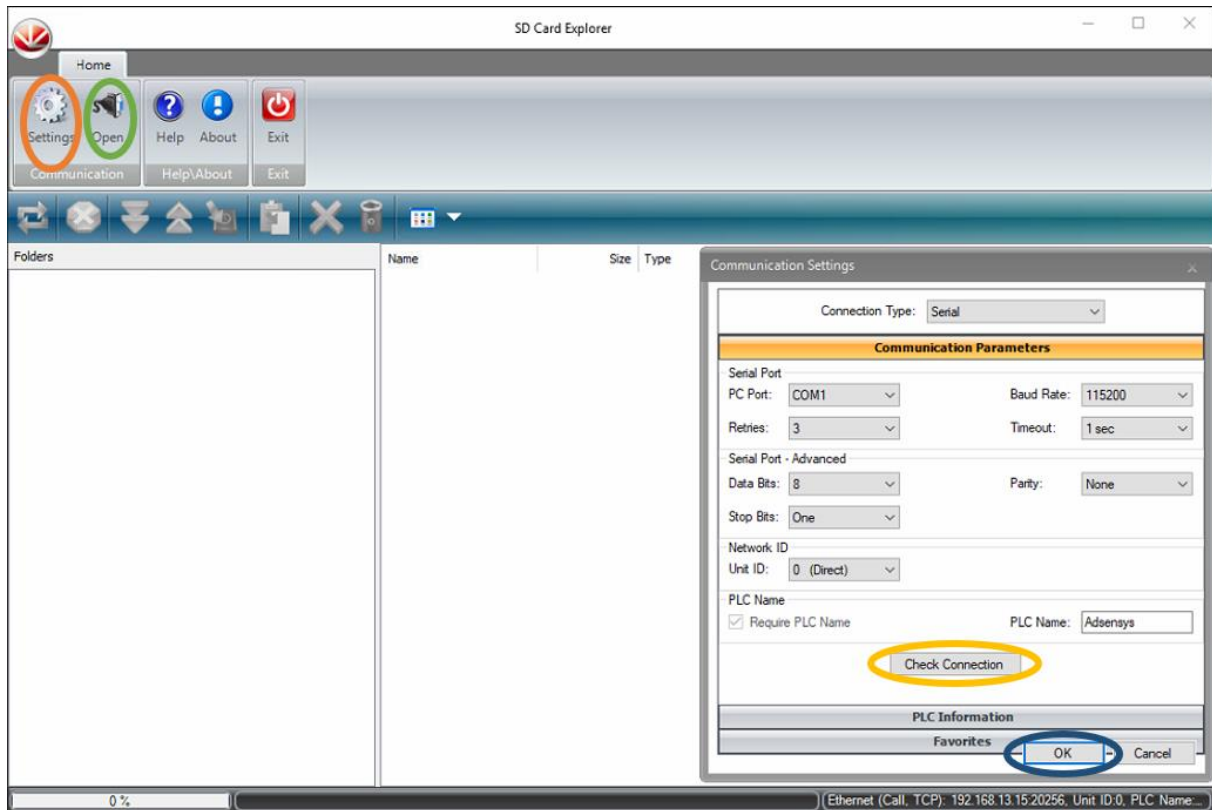


Fig. 99 – SD Card Explorer main screen

### C.1.3.2 Retrieving data by pulling out the SD card and plugging it into a PC

As previously specified, this is not the preferable way for retrieving measurements since it is necessary to shut off the power to the whole system first. It can still be used and it has been actually used during the performed experiments. In this case, the instructions to follow are listed below:

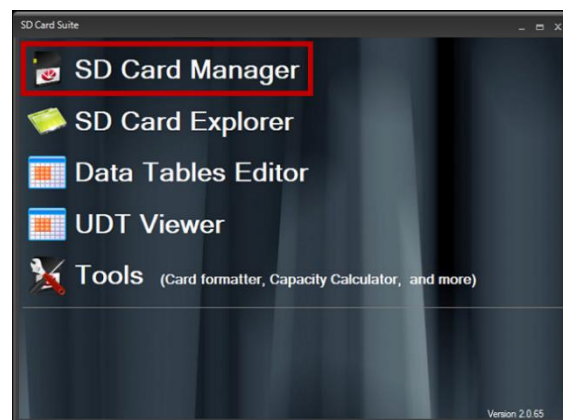


Fig. 100 – SD Card Manager selection

1. After shutting off the whole unit, open the PLC enclosure with the proper key, pull out the SD card from the device SD port and plug it into the PC with the preinstalled software.
2. Start up the SD Card Suite software and select the SD Card Manager program (Figure 100).
3. Create a new file by clicking on the top left **New** icon (Figure 101).

4. Click on the *Import SD folder* icon to import the files stored in the SD card. Here, two options are possible:
  - SD card plugged into a USB port of the PC by using a SD card adapter:
    - In this case, select *Import from SD Card plugged into USB port*.
    - A window will pop up showing the SD card information. Click *Next >>* so that the Alarms, DT, Log and Trend folders saved on the card will be imported in the PC.
    - These data can be exported to Excel through the *Export to Excel* button on the top menu.
  - SD card plugged into the SD port of the PC:
    - In this case, instead, select *Import local folder* to manually copy the files from the SD card.
    - Browse the files to import and convert, then click *Next >>* so that the data will be directly saved in Excel format.

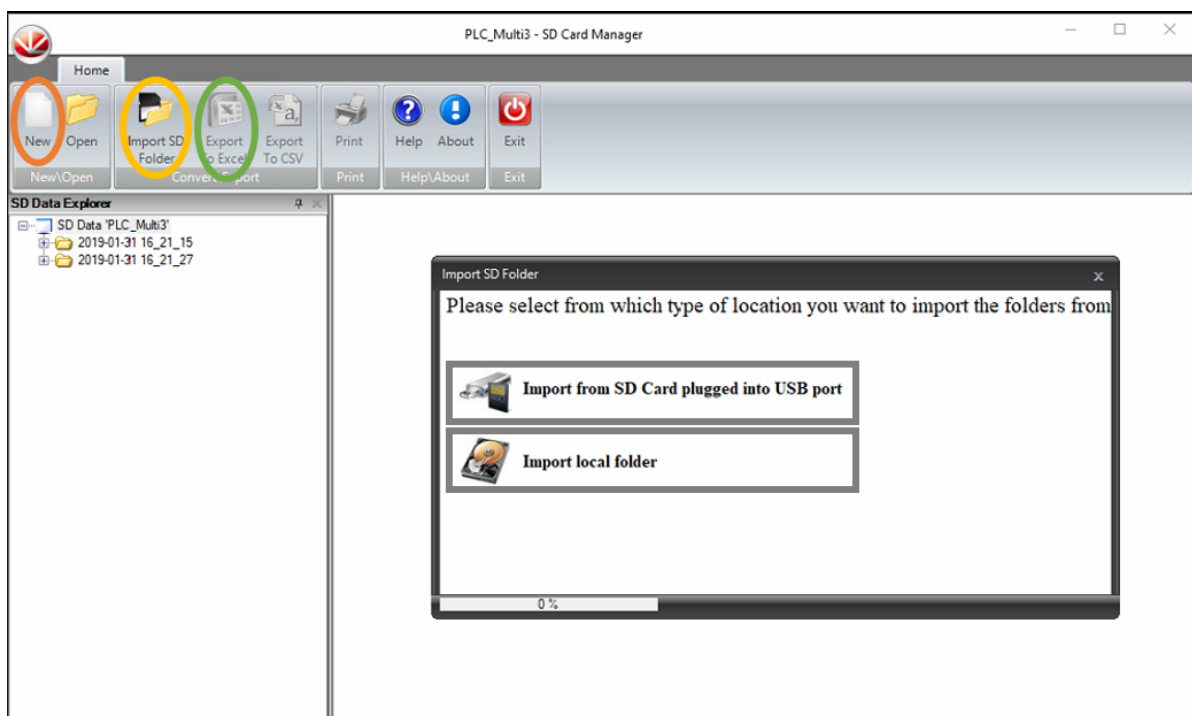


Fig. 101 – SD Card Manager main screen

Note: In order to retrieve data when the PC is connected in remote via Ethernet, it is necessary to use the SD Card Explorer program. The steps to follow are the same already reported for retrieving data via miniUSB-USB cable, beginning with step 2. Steps 4, 5 and 6 must be substituted with the selection of the following options in the Communication Settings window:

- Connection type: Ethernet (Call);
- Target IP: same IP address assigned to the PLC from its own screen;
- PLC Name: Adsensys (Pay attention! It is capital sensitive).

## C.1.4 How to retrieve the measured data from the electrolyser unit

The data can be gained from the electrolyser unit itself by means of the program called HOGEN40. This is the software provided by Proton, the company from which the electrolyser has been purchased, and it is available upon request at Entrance. In particular, this software allows to log real-time data and monitor the process while logging. In what follows, details are provided on how to connect to the unit (either via RS232 serial cable or via Ethernet connection) and how to make use of the program.

### C.1.4.1 Connection via RS232 serial cable

Firstly, the RS232 serial cable provided with the electrolyser equipment has to be used to make a PC communicate with the unit. If the PC has no RS232 serial port, either a USB-RS232 serial converter cable or a RS232-to-USB adapter together with a dedicated driver are needed to establish the connection.

When the installation is completed, the following instructions have to be observed:

- Connect the PC to the unit via the provided cable.
- Start HOGEN40 software and go to: Tools>Options>Communications.  
A window will pop-up reporting the communication settings (Figure 102).
- Check in the PC Device Manager which COM port is used by the USB or RS232 port to which the unit is connected. This explanation has been already provided in the previous section C.1.3.1.
- Select this port in the Comm Port drop-down menu on the HOGEN40 communication window. Click *Apply* and then *Ok*. In this way the PC should be connected to the unit.

**If the COM port in use does not appear in this menu as an option, try and plug the USB in another USB port!**

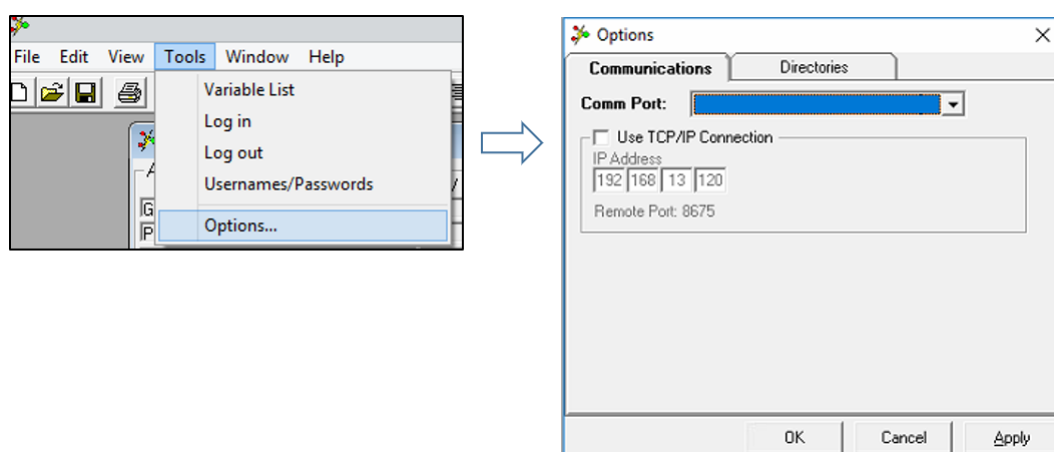


Fig. 102 – HOGEN40 Communications window

### C.1.4.2 Connection via Ethernet

In order to interface with the unit via Ethernet, open HOGEN40 software and get to the Communications window (Figure 102). Here, tick the *Use TCP/IP connection* option and type the IP address assigned to the electrolyser unit.



### C.1.4.3 Data logging

Once established the communication, it is possible to choose between two ways to log the data:

- Logging with the Diagnostic view, available going to View>Diagnostic (Figure 103)

In this screen, all the data that can be logged are listed. It is possible either to choose from this list the desired data by manually selecting the related checkbox or to select all data at once by pressing the *ALL* button. After ticking the *Enable Logging* box, the logging options will show up. By clicking *Change Path*, the log file path can be assigned. The sampling time can only be picked from the discrete list under the *Sampling Rate* drop-down menu, the minimum value being 5 seconds. At last, click *Start Sampling* to make the software start to log.

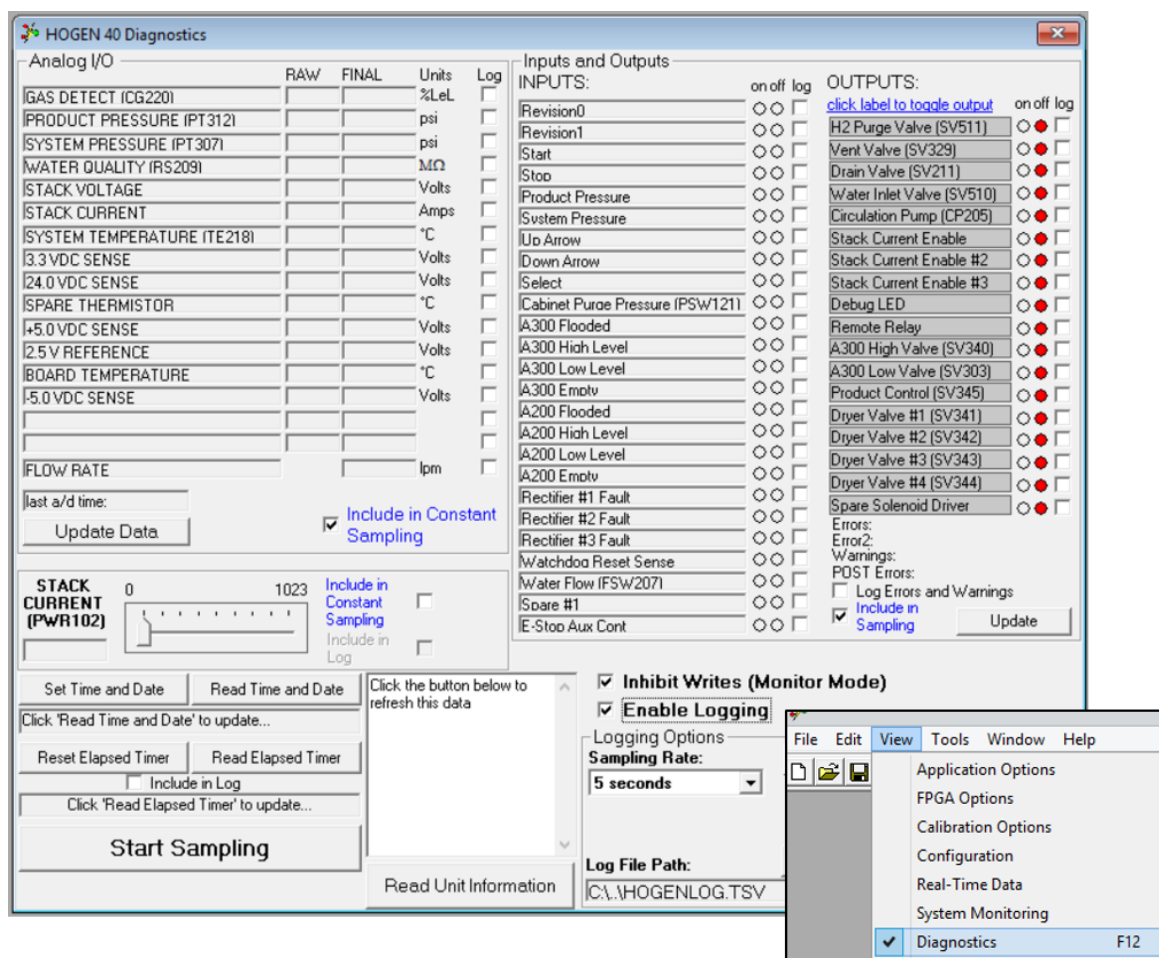


Fig. 103 – HOGEN40 Diagnostics

- Logging with the Monitoring view, available going to View>System Monitoring (Figure 104)

This screen shows a PFD of the process. This allows to monitor the process variables and system state while making it clear where the related sensors are located. Click *Start Monitoring* to make the software start to display the real-time data on the scheme. By clicking *Path*, it is possible to select the path to which the log file will be saved. In order to

start logging, click the switch next to *Data Log On/Off* to make it turn upwards. In order to stop logging, simply click the switch to turn it back downwards again, as it is in Figure 104.

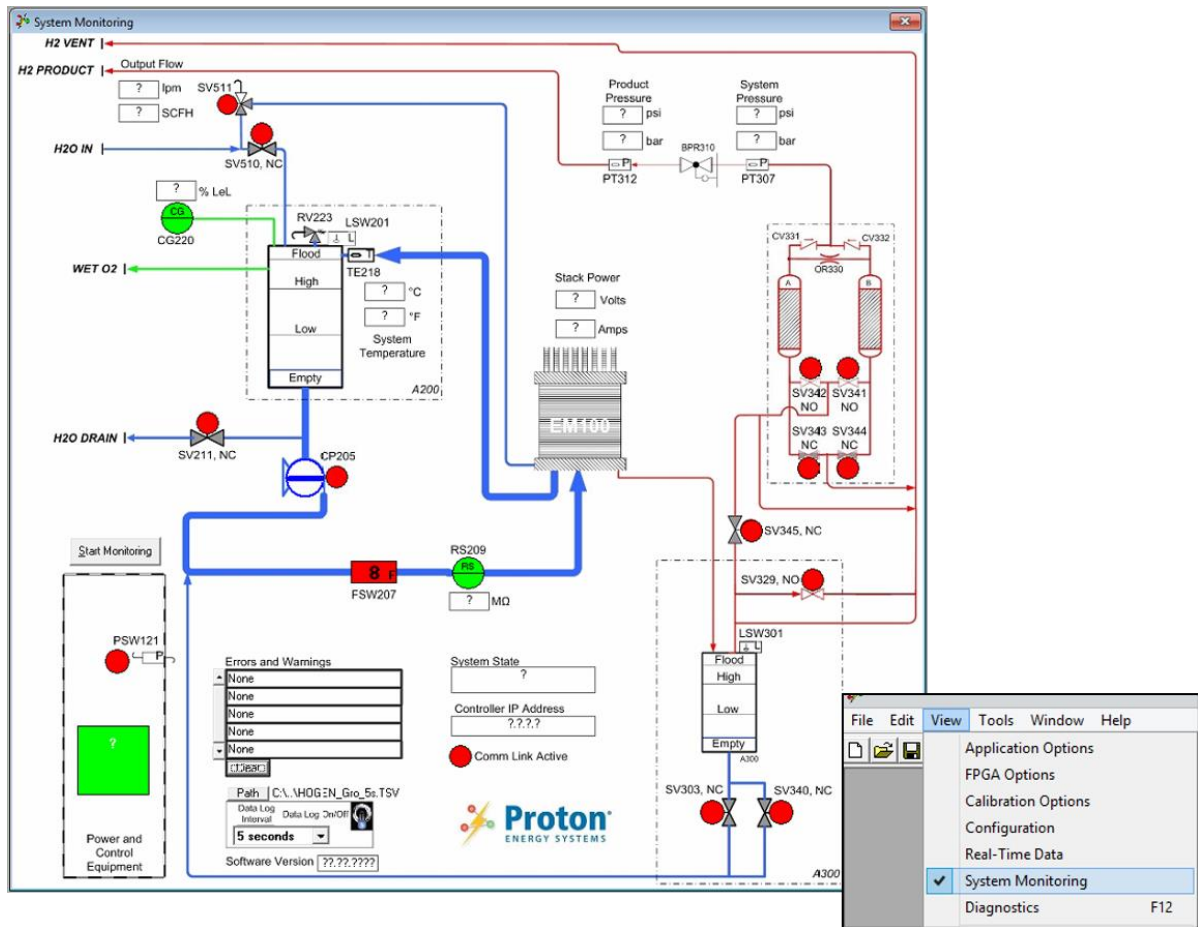


Fig. 104 – HOGEN40 System Monitoring

Note: TSV files gained from the electrolyser unit can be finally loaded into Excel in the same way as the CSV files obtained from the power analyzer.



# Appendix D

The aim of this appendix is to show how to correctly connect PV panels and electrolyser in order to carry out meaningful measurements by means of the power analyzer. This is an integration to the section in Chapter 3 and 4, illustrating the experiments performed for the purpose of modelling these energy transition sources.

## D.1 How to arrange the PV panels connections within the lab setup

In order to perform measurements of the PV-field power output by means of the power analyzer, it is necessary to properly arrange the related connections as follows. Let us suppose that the connections are initially set in such a way to have the PV system sending the generated power into the electrical network (AC socket marked by the yellow circle in Figure 105).

First of all, the inverter has to be shut off and the switch above it (orange square in Figure 105) opened to allow the AC cable downstream to be unplugged from the external grid (yellow circle). After opening the switch which connects the power analyzer to the internal grid (green square in Figure 106), the AC cable can be plugged in downstream of the instrument (blue circle). Afterwards, the switch upstream of the power analyzer can be closed and the inverter can be turned on again. In this way, the inverter no longer injects the produced power into the network, but into the internal circuit in order to be measured.

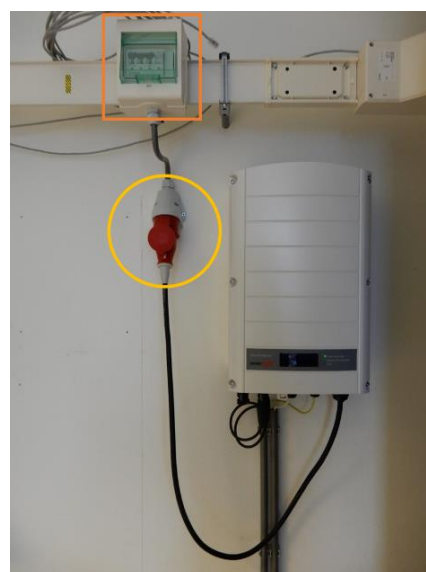


Fig. 105 – Detail switches and sockets (inverter side)

In the other way around, if the previous configuration is intended to be restored, this can be done by following the former steps backwards. It is then necessary to shut off the inverter and open the switch above the power analyzer, so that the AC cable can be put back into the socket to connect the inverter to the external grid. At last, the switch above the inverter can be closed and the inverter started up. This allows the PV power production to be injected into the network while the power analyzer is made available for other operations, such as performing measurements on the electrolyser.

## D.2 How to arrange the electrolyser connections within the lab setup

In order to monitor the electrolyser power input by means of the power analyzer, the respective connections have to be correctly positioned as follows. Let us suppose that the electrolyser is initially supplied by direct connection to the internal circuit (AC socket marked by the white circle in Figure 106).

The first step is then to check that all the electrolyser processes are off. Afterwards, the switch responsible for the direct supply has to be opened (red square), and so does the switch above the power analyzer (green square), allowing the supply by passing through the instrument. At this point, the supply cable can safely be unplugged and then plugged into the socket below the power analyzer (blue circle). At last, by closing the switch upstream of the measuring device, the electrolyser can be powered on and its electrical input variables measured.

On the other hand, to bring the connections back to the previous arrangement, it is necessary to proceed in the opposite way. After making sure the electrolyser is off, both the mentioned switches have to be opened. Lastly, the cable can be put back into the socket providing direct supply from the internal grid and the related switch closed again. In this way, the electrolyser can be started up even if the power analyzer is carrying out other operations, for example the measure of the PV panels output.

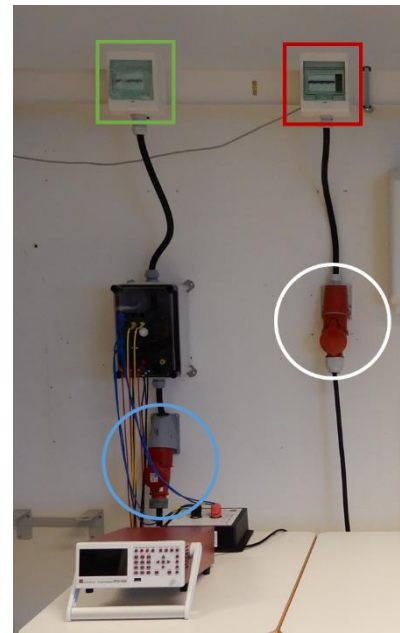


Fig. 106 – Detail switches and sockets (PPA side)

# Appendix E

This appendix contains:

- A section dedicated to the flow controller communication with:
  - Indications on how to use Modbus Tester interface, together with a list of the useful flow controller Modbus registers;
  - Explanation of the conversion applied to the H<sub>2</sub> flow setpoint;
  - The Matlab code used for logging and saving the H<sub>2</sub> flow setpoint and measured H<sub>2</sub> flow data.
- The complete Matlab code of the *Matlab Function* blocks used to integrate power analyzer and flow controller into Simulink, namely:
  - MATLAB Function – Modbus write;
  - MATLAB Function – input translate;
  - MATLAB Function – Modbus read;
  - MATLAB Function – output translate;
  - MATLAB Function – TCP read.

Note: This appendix is not published or publicly available.

# References

- [1] P. Nikolaidis, and A. Poullikkas. “A comparative overview of hydrogen production processes”. In: *Renewable and Sustainable Energy Reviews* 67 (2017), pp. 597–611.
- [2] A. Godula-Jopek, and D. Stolten, *Hydrogen Production: By Electrolysis*, Wiley-VCH Verlag GmbH & Co. KGaA, 2015.
- [3] A. Mazza, E. Bompard, and G. Chicco. “Applications of power to gas technologies in emerging electrical systems”. In: *Renewable and Sustainable Energy Reviews* 92 (2018), pp. 794–806.
- [4] S. Schiebahn, T. Grube, M. Robinius, V. Tietze, B. Kumar, and D. Stolten. “Power to gas: Technological overview, systems analysis and economic assessment for a case study in Germany”. In: *International Journal of Hydrogen Energy* 40.12 (2015), pp. 4285–4294.
- [5] M. Carmo, D. L. Fritz, J. Mergel, and D. Stolten. “A comprehensive review on PEM water electrolysis”. In: *International Journal of Hydrogen Energy* 38.12 (2013), pp. 4901–4934.
- [6] E. Bombard, F. Boni-Castagnetti, G. Chicco, A. Mazza, L. Piantelli, and E. Pochettino (2017). *Innovative large-scale storage technologies and Power-to-Gas concepts after optimization: Report on opportunities and options for PtG in power systems* (Deliverable No. D6.1). Retrieved from STORE&GO Website. URL: [https://www.storeandgo.info/fileadmin/downloads/2017-04-29\\_STOREandGO\\_D6.1\\_IREN\\_submitted.pdf](https://www.storeandgo.info/fileadmin/downloads/2017-04-29_STOREandGO_D6.1_IREN_submitted.pdf)
- [7] A. Kosonen, J. Koponen, K. Huoman, J. Ahola, V. Ruuskanen, and T. Ahonen. “Optimization Strategies of PEM Electrolyser as Part of Solar PV System”. In: *2016 18th European Conference on Power Electronics and Applications (EPE'16 ECCE Europe)*. IEEE. 2016.
- [8] M. Qadrdan, M. Abeysekera, M. Chaudry, J. Wu, and N. Jenkins. “Role of power-to-gas in an integrated gas and electricity system in Great Britain”. In: *International Journal of Hydrogen Energy* 40.17 (2015), pp. 5763–5775.
- [9] Catrinus Jepma, Charlotte van Leeuwen, Daan Hulshof (2017). *Innovative large-scale storage technologies and Power-to-Gas concepts after optimization: Exploring the future for green gases* (Deliverable No. D8.1). Retrieved from STORE&GO Website. URL: [https://www.storeandgo.info/fileadmin/downloads/2017-08-29\\_STOREandGO\\_D8.1\\_RUG\\_submitted.pdf](https://www.storeandgo.info/fileadmin/downloads/2017-08-29_STOREandGO_D8.1_RUG_submitted.pdf)
- [10] Triphase N.V. Triphase HPC Explained white paper: *Shaping dynamic response using Virtual Circuit Control*, 2014.
- [11] Triphase N.V. Triphase HPC Explained white paper: *Under the hood of Triphase Virtual Circuit Control*, 2014.
- [12] Triphase. *Triphase Support Website*: global documents. URL: <https://triphase.com/support/>

- [13] Triphase. *Triphase Support Website: project-specific documents*. URL: <https://triphase.com/support/project-list/>
- [14] A. S. Tanenbaum, and D. J. Wetherall, *Computer Networks*, Pearson College Div, 2010.
- [15] Newtons4th Ltd. *PPA5xx/15xx series Start Up Guide, Firmware v2.74*. 2017. Retrieved from Newtons4th Ltd Website. URL: [https://www.newtons4th.com/wp-content/uploads/2014/07/PPA5\\_15-Start-up-guide-1.pdf](https://www.newtons4th.com/wp-content/uploads/2014/07/PPA5_15-Start-up-guide-1.pdf)
- [16] Newtons4th Ltd. *PPA500/1500 User Manual, Firmware v2.90*. 2018. Retrieved from Newtons4th Ltd Website. URL: [https://www.newtons4th.com/wp-content/uploads/2014/07/PPA5xx\\_15xx-User-Manual-v2-91.pdf](https://www.newtons4th.com/wp-content/uploads/2014/07/PPA5xx_15xx-User-Manual-v2-91.pdf)
- [17] Newtons4th Ltd. *PPA500/1500 Communications Manual, Firmware v2.83*. 2018. Retrieved from Newtons4th Ltd Website. URL: [https://www.newtons4th.com/wp-content/uploads/2014/07/PPA5xx\\_15xx-Comms-manual-v2\\_83.pdf](https://www.newtons4th.com/wp-content/uploads/2014/07/PPA5xx_15xx-Comms-manual-v2_83.pdf)
- [18] Newtons4th Ltd. *PPA DataLogger - Data Logging Software User Manual, Software Version v3\_2a*. 2015. Retrieved from Newtons4th Ltd Website. URL: <https://www.newtons4th.com/wp-content/uploads/2014/07/PPA-Datalogger-User-Manual.pdf>
- [19] Proton OnSite. *HOGEN S Series 2 Hydrogen Generator: Installation & Operation Instructions*. 2011.
- [20] Proton OnSite. *HOGEN S Series 2 Hydrogen Generator: Service Manual*. 2011.
- [21] Proton OnSite. *HOGEN S Series 2 Hydrogen Generator: Maintenance Manual*. 2011.
- [22] A. Ursúa, L. M. Gandía, P. Sanchis. "Hydrogen Production From Water Electrolysis: Current Status and Future Trends". In: *Proceedings of the IEEE 100.2* (2012), pp. 410–426.
- [23] D. W. Green, R. H. Perry, *Perry's Chemical Engineer's Handbook*, McGraw-Hill Education, 2007.
- [24] Modbus Organization. *Modbus Application Protocol Specification V1.1b*. 2006. Retrieved from Modbus Org Website. URL: [http://www.modbus.org/docs/Modbus\\_Application\\_Protocol\\_V1\\_1b.pdf](http://www.modbus.org/docs/Modbus_Application_Protocol_V1_1b.pdf)
- [25] Bronkhorst. *Document 9.17.022 - Instruction manual: General instructions digital Mass Flow / Pressure instruments laboratory style / IN-FLOW*. 2018. Retrieved from Bronkhorst Website. URL: <https://www.bronkhorst.com/getmedia/50bed9ce-0445-4eba-9d37-f113ec53cb34/917022Manual-general-instructions-digital-laboratory-style-and-IN-FLOW>
- [26] Datasheet of Trina Solar's PV module, model TSM-260PC05A. Retrieved from Trina Solar Website. URL: <https://www.totalsolarsolutions.com.au/wp-content/uploads/downloads/TRINA-PC05A-250W.pdf>

- [27] Datasheet of SolarEdge's three-phase inverter, model SE4K. Retrieved from SolarEdge Website. URL: <https://www.solaredge.com/sites/default/files/se-three-phase-indoor-inverter-datasheet.pdf>
- [28] Datasheet of Kipp&Zonen's pyranometer, model SMP3. Retrieved from Kipp&Zonen Website. URL: <https://www.kippzonen.com/Product/201/SMP3-Pyranometer#.XIVTQShKhPY>
- [29] The MathWorks. *SimPowerSystem User's Guide, Version 3*. 2003. Retrieved from The MathWorks Website. URL: [https://www.mathworks.com/help/releases/R13sp2/pdf\\_doc/physmod/powersys/powersys.pdf](https://www.mathworks.com/help/releases/R13sp2/pdf_doc/physmod/powersys/powersys.pdf)
- [30] F. Spertino, F. Corona, and P. Di Leo. "Limits of Advisability for Master-Slave Configuration of DC-AC Converters in Photovoltaic Systems". In: *IEEE Journal of Photovoltaics* 2.4 (2012), pp. 547-554.
- [31] G. Chicco, V. Cocina, A. Mazza, and F. Spertino. "Data Pre-Processing and Representation for Energy Calculations in Net Metering Conditions". In: *2014 IEEE International Energy Conference (ENERGYCON)*. IEEE. 2014.
- [32] E. Bompard, S. Bensaid, G. Chicco, and A. Mazza (2018). *Innovative large-scale storage technologies and Power-to-Gas concepts after optimization: Report on the model of the power system with PtG* (Deliverable No. D6.4). STORE&GO project.
- [33] H. Lok, A. Estebarsari, and A. Mazza (2018). *Innovative large-scale storage technologies and Power-to-Gas concepts after optimization: Status P2G grid integration experiment* (Deliverable No. D6.2). STORE&GO project.
- [34] STORE&GO Website. URL: <https://storeandgo.info/>
- [35] E. Bompard, A. Monti, A. Tenconi, A. Estebarsari, T. Huang, E. Pons, M. Stevic, S. Vaschetto, and S. Vogel. "A multi-site real-time co-simulation platform for the testing of control strategies of distributed storage and V2G in distribution networks". In: *2016 18th European Conference on Power Electronics and Applications (EPE'16 ECCE Europe)* (2016), pp. 1-9.
- [36] Opal-RT Website. URL: <https://www.opal-rt.com/>
- [37] WireShark. Wireshark User's Guide. Retrieved from WireShark Website. URL: <https://www.wireshark.org/download/docs/user-guide.pdf>
- [38] Bronkhorst. *Document 9.17.023 - Instruction manual: Operational instructions for digital Multibus Mass Flow / Pressure instruments*. 2018. Retrieved from Bronkhorst Website. URL: <https://www.bronkhorst.com/getmedia/ad6a26ef-e33f-4424-b375-21d5811e3b04/917023-Manual-operation-instructions-digital-instruments>

- [39] Bronkhorst. *Document 9.17.035 - Instruction manual: Modbus slave interface for digital Mass Flow / Pressure instruments*. 2017. Retrieved from Bronkhorst Website. URL: <https://www.bronkhorst.com/getmedia/bb0e02ab-2429-4638-b751-7186bd7178fb/917035-Manual-Modbus-slave-interface>
- [40] The MathWorks. *Instrument Control Toolbox User's Guide, Version 2.5*. 2007.
- [41] The MathWorks. *Instrument Control Toolbox User's Guide, Version 3.14*. 2018. Retrieved from The MathWorks Website. URL: [https://it.mathworks.com/help/pdf\\_doc/instrument/instrument.pdf](https://it.mathworks.com/help/pdf_doc/instrument/instrument.pdf)